DESIGN AND DEVELOPMENT OF FPGA BASED NUCLEAR QUADRUPOLE RESONANCE SPECTROMETER

By

Preeti Hemnani

ENGG01201104007

Bhabha Atomic Research Centre, Mumbai

A thesis submitted to the

Board of Studies in Engineering Sciences

In partial fulfillment of requirements

for the Degree of

DOCTOR OF PHILOSOPHY

of

HOMI BHABHA NATIONAL INSTITUTE

May, 2018

Homi Bhabha National Institute

Recommendations of the Viva Voce committee

As the members of viva voce committee, we certify that we have read the dissertation prepared by **Preeti Hemnani** entitled "**Design and Development of FPGA based Nuclear Quadrupole Resonance spectrometer**" and recommend that it may be accepted as fulfilling the thesis requirement for the award of Degree of Doctor of Philosophy.

Date 02.05.2018

Chairman – Dr. Archana Sharma

Date: 02/5/2018

Guide / Convener – Dr. A.K. Rajarajan

Date:

Co-guide - Dr. S.V.G. Ravindranath

Date: 02.05.2018

Technology Adviser- Dr.Gopal Joshi

02.05.2018
Date:

Member 1- Dr. Vaibhav Hanamant Patankar

Date:

Member 2- Dr. Gopika Vinod

Date: 2/5/2018

Member 3- Dr.B.Dikshit

Date: 2/5/2018

Examiner - Prof. Sidhartha P. Duttagupta

Final approval and acceptance of this thesis is contingent upon the candidate's submission of the final copies of the thesis to HBNI.

I/We hereby certify that I/we have read this thesis prepared under my/our direction and recommend that it may be accepted as fulfilling the thesis requirement.

Date: 2-05-2018

Place: HBNI, Mumbai

Guide-Dr.A.K.Rajarajan

Co- Guide-Dr.S.V.G.Ravindranath

STATEMENT BY AUTHOR

This dissertation has been submitted in partial fulfilment of requirements for an advanced degree at Homi Bhabha National Institute (HBNI) and is deposited in the Library to be made available to borrowers under rules of the HBNI.

Brief quotations from this dissertation are allowable without special permission, provided that accurate acknowledgement of source is made. Requests for permission for extended quotation from or reproduction of this manuscript in whole or in part may be granted by the Competent Authority of HBNI when in his or her judgment the proposed use of the material is in the interests of scholarship. In all other instances, however, permission must be obtained from the author.

Mumbai, May 2018 Preeti Hemnani

DECLARATION

I, hereby declare that the thesis entitled "**Design and Development of FPGA based Nuclear Quadrupole Resonance spectrometer**" submitted to Homi Bhabha National Institute (HBNI), Mumbai, India, for the award of Doctor of Philosophy in Engineering Science, is the record of work carried out by me during the period from March 2011 to August 2016 under the guidance of Dr.A.K.Rajarajan, Dr.Gopal Joshi and Dr. S.V.G.Ravindranath. The work is original and has not been submitted earlier as a whole or in part of degree/diploma at this or any other Institute/ University of higher learning.

Mumbai, May 2018 Preeti Hemnani

LIST OF PUBLICATIONS ARISING FROM THE THESIS

Peer Reviewed Journals

1. Preeti Hemnani, A.K. Rajarajan, Gopal Joshi, S.V.G. Ravindranath, "Development of low frequency FPGA based NQR/NMR spectrometer", Global journal of Researches in Engineering: F, Electrical and Electronics engineering, March 2016 Volume 16, Issue 2 Online ISSN: 2249-4596

2. Preeti Hemnani, A.K. Rajarajan, Gopal Joshi, S.V.G. Ravindranath, "Detection of NQR signals using Wavelet Transform and Adaptive filters", International journal of Instrumentation Technology (March 2018), Vol,2,No.1, pp.34-49, Inderscience Publications.

DOI: 10.1504/IJIT.2018.10011916

3. Preeti Hemnani, A.K. Rajarajan, Gopal Joshi, S.V.G. Ravindranath, "The Building of NMR/NQR spectrometer", International Journal of Electrical and Computer Engineering Vol.8, Issue.3, June 2018, pp-1442~1450, DOI: 10.11591/ijece.v8i3.pp1442-1450

Conference Proceedings

1. Preeti Hemnani, A.K. Rajarajan, Gopal Joshi, S.V.G. Ravindranath , "FPGA based ^{14}N pulsed NQR spectrometer" , National symposium on Nuclear instrumentation, HBNI, Mumbai, November 2013,ISBN: 81-88513-59-8
2. Preeti Hemnani, A.K. Rajarajan, Gopal Joshi, S.V.G. Ravindranath, "FPGA

based pulsed NQR spectrometer" , DAE-SSPS Symposium, Thapar University, Patiala on December 2013 ,published in AIP Proceedings, 1591, 661-663 April 2014,doi:10.1063/1.4872710.

3. Preeti Hemnani, A.K. Rajarajan, Gopal Joshi, S.V.G. Ravindranath , "FPGA based RF pulse generator for NQR/NMR spectrometer" in International Conference on Advances in Computing and Communications, Cochin, September 2016, published in Proceedings Computer Science, Volume 93,2016 ,pages 161-168, **Elsevier, Science Direct ,**doi :10.1016/j.procs.2016.07.196
4. Preeti Hemnani, A.K. Rajarajan, Gopal Joshi, S.V.G. Ravindranath, "^{14}N NQR spectrometer for explosive detection: A Review", International Conference on Automatic Control and Dynamic Optimisation Technique, Pune, September 2016 to be published in **IEEE Xplore, doi:** 10.1109/ICACDOT.2016.7877761

ACKNOWLEDGEMENTS

This project would never have been possible without the support and guidance of various people at BARC.

Firstly I would like to thank Dr. A.K.Rajarajan for giving me the wonderful opportunity to complete my project work under his supervision. It is truly an honour. Special Thanks for all the advice, ideas, moral support and patience in guidance throughout this project. His wealth of knowledge in the field of Nuclear Quadrupole Resonance in particular is inspiring. I have learned many things from him including technical knowledge, research methodology and communication skills. I appreciate all his contributions of time, ideas to make my PhD experience productive and stimulating.

Special thanks also to be given to Dr. Gopal Joshi for introducing me to the instrumentation part of NQR and for continuous support and guidance in the years that followed and for keeping me motivated throughout my project work. Thank you for believing in me and giving me necessary pep talks whenever I started doubting myself.

I would like to thank Dr S.V.G. Ravindranath for guiding and setting the path for my work. It helped me to move in focused manner towards project objectives.

My special thanks to committee members Dr. Archana Sharma, Dr. V. H. Patankar, Dr. Gopika Vinod, Dr. B. Dixit, for serving on my supervisory committee and for their time, interest and helpful comments which helped me a lot during my research work.

I would also like to express my sincere thanks to Ms. C.I. Sujo for generously sharing her time and knowledge on RF amplifier. In my initial work I am particularly indebted to Mr Paresh Motiwala for sharing the information on FPGA and VHDL programming that enabled me to develop model. I must also thank Ms.Charulata, Mr. Shyam Mohan and ED workshop for helping me on, making the box for probe.

I would like to thank administrative and technical staff members of BARC and HBNI who had been kind enough to advise and help in their respective roles.

I am deeply thankful to my parents, my husband and my daughters for their help, encouragement and support. Finally I would like to thank all the people who helped me during my PhD.

CONTENTS

SYNOPSIS

Nuclear Quadrupole Resonance (NQR) is spectroscopy of nuclear energy levels resulting from the interaction of nuclear quadrupole moment with the electric field gradient in crystalline (non-cubic) solids. The nuclear energy levels pertaining to this interaction absorb and emit electromagnetic radiation in the RF range. In the pulsed NQR spectrometer, the sample is exposed to intense RF radiation of resonance frequency (1MHz to 100MHz) from which the nuclei absorb power. When the RF radiation is switched off the absorbed energy is radiated from the nuclei at the same frequency as it was absorbed in a typical time constant (T_2^*) of few tenths of microseconds to a few milliseconds. The resonance frequency depends on both the quadrupole moment of the nucleus and the electric field gradient surrounding it hence is a property of not only the nucleus but also its surroundings. For most of the organic crystals the resonance frequency lies below 10 MHz. ^{14}N NQR frequencies for organic compounds like urea, $NaNO_2$, RDX etc lies in the range of 1 - 5 MHz.

NQR spectrometer developed as part of this thesis is composed of four modules; Transmitter, Probe, Receiver and computerized control (FPGA & Software) module containing frequency synthesizer, synchronous demodulator, pulse programmer and display. The function of the transmitter module is to amplify the RF pulse sequence to about 200 W power level into the probe (50 Ohm) which is a parallel resonance circuit with a tapped capacitor. The probe excites the nucleus and picks-up the signal emitted from the nuclei. The nuclear signal at the same frequency as the excitation, which is typically in the range of a few micro volts is amplified, demodulated and filtered by receiver module. Direct digital synthesizer (DDS), pulse programmer, digital demodulator, finite impulse response filter (FIR), Signal accumulator have been implemented in single FPGA chip. The FPGA chip along with high speed ADCs (105MSPS), DACs (300MSPS), RF power amplifier, pre-

amplifier, cross diodes and quarter wave transformer has been used to build prototype of NQR spectrometer as part of this thesis. The whole instrument is developed in Electronics Division (ED), BARC from which RF power amplifier was available in-house at ED and other parts as explained above were developed as part of this thesis. The same was used to observe ^{14}N NQR signal from $NaNO_2$. Using a permanent horse shoe magnet same spectrometer has also been used as NMR spectrometer to observe ^{1}H NMR signal from H_20 and ^{2}H NMR signal from D_2O.

The NQR technique suffers mainly from its inherently low signal to noise ratio (-60dB and less) and RF interference. The low SNR can be remedied by repeating the measurements as NQR signals can be added coherently, however time needed for accurate detection can be too long (can be in hours). RFI on other hand can be alleviated using proper shielding which is only possible in laboratory environments and not in the fields. Adaptive filters and wavelet transforms are used in this work as these do not need prior knowledge of signal and also parameters of adaptive filter changes to meet the optimization parameters. ANC (Adaptive Noise Canceller) and ALE (Adaptive line Enhancer) based on Adaptive algorithm are studied here and applied to NQR/NMR signals as post signal processing techniques. Simulation results show that ALE and wavelet transforms along with coherent accumulation are faster detection method with improved SNR.

List of Figures

List of Tables

List of Abbreviations

ADC..... Analog to Digital Converter

ANC…… Adaptive Noise Cancellation

ALE…… Adaptive Line Enhancer

ALS……. Alternating least Squares

CFM…… Cubic feet per Minute

CORDIC……. Coordinate Rotation Digital Computer

CVI……..... C for Virtual Instrumentation

CW……..... Continuous Wave

DAC…… Digital to Analog Converter

DDS……..... Direct Digital synthesizer

DPRAM…….. Dual Port Random Access Memory

DSP……..... Digital Signal Processing

EFG……. Electric Field Gradient

FID…….. Free Induction decay

FIR…….. Finite Impulse response

FPGA…….. Field Programmable Gate Array

FT…… Fourier Transform

FFT……..... Fast Fourier Transform

GUI……. Graphical User Interface

IF……. Intermediate Frequency

ISE…….. Instantaneous Square Error

LMS…… Least Mean Square

LUT…… Look Up Table

MOSFET……..... Metal Oxide Semiconductor Field Effect Transistor

MRI……..... Magnetic Resonance Imaging

MSE…… Mean Square Error

NLMS……..... Normalised Least Mean Square

NMR……... Nuclear Magnetic Resonance

NQR …….. Nuclear Quadrupole Resonance

PCI……. Peripheral Component Interconnect

PTFE…….. Poly Tetrafloro Ethylene

RDX……... Research Development Explosive

RF…….. Radio Frequency

RFI……. Radio Frequency Interference

SNR…… Signal To noise ratio

TNT…… Trinitrotoluene

TTL……... Transistor Transistor Logic

USRP……..... Universal Software Radio Peripheral

VHDL…… Hardware Description Language

Chapter 1

1. Introduction

Nuclear Quadrupole Resonance (NQR) is a solid state radio frequency technique that can be used to detect the presence of quadrupolar nuclei existing in several drugs, narcotics and explosives [1]. It provides a unique signature of the material of interest i.e. the set of resonance frequencies is unique to the material. The NQR frequency depends on the electric field gradient (EFG) and the quadrupole moment of the resonant nucleus which further depends on the crystal structure of the solid and chemical components of the molecule. In case of explosive detection, the NQR frequencies are quite specific and are not shared by other nitrogenous materials, where NQR detects ^{14}N of the explosive, without suffering interference from any nitrogen based fertilizer in the soil. NQR is utilized for the application of detecting explosives at airport security, military areas, post offices, government buildings and landmine clearance [2]. It is also used in drug developments for studying and analysing pharmaceutical ingredients, polymorphic forms, drug structures and characterization between the components [3].

Nuclear Magnetic Resonance (NMR) is a RF technique that is able to detect any compound by sensing the excited resonance signals from atomic nuclei having non-zero spin. NQR is similar to NMR but the only difference is NMR needs a DC magnetic field and due to this its application in the field is limited, and therefore most of the NMR-based explosive detection systems are developed for luggage screening. However, unlike NMR, the job of producing the spectroscopic energy levels in NQR is carried out by the crystalline electric field gradient and hence, NQR does not require a static magnetic field. This property makes it

attractive as a non-invasive technique to detect explosives in landmines, drug ingredients chemical compounds [4].

NQR detection is applicable for the quadrupolar nuclei with spin, $I > 1/2$ i.e. the nuclei need to have quadruple moments due to non-spherical shape of its charge distribution. For the application of explosive detection, ^{14}N NQR is a suitable technique as most of the explosive substances are typically rich in ^{14}N nuclei with $I = 1$. The process of NQR detection in various applications is commenced with exciting ^{14}N by using radio frequency (RF) radiation, which is produced by passing RF power through solenoids of series or parallel resonance circuits and the same (or another set of coils as per the convenience) is used for its detection as well. Then, the radiation resulting from the decay of the excited ^{14}N nuclei to their ground state is detected. Since the frequencies of resonance depends on the crystalline and molecular environment of ^{14}N in the explosive, the NQR spectra are unique for a given material and are not influenced by the interference of other nitrogen containing materials during the NQR measurements. Before the advent of plastic explosives (TNT, RDX etc), the explosives contained chlorates as the oxidizing materials. Chlorine-NQR served as a technique for detecting these materials [5].

1.1 Review of NQR spectrometers

Previously, NQR and NMR spectrometers were based on relatively simple oscillator designs such as marginal oscillator and self-limiting oscillator circuit [6]. These were referred as continuous wave (CW) techniques and spectrometers. The CW spectrometer scans through a range of frequencies, which are determined by an LC circuit with sample placed inside or near the coil. With advent of modern electronics, the method of pulsed excitation and detection of NMR / NQR signals have largely improved the stability and efficiency of the spectrometer while simplifying the signal detection circuits. Pulsed NMR spectrometers

utilize a high power pulse (in kW) of RF radiation to excite the magnetized nuclei across the Zeeman energy levels. The tiny RF signal (in range of μV) observed from the nuclei relaxing to the ground state after the excitation stops is called the free induction decay (FID). The frequency is extracted from FID using a Fourier transform (FT) of time based data. A pulsed NMR spectrometer consists of a control console, a magnet and a coil that can be used for transmitting as well as receiving the RF radiation. Only one coil is required as signal reception does not begin until the end of excitation pulse. Many of the pulse techniques began as NMR and have been adapted for NQR as well. While the development of NMR/NQR as a technique itself is significant, the role of advancement in digital electronics in the instrumentation and techniques of NMR cannot be overstated. Since the invention of the original CW NMR, digital signal processing (DSP) and advanced Fourier transform techniques have become an integral part of the modern day pulsed NMR techniques.

NQR shares the same electronics and detection technique except for the presence of magnet. In the place of a magnet, the electric field gradient of the non cubic environment of the quadrupolar nucleus in a crystal creates the necessary splitting of nuclear energy levels to give rise to NQR. So the condition for observing NQR signal is a quadrupolar nucleus in a non cubic site of a crystal. NQR is not only nucleus -specific but also compound –specific, thus making it a tool for detection, quantification and characterization of various chemicals for remote detection of drugs, explosives or quantifying the chemicals in already packed medicines [7][8].

Both NQR and NMR were experimented and explored in a similar time span of late 1940s, where the first experiment showing the NQR phenomenon was performed by Dehmelt and Kruger [9] in 1950. Later, several groups investigated NQR as an explosive detection technique but due to its weak signals (typically micro volts), NMR was mainly deployed as it lead to higher detection accuracy and simple electronic circuit configuration [10]. Nonetheless, as

the NMR cannot be used for field applications due to its size, the NQR gained popularity for mine and explosive detection.

Utilizing NQR technique for detecting nitrogen-containing substances originated in 1960s [11] [12], where several researchers have determined that NQR of nitrogen is a convenient and relatively inexpensive tool for explosive detection. As ^{14}N is the main component of explosives and as ^{14}N NQR transitions in most of the explosives fall in frequency range of 500 kHz to 5 MHz, a pulsed NQR spectrometer system in the same range with Fast Fourier Transform (FFT) capabilities was designed in [13].

NQR spectrometers as detection systems are developed in two aspects, which are hardware configuration and NQR signal processing techniques. The conventional NQR configuration was large and consisted of standalone analog devices. The challenge in the configuration was to reduce the size of the instrument and also detect the weak signals by constructing a specialized sensitive spectrometer system using optimum experimental techniques. To overcome the challenge the mentioned functionalities, the RF signal generator and pulse programmer were replaced from analog components to digital signal processing (DSP) chips [14]. Then, all the digital jobs of NMR spectrometer were performed by field-programable gate array FPGA [15]. FPGA is the most popular technology for implementing prototype and testing new algorithms, due to its reconfigurable feature. The next sections address the detection of ^{14}N signal using NQR based on two main aspects of detection system- hardware configuration and NQR signal post processing techniques.

1.1.1 Hardware Configuration

The NQR spectrometers for detection systems comprises of two functionalities, transmitting and receiving. The function of a transmitter is to provide a high output power (in

kW), the receiver section requires high resolution (display should be in μV scale) for detecting weak NQR signals. Also, the NQR probe must be designed with high sensitivity (Q = 100) to the NQR signal and high rejection to radio frequency interference (RFI).

In a pulsed NQR spectrometer[13] the transmitter and receiver used a heterodyne configuration to eliminate carrier feed through problems present in standard autodyne NQR spectrometers, a sequencer unit was used to select the type of pulses. A single knob tuning and matching network was used for allowing simultaneous tuning of both the transmitter output and receiver input by single control. Versatile pulse sequencer was used for gating of a system which can generate Carr-Purcell, Meiboom-Gill, modified Carr-Purcell, and spin-locked spin-echo sequences, as well as a standard sequence of $\pi/2$ pulses for collection of FID and echo signals. In 1993, Zhu [16] proposed "Detection of Explosives by ^{14}N NQR technique". The researcher constructed a super regenerative NQR spectrometer with a pair of cylindrical solenoid coils. The cylindrical solenoid was made with the bare of copper wire on cylindrical Poly Tetrafloro Ethylene (PTFE) former. The sample of interest was made to move between the coil gaps. The RF power of about 8000 W was available. The signal level was compared with the preset threshold value and if the signal obtained from spectrometer exceeded the preset threshold value, an alarm was activated.

In 1993, Peterson [17] applied modern circuitry and signal processing techniques towards the production of pulsed spectrometer for low frequency (0.5 -10 MHz) NQR. This spectrometer constituted a personal computer containing data acquisition card, an advanced measurement system, a low frequency NQR impedance matching network, a shielded sample coil and oscilloscope. In the proposed technique, the analog information produced by the nuclear resonance was digitized by data acquisition card and processed by computer to produce a Fourier Transform of the resonance. Averaging and other digital signal processing was

performed by the computer. Also, the signal processing scheme of the spectrometer used super heterodyne techniques in both the receiver and transmitter sections.

In 1996, T.N. Rudakov [18] developed a pulsed NQR spectrometer for detection of ^{14}N chemical compounds in the frequency range of 0.5- 10 MHz. The researcher used a master oscillator controlled by personal computer with A/D and D/A converter, a sequencer, a digital phase shifter, a transmitter irradiator consisting of power amplifier and a transmitting and receiving coil system that further consisted of receiving coils, a key and a Q switching device and a preamplifier unit. This instrument has been used to detect large samples (anti-tank mines).

In 1999, Schiano [19] modified the spectrometer [17] that can automatically adjust the pulse parameters in response to observed NQR signals. The novelty of the spectrometer was its ability to change pulse sequence parameters during the progression of the experiment. This feature enabled the use of feedback control algorithm that automatically adjusts the pulse parameters to maximize the signal to noise (SNR) ratio of the detected signal. Both the transmitter and receiver are taken in a single conversion heterodyne system to prevent the coherent interference signals from being produced in receiver during the detection of NQR signal. A matching network transforms the impedance of the transmitter to the high impedance load of parallel combination of the sample coil inductor and tuning capacitor so that the nuclear signals induced in the sample coil are coupled to the high impedance input of receiver. There is a provision of acquisition of both in phase and quadrature components of NQR signal, where a unit digitizes and averages both these components.

In 2007, Ferrari [20] constructed a fully homemade NQR spectrometer in an attempt to gain versatility and possibility of implementing new experiments. The researcher used frequency synthesizer of direct digital synthesis type, which has the ability to produce two independent outputs. The 90^{o} out of phase was used for quadrature detection. Also, a pulse unit

and data acquisition board was replaced by digital signal processor accommodating personal computer.

In 2008, Takeda [15] [21] developed an FPGA-based NMR spectrometer. The researcher built handy and operational NMR spectrometer by combining latest available devices and RF components. The designed spectrometer was capable of giving output of an RF of up to 400 MHz and modulating the amplitude, phase, and frequency of RF irradiation. A part of transmitter and receiver were implemented inside the FPGA. Also, the digital circuits required for NMR spectrometer including pulse programmer, direct digital synthesizer, digital receiver and a PC interface were built inside a single chip of FPGA. It was concluded that by combining FPGA chip with peripheral analog components, a compact laptop sized home built spectrometer was developed which is capable of a RF output up to 400 MHz with amplitude, phase and pulse modulation.

In 2014, Begus [22] designed a low power (5 W) and low frequency (0.5 – 5MHz) pulsed ^{14}N NQR spectrometer based on microelectronic components. The researcher constructed a NQR spectrometer of 2 kg mass using Universal Software Radio Peripheral (USRP) platform, FPGA, high speed A/D and D/A converters (100MSPS) together with lab view software. He considered the cases where ^{14}N NQR line parameters (line width, T_2 ,T_1) allows a longer duration of π pulses. The researcher revealed that the maximal RF power of 5 W is required to excite the nuclei. A notebook PC is needed for communication with this spectrometer and for data acquisition and analysis.

1.1.2 NQR signal post processing techniques

One of the most intimidating drawbacks of NQR is that it is heavily affected by interference more than any other detection techniques. Since NQR signal is often weak, the

SNR is very low (< -60dB), for which rigorous and continuous research is required to develop post processing algorithms for NQR signal processing that are capable of enhancing the detection performance. The challenge for NQR signal detection is to reduce the effect of RFI and to detect the weak NQR signal from background noise.

Several researchers have developed mechanisms to rectify the situation and resolve the issues of SNR. In [23], a feedback algorithm is proposed that automatically adjusts NQR pulse parameters to increase SNR. As NQR provides a means for detecting explosives by revealing the presence of ^{14}N but the distance between the search coil and the explosive, as well as the temperature of the explosive, is unknown. So with fixed pulse parameters it is not possible to increase the SNR. And thus the proposed approach is useful in situations where the optimal pulse parameters cannot be chosen beforehand due to lack of knowledge regarding the system. The proposed feedback algorithm that used measurements of the NQR signal to adjust the pulse width automatically in the strong off-resonant comb sequence to increase the SNR of the NQR measurement.

In [24], the same feedback control methodology was suggested for adjusting pulse parameters, wherein the tuning was applied in the pre-screening stage. In the pre-screening stage, the NQR equipment is placed over a test mine such that the algorithm finds optimal pulse parameters for the explosive material.

NQR is highly effective for landmine detection NQR sensor is not exposed to radio frequency interference (RFI). But strong non-stationary RFI cannot be avoided in the field, a robust detection method is proposed. Using reference antennas, LMS algorithm is applied in frequency domain to cancel the RFI in field data. An average power detector based on power spectral estimation algorithm is also proposed by Y.Tan in [25]. The experimental results showed that the average power detector outperforms the non-adaptive bayesian detector and

can provide robust detection performance by distinguishable features of NQR signals and RFI in the frequency domain.

In the field applications, where the detection system cannot be shielded, NQR has been proved highly effective method if the NQR sensor is not exposed to radio-frequency interference (RFI). However, strong non-Gaussian RFI in the field is unavoidable. A statistical model of such non-Gaussian RFI noise is proposed by Tantum [26]. Also, the asymptotic Cramer–Rao lower bound for estimating a deterministic QR signal in this non-qaussian noise is presented. The performance of several convenient estimators was compared to Cramer–Rao lower bound. Considering the RFI as a colored non-gaussian process, Tantum [27] proposed a two step adaptive kalman filtering to estimate and detect the NQR signal in the post mitigation signal.

Using the least mean square algorithm to suppress RFI with the help of secondary antenna is a major contribution to the design of NQR detection systems. In addition G.Liu [28] claimed that RFI signals collected by the main NQR probe and secondary antenna array are not only spatially but also temporally correlated. The researchers proposed several methods, i.e. alternating least squares (ALS) for RFI suppression [29]. The advantage of this method is that both spatial and temporal information of collected RFI signals from antenna array is utilized.

Stegana, [29] investigated several detection algorithms for NQR signals which included bayesian method, matched filter and maximum entropy method. The Bayesian method was the most robust method against noise, however it requires prior information. The performance of matched filter and maximum entropy method degrades as SNR decreases. In addition, the maximum entropy method is found to be most computationally intensive method among the other three methods.

The current techniques only measure the response of a known resonance frequency i.e it is assumed that with knowledge of the sample temperature, the most dominating resonance

frequency is exactly known. But the sample temperature may be within 5 degrees (K) accuracy, the author [30] included the estimate for a sample with 5 degrees offset, compared the performance gain of the detectors as the gain factor between the detection thresholds for a sample containing TNT and for one without TNT, as a function of the measured echo number. By exploiting the temperature dependency of NQR frequencies, Jacobson [31] developed several methods, which are non-linear square method and an approximate maximum likelihood detector to enhance SNR and improve NQR signal detection performance.

S.D Somasundaram [32] presents an NQR signal model, which is further exploited for detection algorithm development. In the traditional detection algorithm, NQR signal segments are captured after the stimulus pulses, wherein one pulse sequence are averaged to produce one NQR signal segment with high SNR, thus to improve the accuracy of decision. On the contrary, Somasundaram proposed to utilize the captured NQR signal segment as sequence of detection, instead of averaging them to produce one segment. In this way, the decaying characteristic of each NQR signals segment can be used. In [33],[34],[35] the authors proposed to refine generalized maximum-likelihood ratio test methods and then used these methods to work on a serial NQR signal sequence. In [36], this approach is further improved to deal with the stochastic NQR (sNQR), where author proposes acquiring signal of interest free samples, having only corrupted signals, and using them to reduce the effects of RFI on conventional NQR measurements. Here author has shown that the sNQR detectors performed well as compared to conventional NQR detectors. In [37], the authors have presented a method where NQR probe is utilized for RFI mitigation. The data are also collected before or after the real detection without the presence of stimulus RF pulses. These data contain only RFI signals, not the NQR signals. Then, NQR signal data are captured during RF pulse sequence, which contains both NQR signal and RFI. The RFI signals in these two different data sets have

temporal correlation. Thus, the signal of interest data can be subtracted from NQR signal to remove RFI.

An adaptive noise cancellation method has been used by Tantum et al [38] to reduce the RFIs for NQR signals. It is reported that by using least mean square algorithm the adaptive noise cancellation method can reduce RFIs by more than 50 dB. However, this method may amplify the white noise and it may suffer from signal cancellation due to minimizing the total output power. Therefore, a challenge in NQR signal detection is to mitigate the impact of RFI and identify the poor NQR signal from the external noise.

Also, in NQR spectrometers, the uncertain amplitude has been observed to be a potential hindrance of detecting signals in an accurate manner. For this purpose, several post processing algorithms for NQR signal processing have been developed, as mentioned in the previous section, yet they lack in terms of detection performance. From the review of NQR signal post processing techniques, it is evident that to fulfill this complicated detection system must be equipped with a versatile computation platform.

1.2 Contributions and Thesis Outline

In view of the aforementioned limitations of current NQR detection systems, an FPGA based pulsed NQR spectrometer is proposed in this work. FPGA is used to perform the entire digital task required for spectrometer such as Pulse Programmer, DDS, Digital Receiver composed of quadrature demodulator, a low pass FIR filter and data acquisition. Also, the analog peripheral components such as pre-amplifier, cross diodes and quarter wave transformer (used for isolation of transmitter and receiver) and Probe (Coil designing along with resonance circuits) were designed and developed as part of this thesis.

In the field, the time of detection is the important parameter. The quantities that limit time of detection mainly are the SNR and the relaxation time of the material. The latter being

the property of the material, it severely limits the rate at which the signal can be acquired. The only option to improve the SNR is by improving the signal detection technique. To improve SNR per unit time several other techniques have been used i.e. FIR filter, wavelet transform and adaptive filter. FIR filter is generally based on prior knowledge of spin echo. Wavelet transform is not suitable due to computational complexity. Adaptive filter algorithms are used in this work as these do not need prior knowledge of the signal and also the parameters of adaptive filter, changes to meet the optimization parameters. The detailed discussions of the contributions are presented in rest of the chapters.

Second chapter is NQR background which presents the principles of NMR and NQR. Apart from these this section also focuses on NQR signal model.

Third chapter is the NMR/NQR detection system which presents traditional NQR system design, NMR/NQR probe, sensitivity of NQR detection, radio frequency interference and NQR signal processing. Finally an overview of developed FPGA based pulsed ^{14}N NQR spectrometer is presented.

Fourth chapter is the Implementation of spectrometer which illustrates the design and implementation of the NMR/NQR spectrometer. All the components of the developed system are explained.

Fifth chapter is the results chapter that presents the experimental results of the NMR/NQR spectrometer. It elaborates on the NMR and NQR signal detection system and its performance.

Sixth chapter is Post processing of NQR signals that presents the results of the NMR/NQR spectrometer concerned with the post processing of NQR signals. It elaborates on the adaptive filters and wavelet transforms , adaptive noise cancellation, adaptive line enhancer, adaptive filter structure, related algorithms and system performance. It further presents the simulation results of the proposed technique.

Seventh chapter is Summary and Future work which is last chapter that explains about the summary of outcomes obtained through the results section as well as provides conclusion to the research followed by best strategies to be adopted for further explosive detection with NQR/NMR spectrometer with specific reference to FPGA and signal processing in an effective way.

Chapter 2

Nuclear Resonance Spectroscopy

Originally conceptualized and observed by I. I. Rabi [39], technology of NMR developed in instrumentation and theory along with the development of RF technology during the world war and later commercial instruments for observation of NMR and Magnetic Resonance Imaging (MRI) were available for various companies. NQR however remained as a specialized field and the development in this field was limited to specialized applications like mine and drug detection. The theoretical development in NMR is very advanced to the extent that NMR devices are being developed for quantum computing purposes [40].

2.1 NQR Theory

This section describes the basic principle behind NMR/NQR and elementary detection techniques used for observing signal.

2.1.1 Principles of NMR

Most of the atomic nuclei possess a non zero spin. Given in the table given below are the information on the origin and value of spin observed in various nuclei.

Table 2.1 Spin of Nuclei

Mass number	Atomic Number	Spin	Example
Even	Even	0	^{4}He,^{12}C,^{16}O
Odd	Odd	1/2,3/2,5/2(Half Integer)	^{1}H,^{15}N
Even	Odd	1,2,3(Integer)	^{2}H,^{14}N

These tiny magnets, when placed in a uniform magnetic field (B_o), orient in $2I + 1$ directions with respect to B_o. This is known as the Zeeman Effect.

For nucleus with spin $I = 1/2$ (e.g. ^{1}H, ^{13}C, ^{15}N, ^{19}F, and ^{31}P), $2I + 1$ is = 2 states. Thus, whenever the nuclei are in a magnetic field, a nucleus with spin =1/2 can be in one of the two states. These two states correspond to the orientation of spin in the direction and opposite to the direction of the applied field. The energy of the parallel orientation is less than energy of the anti-parallel orientation. The transition of the nuclei from one orientation to the other can be achieved by applying electromagnetic (EM) radiation of energy (hυ), which is equal to the energy difference of the two orientations., Here h is the Planck's constant and υ is the frequency of EM radiation.

The magnetization of the sample nuclei is the sum of all the individual nuclear magnetic moments (spins). There is a slight excess of nuclei oriented with the magnetic field, i.e. in the lower energy state, such that the sum will yield a magnetization (M) along the positive z-axis. It is noteworthy that the total magnetization and not the magnetic moment of an individual nucleus which determines an NMR signal.

Classically, the magnetic moment of a spinning nucleus precesses with a characteristic angular frequency, which is called Larmor frequency. (Fig 2.1)

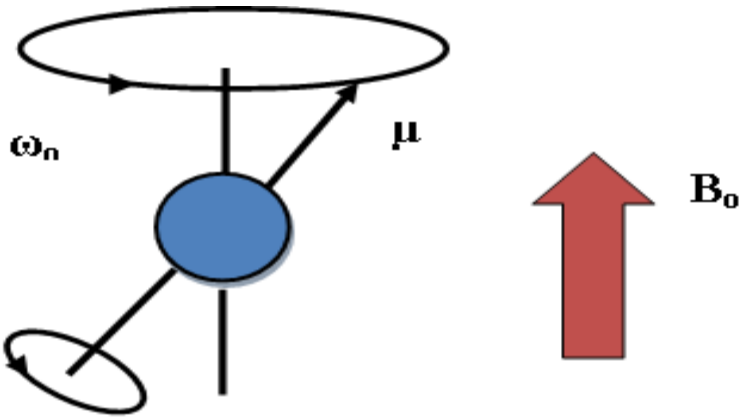

Fig 2.1 Nuclei placed in Magnetic Field B_o (classical picture)

Larmor frequency is given by:

$$\omega_o = \gamma Bo \qquad [2.1]$$

where γ is gyro magnetic ratio and B_o is applied magnetic field.

In relation to quantum mechanics, the $2I + 1$ orientation determines that a nucleus magnetic moment taken against an external magnetic field is not of equal energies. The Hydrogen nucleus (proton) has a spin $I = 1/2$ and its magnetic quantum number (m_I) can take values $\pm 1/2$ and therefore results in two possible orientations. The two orientations have corresponding energies $\mp\frac{1}{2}\gamma(\frac{h}{2\pi})B_0$, which results in energy difference (Fig 2.2) of:

$$\Delta E = \gamma\left(\frac{h}{2\pi}\right)B_0 \qquad [2.2]$$

where h is Planck's constant (6.63 x 10^{-27} erg sec). Replacing $\Delta E = h\upsilon$, we get the resonance condition $\omega_o = \gamma Bo$

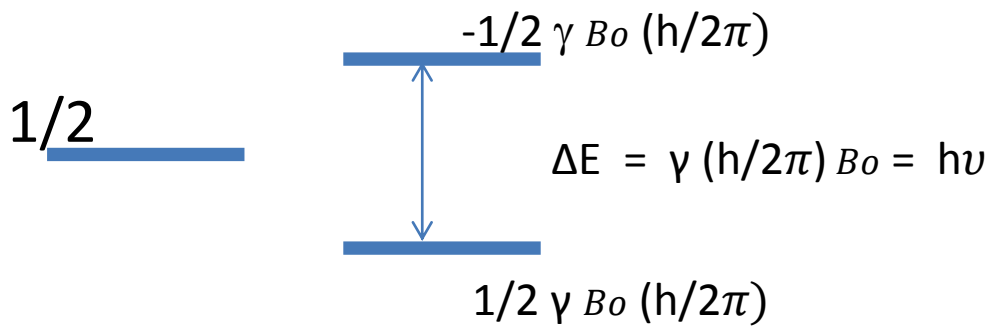

Fig 2.2 Energy level diagram for nuclei of spin I = ½.

From Macroscopic view, the NMR phenomenon can be explained as shown in Fig 2.3 and 2.4 [6]. As demonstrated in the figure, the addition of all unevenly distributed magnetic moments results to net Magnetization (M). At thermal equilibrium, in the presence of large static field B_o, M aligns with B_o. This is shown in Fig 2.3. When M is perturbed from

alignment with B_o, it exhibits precessional motion about the axis B_o , which is generally in z direction.

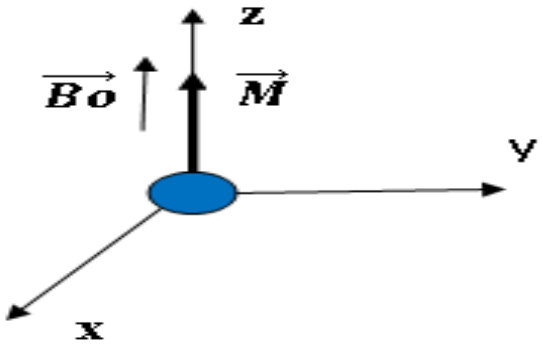

Fig 2.3 Classical picture of nucleus in static field B_o

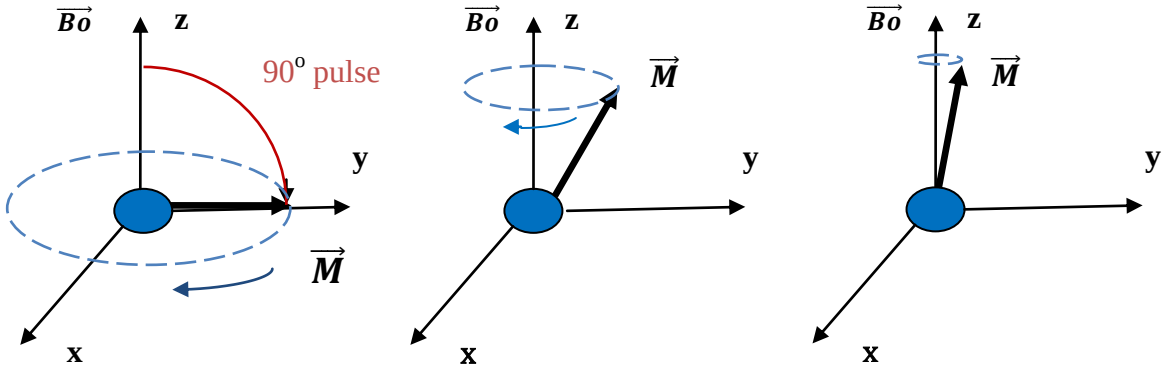

Fig 2.4 Precession of Magnetization after 90° pulse

The magnetization vector can be decomposed into transverse component M_{xy} and longitudinal component M_z. At thermal equilibrium M is aligned with B_o thus $M_z=M_{eq}$, M_{xy} = 0 and precession is not visible. However when another magnetic field that is orthogonal to B_o perturbs M from equilibrium, M_{xy} is non-zero and precession can be observed. Precession is most obvious when M is perturbed 90° from B_o as shown in Fig 2.4 a). After the Magnetization is perturbed from equilibrium it begins to realign with Bo while it is precessing (Fig 2.4 b and Fig 2.4 c). This process is called relaxation, which induces an RF signal oscillating at the NMR frequency which can be picked up by nearby coil.

2.1.2 Principles of NQR

The NQR working principles are similar to those of NMR. The only difference is in the interaction between nuclear magnetic moment and the external magnetic field, where unlike NMR, NQR exploits the interaction between the electric quadrupole moment of nucleus and EFG that surrounds the nucleus. Therefore, NQR does not require an external magnetic field. Atomic nuclei with spin I > 1/2, such as ^{14}N (I = 1), ^{17}O (I = 5/2), ^{35}Cl (I = 3/2), ^{63}Cu(I=3/2) possess a non spherical charge distribution (shape) and hence a quadrupole moment. In NQR, the electric quadrupole moment (denoted by **Q**) interacts with EFG of the non-cubic crystal site which, much like the Zeeman Effect of NMR, results in the energy splitting of the nucleus, depend on its orientation with respect to EFG. This quadrupole moment is associated with the non-spherical charge distribution. The $2I + 1$ energy levels for nuclei (spin =1) (Fig 2.5) having quadrupole moment are given by:

$$E_o = -\frac{2}{3}\, hv_Q \qquad\qquad E_{\pm} = (1 \pm \eta)h\frac{v_Q}{3} \qquad [2.3]$$

All the three possible transition frequencies are:

$$v_o = \frac{2}{3}\,\eta v_Q \quad , \qquad v_{\pm} = (1 \pm \frac{\eta}{3})v_Q \qquad [2.4]$$

Where, $$v_Q = \frac{3e^2qQ}{4h} \qquad [2.5]$$

Where, $\frac{e^2qQ}{h}$ represents the nuclear quadrupole interaction between **Q** and EFG. Also, η is asymmetry parameter of EFG [11].

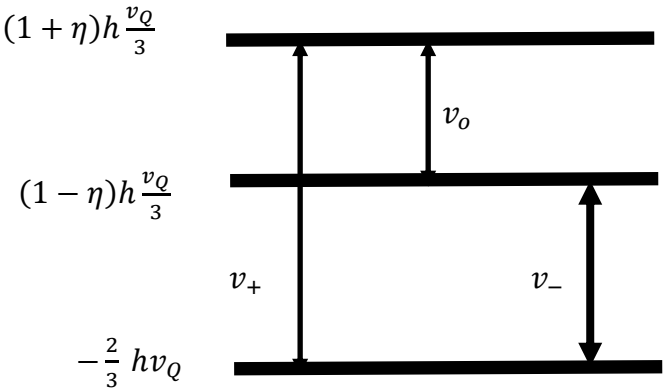

Fig 2.5 Energy splitting and resonance frequencies for spin I = 1 nuclei.

The three frequencies (Fig. 2.5) are well separated and can be excited and observed individually. These frequencies are proportional to principal values of EFG tensor around the nuclei, which further depends on factors such as bonding, valence electrons etc. Some of the materials containing nitrogen have multiple molecules on crystal lattice. Each of these molecules may have several ^{14}N nuclei that experience different local EFGs, where the different NQR frequencies are determined by its chemical structure. Thus, NQR signal is unique for each type of materials [41]. Additionally, the ^{14}N NQR transitions in various solids including some of the explosives fall in the frequency range 500 kHz to 6 MHz.

For the detection of materials containing ^{14}N, one of the resonance frequencies that carry the strongest energy is captured and regarded as the feature frequency of the sample material. However, in real time, due to imperfections in crystal lattice, the actual NQR signal has a line width. The energy absorbed by the nuclear spins induces a voltage that can be detected by a suitably tuned coil, amplified to the level of observation on an oscilloscope.

As explained for NMR, NQR detection can be explained by irradiation and precession of ^{14}N spins. Before the application of RF pulse, the ^{14}N spins are along reference axis. The RF pulse is high power pulse (in kW) at resonance frequency. The width of RF pulse is denoted by $\boldsymbol{\tau}$. This RF pulse is applied to a coil that contains the sample to induce an oscillating magnetic field (B_1). The magnetic field tilts the ^{14}N spins from the reference axis

by an angle θ, which depends on the power and duration of RF pulse.

$$\theta = \gamma B_1 \boldsymbol{\tau} \qquad [2.6]$$

The power requirements of the RF transmitter used in an NMR /NQR experiment depend not only on γ of the nucleus but also on the sample coil geometry. It has been shown that B_1 power in the sample coil is given by [42].

$$B_1 = 3(PQ/v_o V)^{1/2} \qquad [2.7]$$

Where P is transmitter power in watts; Q is the quality factor of the probe, $v_o$is resonance frequency in MHz and V is the volume of the sample coil in cm^3.

During the process where the ^{14}N spins precess back to the equilibrium state, a decaying RF signal, called FID signal, is emitted and can be detected. The time constant by which nuclear spin systems returns back to the equilibrium state is called spin –lattice relaxation time (T_1). As the NQR signal has narrow band spectrum, the NQR frequencies of the ^{14}N nuclei will be slightly different from the ideal values.

When ^{14}N spins precess after the RF pulse is applied, the small frequency difference from different spins lead to phase differences between the signals, due to which they add up incoherently and cancel out. This occurs before the spins return to the equilibrium state. The time constant for FID decay is denoted by T_2^*, which is affected by the molecular structure and current condition of the sample. Therefore, even for the same material, T_2^* may vary from sample to sample. The strength of FID signal depends on the flip angle θ. Highest NQR signal is achieved when $\theta = \pi/2$ thus, the pulse width that results to maximum FID signal power is referred as $\pi/2$ pulse width. The FID signal induced by one excitation of RF pulse is weak (μV) and thus, the SNR of the signal is low to make an accurate detection. Thus, most of the NQR detection systems perform the detection by repeating the detection cycle. Also the

NQR FIDs are acquired in time intervals between the RF pulses. The numbers of NQR FIDs are averaged to increase the SNR such that the detection accuracy can be improved. The nuclei has to begin with equilibrium state for each individual detection cycle, for this reason, the spacing between the pulses (t_{gap}) should be longer than $5T_1$ to guarantee this initial condition.

The other type of NQR signal that can be generated is called spin echo. It requires two RF pulses with different phases to produce an echo signal. FID and spin echo signals are shown in Fig 2.6. The mechanism of generating echo signals can simply be interpreted as refocusing the out of phase FIDs.

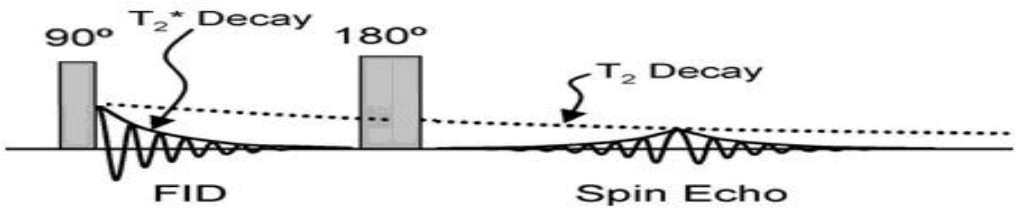

Fig 2.6. FID and Spin Echo in time domain.

After application of first 90^o RF pulse, an FID is generated. As the ^{14}N spins have slightly different NQR frequencies, the spins are soon out of phase and resultant NQR FID decays at a faster speed. Then a second 180^o RF pulse is applied after a spacing of t_1. Thus, all out of phase ^{14}N spins are flipped by 180^o which makes the spins start to precess in opposite direction. Hence, the spins are refocused at time t_1 after second pulse and spin echo is radiated. Formation of spin echo in NQR is similar to its formation in NMR which is shown in Fig 2.7.

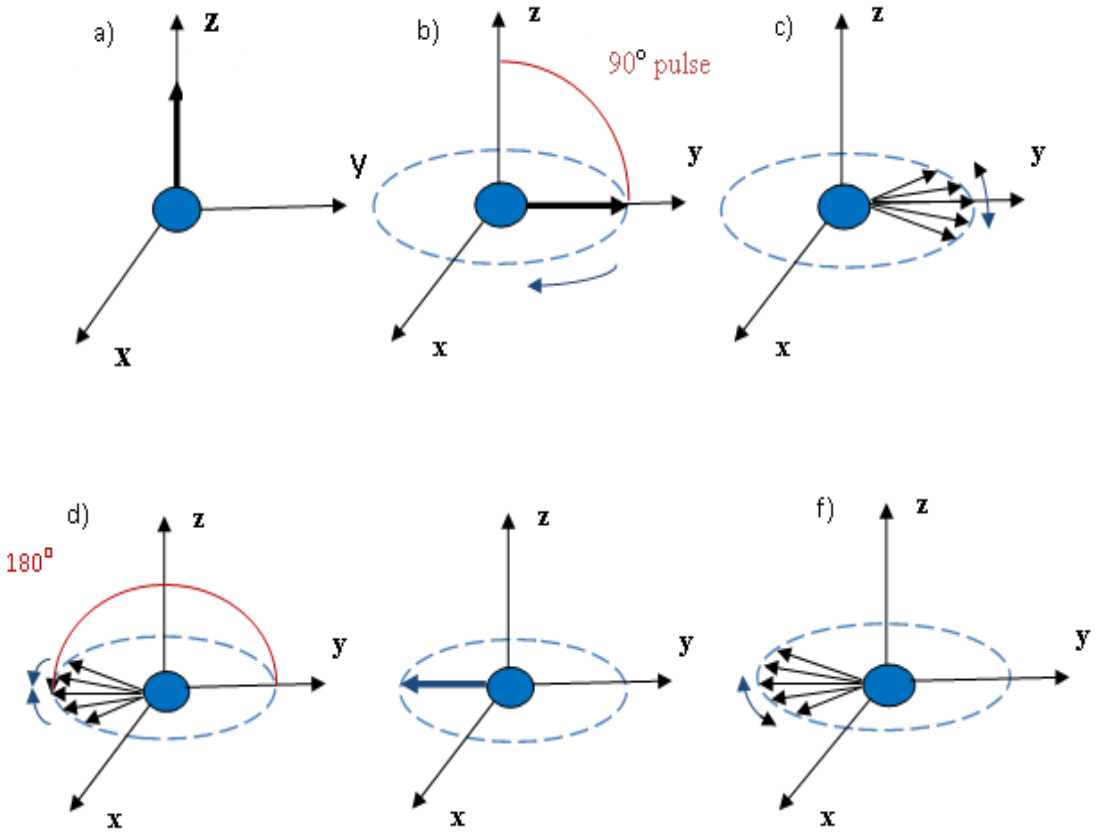

Fig 2.7 The Status of magnetic moments during spin echo generation

Fig 2.7 illustrates the formation of spin echo from magnetic dipole moments view. In the beginning, the Magnetization M is at its equilibrium state (in the direction of external magnetic field) shown in (a). After the pulse width τ_1 it rotates with angle of 90^0as shown in b) and then these spins start to dephase immediately as some precess faster, and some slower, than the average as shown in Fig c). As the spins move further out of phase with each other they don't add together as effectively and the sum of all the spins starts to decrease (or "decay"). Application of 180^o pulse flips the spins in the transverse plane. The spin phases are reversed, the faster ones and slower ones have flipped their positions (Fig d). From this new starting point the spins continue to precess at their individual rates. As the spins continue to precess they are now rephasing instead of dephasing. After rephasing for a time t_1 (same as dephasing time), an echo forms (Fig e). The Echo signal is named as Hahn echo to honour Edwin Echo, who first demonstrated the echo signals in NMR experiments [43].

2.2 NQR Signal Model

As discussed in previous sections there are two popular methods of observing NQR signals i.e. observing FID using a single pulse excitation and observing spin echo using a double pulse sequence. The choice of the sequence depends mainly on $\boldsymbol{T_2^*}$ of the sample material. For a long relaxation time of milliseconds, as in the case for ^{14}N signal from $NaNO_2$, a single pulse sequence is appropriate. Depending on the detection environments and experimental setup, the noise and interference may corrupt the NQR signals. Thus, the noise corrupted FID signal $\boldsymbol{X_o}$ is modeled as linear combination of signal $\boldsymbol{S_o}$ with strength $\boldsymbol{A}$ and background noise $\boldsymbol{W_o}$ as shown in equation no.2.7 [44]:

$$X_o(t) = AS_o(t) + W_o(t) \qquad [2.7]$$

Where, $X_o(t)$ is the NQR response signal, $W_o(t)$ is the background noise, which is assumed to be Gaussian random process with mean value zero. The pure FID signal $S_o(t)$ is modeled as:

$$S_o(t) = e^{\frac{-t}{T_2^*}} \cos(2 * pi * fc * t) \qquad [2.8]$$

Where, T_2^* denotes decay time constant and f_c denotes the difference between FID frequency and reference frequency. The reference frequency is the frequency of RF excitation pulse, which may vary slightly from FID frequency.

The FID signal model is fairly simple and straightforward to understand. The echo signal sequence, however, is very complicated to model as it results from two RF pulses and comprises of multiple decaying factors. An NQR echo signal sequence induced by RF excitation pulse sequence can be represented by:

$$S_o(t) = \cos(2 * pi * fc * t)\, e^{\left(-\frac{abs(t-\boldsymbol{t_1})}{T_2^*}\right)} e^{-\frac{t}{T_t}} \quad [2.9]$$

Where, T_t , T_2^* denotes echo train decay constant, and sinusoidal damping constant.

Also, $\boldsymbol{t_1}$ is the time interval between the first and second pulse.

2.3 Summary

This chapter provides a brief introduction to the NMR and NQR techniques by comprehensively emphasizing on the principles of both the techniques. The NMR utilizes the interaction between the nuclear magnetic moment and external magnetic field, while NQR exploits the interaction between electrical quadrupole moment of the nucleus and electric field gradient that surrounds the nucleus. Thus, the advantage of the NQR over NMR is that NQR does not require the presence of an external magnetic field.

The detection of explosive detection via NQR is based on the presence of nitrogen ^{14}N, as all explosives contain nitrogen. As the frequencies of the nitrogen nuclei contained in explosives and other materials are different, explosives can be efficiently and uniquely identified by ^{14}N NQR frequency. For these types of materials, the excitation by an applied RF pulse will lead to the transmission of ^{14}N spins from equilibrium state to an excited state. After the RF pulse, the spins precess back to equilibrium state and thus emit NQR signals. These signals can be captured by the coil. As the SNR of NQR signals are weak (< -60dB), an RF pulse sequence might be used instead of single RF pulse to improve the SNR. There are two types of NQR signals that can be captured during detection, FID and echo signals.

Chapter 3

NMR/NQR Detection System

Original NQR systems are continuous wave systems where the nuclei are continuously excited with low power (in Watts) frequency scanned RF signal. The impedance variation observed due to the resonance served as the signal. The continuous wave spectrometers are not in use any more hence it is not being discussed here. The Pulsed technique uses short pulses (μs) of intense RF and observes the FID or the spin echo. In this chapter configurations of pulsed spectrometers are discussed. The author further proposes an FPGA based pulsed ^{14}N NQR spectrometer.

3.1 Pulsed NQR System Design Requirements

An NQR system, in general, is composed of four modules, namely, transmitter module, probe module, receiver module and computer control module. The transmitter section is designed to excite the nuclei using a high power (kW) RF pulse; hence it is comprises of an RF source, a pulse programmer and a power amplifier. The receiver section is designed to receive weak signal (μV) following the strong excitation and it comprises of a preamplifier, detectors, and filters. The computer control could produce the required pulse sequence for excitation of nuclei; however it is designed to acquire, digitize, store and process the data. In highly sophisticated commercial systems the computer control module runs the entire process.

3.1.1 Transmitter Section

The transmitter consists of RF signal generator of sinusoidal frequency and amplifiers to boost the RF signals to the desired level (typically 1 kW). For pulsed NMR/NQR, the irradiation must be modulated into pulses. For this purpose, the simplest scheme is to have an oscillator which works at low voltage level (typically TTL) that can be switched on and off. However a more common scheme used in pulsed NMR/NQR is gating continuous RF signal with TTL logic pulses using the amplitude modulation technique. This low voltage signal is then amplified by the power amplifier to generate the high power excitation signal.

While the transmitter delivers high power (kW) signals to NQR probe during the excitation period, a switch is needed to isolate the sensitive receiver from the high voltage. During the receiving period, the switch connects the receiver to the probe and disconnects the transmitter section. Since NQR signals are extremely weak (of the order of μV), the switch needs to have low signal attenuation while it is connecting the probe to the receiver section. Also, the switch should have a fast (a few μs) switching capability for collecting FID signals.

Programmability is another property that enables the successful detection of FID or echo. To adapt the RF pulses to various samples, the parameters of RF pulses such as pulse width, gap between two pulses, and frequency and amplitude of the RF signal must be programmable.

3.1.2 NMR/NQR Probe

The job of an NQR probe is twofold. It is required to produce the RF magnetic field that is sufficiently strong to excite the nuclei and required to be sensitive enough to detect the weak signal after the excitation is complete. The most suitable probe circuit for this purpose is the tuned LCR tank circuit. The Fig 3.1 shows series and parallel tank circuits that can be used for this purpose. Since in the tuned condition, the tank circuits have extreme impedances (zero or

infinity theoretically), the transfer of power into the coil as well as transfer of signal from the coil require additional components that could match the impedance of these circuit to the output/input impedances of the amplifiers. This is typically achieved by making use of standard impedance configuration for the components in the circuit and matching the probe impedance to that value. The author has used 50 Ohm components where as 75 Ohm standard configurations are also available commercially.

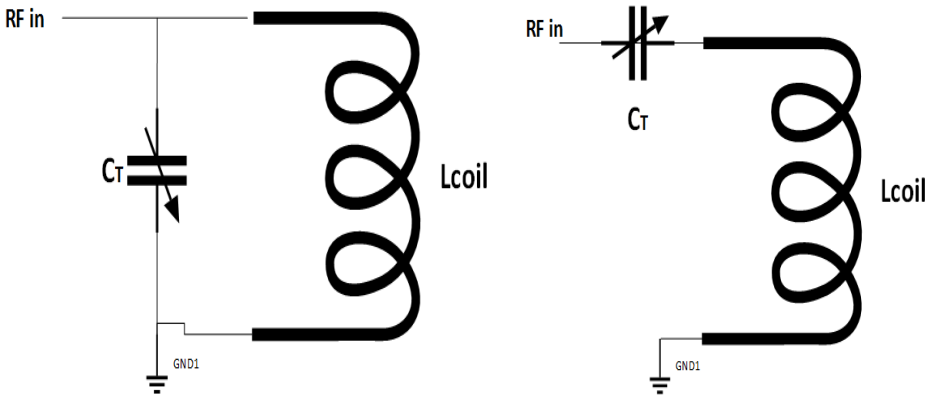

Fig 3.1 The parallel and series LC probe.

The Q factor of the tank circuit plays an important role in amplifying the exciting signal further. However this is both a boon and a bane as the voltages in the coil could easily go beyond the breakdown voltages of the various components of the circuit and result in breakdown or sparking etc. So the probe needs to have a good insulation and need to use components with high voltage ratings wherever required. A coil always has a resistance associated with it and the same serves as a damping to the Q of the circuit. One may add additional resistances to the circuit in order to further dampen the Q or for the purposes of matching the impedance of the probe with rest of the electronics. The high Q is also associated with a long recover time (ringing) of the probe. Additional circuitry can be used in such case to switch the Q to dampen the ringing [45].

In most of the modern circuits, a single coil is used for both excitation of the nuclei and detection of signals. This poses some stringent requirement of the probes and additional circuitry to isolate the excitation and detection circuits.

In some of the designs [46] [18], the transmitter and receiver coils are different, which simplifies the electronics and also makes it easier to optimize the independent requirements of both transmitter and receiver. However, mechanically, the cross coil arrangement is more complicated than the single coil system because a larger volume is required in the crossed coil arrangement. Moreover isolating the transformer coupling between the excitation coil and the receiving coil could be quite a challenge.

Several designs have been proposed for NQR coil. For lab designed spectrometers, a simple solenoid is often employed, where the sample under study is placed inside the coil that enables the effective utilization of the magnetic fields. For field applications requiring the detection of chemical compounds, a flat pattern coil is often used. There are also some coil designs that provide more robust interference rejection [47]. In order to make the receiver configuration simpler, it is observed that the parallel tank circuit is more desirable for an NQR probe.

3.1.3 Receiver Section

The receiver section should provide the amplification of the weak NMR/NQR signal(μV) with minimum degradation and distortion. It should also be able to detect the RF signals for display and measurement. The total gain required in NMR/NQR receiver is typically between 60-100 dB. The NMR/NQR frequency is amplified by about 20-30 dB and then converted to a fixed intermediate frequency (IF) by mixing with a local oscillator frequency derived from the transmitter. This provides a more stable receiver and allows most of the amplification at the fixed frequency.

For pulse application, it is necessary to deactivate the receiver during transmitter pulses to prevent overload and subsequently avoid slow recovery for gaining optimum performance, which can be achieved using RF switch as discussed in section 3.1.1.

The output of the mixer contains both the sum and difference frequencies of the two inputs, only one of which is at the desired frequency. The unwanted frequency is easily rejected by limiting the bandwidth at the following receiver stages.

3.1.3.1 Sensitivity of NQR Detection

The RF signal resulting from the nuclear precession is extremely weak; the voltage signals picked up by the NQR probe are of the order of μV. The signal strength is at the same power level as the thermal noise in the NQR coil. Hence, the major concern in the NQR detection system design is the low SNR.

Fig 3.2 demonstrates the traditional NQR probe, where L_{coil} is the inductance of NQR coil. For this type of NQR probe, a power matching network is usually used to form the input impedance of 50Ω, which further matches the output impedance of driving power amplifier in transmitter section with receiving signal amplifier in receiver section. The power matching scheme is referred as 50Ω power matching network.

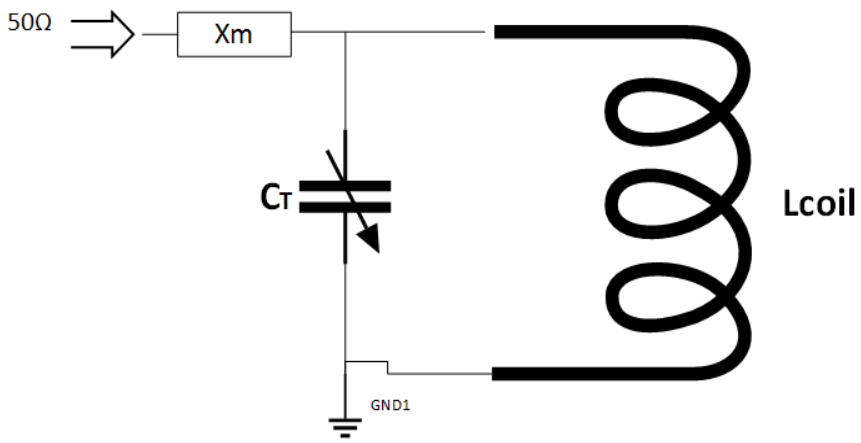

Fig 3.2 The NQR probe with 50Ω matching network

The NQR voltage signal is proportional to quality factor Q of the NQR coil, thus a high Q value (100) is desired during the excitation and detection period, but just after excitation pulse Q has to be low to reduce the ringing time of probe. That can be done through Q damping circuit to switch Q to a low value during the emergence of ringing. After the ringing suppression, the Q value can be shifted to the higher value.

The thermal noise of the NQR probe is the main contributor of noise. The thermal noise for NQR probe is given by:

$$\sqrt{V_n^2} = \sqrt{4kTR_oB} \qquad [3.1]$$

where B is the bandwidth of the NQR signal and k is the boltzman constant.

In this case, the Signal (V_s) to noise (V_n) ratio (SNR) is defined as $\frac{V_s}{\sqrt{V_n^2}}$

In realistic detection systems, the pre–amplifiers in detection stage also contribute to the noise power. The noise factor of detection system is defined as the ratio of total output noise power of the system to the portion of output noise generated due to the input noise power. As the noise factor is mainly constrained by the first amplifier stage, a low noise amplifier is desired to amplify the NQR signals initially.

Another method to improve the SNR is to average the signal obtained over many detection cycles. Signal being coherent adds up linearly while the incoherent noise adds only as the square root of the number of cycles averaged. Hence, if n signal cycles are added, the noise voltage goes up by $\sqrt{n}$ while NQR signal voltage goes up by n .Thus, the SNR (voltage) is increased $\sqrt{n}$-fold.

3.1.3.2 Radio Frequency Interference

As the NQR signals are inherently weak (μV), they are vulnerable to RFI from other sources as well. The interfering sources may include electrical equipment, power lines and most severely, commercial and amateur radio stations. Depending on the distance from the interfering source, they can be divided into two categories, i.e., Far field RFI and near field RFI. Commercial AM radios whose frequencies range from 500 kHz-1.5 MHz are the biggest far field RFI sources, which are mostly uniformly distributed. On the contrary, the near field RFI is generated from the source close to test equipment. It can also come from NQR test equipment itself. If no precaution is taken, the ratio of NQR signal to RFI power can be as low as -60dB [1]. So far, the most effective method for rejecting RFI is shielding.

For lab testing and stationary security screeners, shielding the testing sample and the detection system is feasible. But for field applications such as landmine detection, the targets cannot be enclosed.

There is another RFI cancelling method, where one or more multiple auxiliary probes (RFI probes) are employed, dedicated to picking up RFI. Whereas, RFI can be picked up by both the RFI probe and NQR probe, the NQR signals can only be sensed by NQR probe. The RFI captured by RFI probes is subtracted from the signals captured by NQR probe such that the RFI portion is suppressed, and the NQR signal is left for detection. The assumption made is that the RFI probes can only pick up RFI and not the NQR signals. This is possible if RFI probes are positioned far enough from the NQR test sample such that the NQR signals vanish to a much lower level than the noise power level [25]. Another assumption is that the RFI signals on the NQR probe and RFI probes are correlated.

3.1.3.3 NQR signal post processing

The SNR of NQR measurements is determined by both the statistical properties of the noise and selection of pulse sequence parameters. The standard approach of improving the SNR uses multi-pulse sequence that facilitates coherent signal averaging [48]. The other method includes correlation detection [49] and matched filter [50]. The key point of both methods is that the interference and noise generated are eliminated through the commencement of correlation processing between the acquisition NQR signal and the local signal of the same frequency. Nonetheless, these methods have limitations due to phase and intensity uncertainties in the NQR signal. They also meet difficulties in accurate measurements of the temperature in the environment. Also, traditionally, the signal is first demodulated with the known NQR frequency, and then digitized. However, to avoid the loss of information, direct digitization without demodulation is preferable.

From hardware perspective, direct digitization without demodulation requires a much higher sampling frequency. With the advancement of ADC circuits, the NQR signals which range from 0.5 – 6 MHz can be oversampled with a high resolution (100 MHz) to preserve more useful information. Based on this hardware development, more advanced signal processing techniques are proposed (discussed in Chapter 1).

3.2. Proposed FPGA based NMR/NQR Spectrometer

Many NQR based detection systems have been proposed since the NQR phenomenon was first demonstrated in 1950's. Depending on the different applications there have been various ways to build the system. No matter what configuration is adopted, the detection system has to meet general requirements. The traditional NQR system configuration was large and consisted of standalone analog devices. The challenge in the configuration was to reduce the size of the instrument and also to detect the weak signals by constructing a

specialized sensitive spectrometer system using optimum experimental techniques. Therefore, the goal of this work is to develop a FPGA based ^{14}N NQR spectrometer, so as to overcome some of the limitations of the existing techniques. NQR provides a noninvasive means of detection by revealing the presence of ^{14}N. In order to bring new ideas into practice, it is often necessary to make some modifications to the hardware inside the spectrometer which cannot be done in commercial spectrometers. Since NMR/NQR is a field in which progress has never declined and is likely to grow in future also, it is better to build a new spectrometer.

The key strategy for developing this spectrometer is to fully exploit a FPGA as FPGA chip is composed of large number of programmable logic gates, in which digital circuits can be built with hardware description languages such as VHDL and verilog. FPGA circuits can be reused after their development as per the requirement. Individual circuits in FPGA run concurrently with reconfigurable capability. FPGA can realize any digital circuits with limitations set by the available number of logic elements and the operation speed. The proposed FPGA based spectrometer employs a single FPGA, which performs all the digital jobs required for NMR/NQR spectrometer including pulse programmer, direct digital synthesizer (DDS), digital receiver composed of quadrature demodulator and a low pass filter and PC interface for data transfer. The block diagram of proposed spectrometer is shown in Fig 3.3.

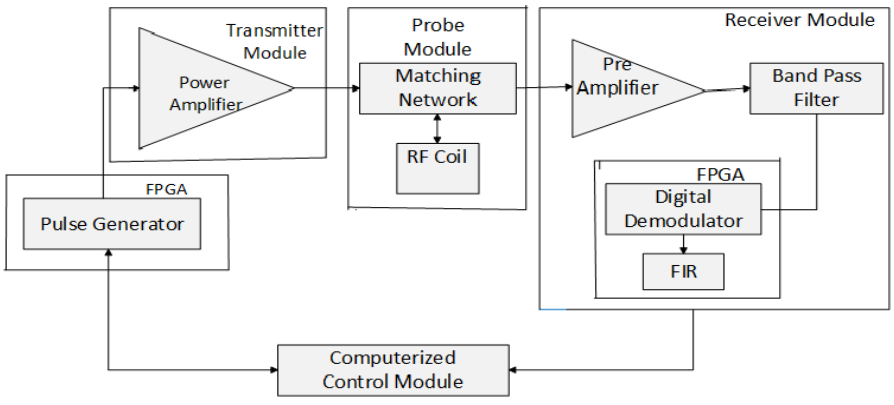

Fig 3.3 Block Diagram of Proposed FPGA based NQR spectrometer.

Thus, the proposed FPGA based NQR instrument is designed using a digital technique which includes a FPGA chip, ADCs, and DACs. With the field programmability, the digital part of an NQR instrument could be constructed with FPGA resulting in a compact and completely programmable NQR instrument with high sensitivity (detect in range of μV) and suitability for applications such as mine detection, noninvasive compound identification etc. Moreover, by adding a permanent magnet of uniform field, one could carry out NMR as well which can be a useful tool for quantitative analysis of trace elements such as Proton, Tritium, and Deuterium etc.

3.3. Summary

This chapter has presented the design requirements for the traditional NQR detection system. It is comprehended that the NQR detection system usually consists of an NQR probe, transmitter section, and receiver section. Further, the design concerns and commonly used methods for detection of diverse materials are discussed. The traditional NQR detection system and their limitations for each section are briefly reviewed. Lastly, the chapter discusses the proposed spectrometer for efficient detection system.

Chapter 4

Implementation of proposed NMR /NQR spectrometer

A schematic diagram of the experimental setup is shown in Fig. 4.1 and photograph is shown in Fig 4.2. Single coil configuration is used in this setup where the same coil is used for exciting the nuclei as well as for detecting the signal. The FPGA part of the spectrometer houses a Direct Digital Synthesizer (DDS) as a RF generator, a pulse sequencer to coherently switch on and off the RF oscillations. The resulting low power (mW) RF pulses are then amplified by a RF Power amplifier which delivers the power to the probe circuit.

The signal generated in the coil after the excitation, is amplified by the low noise amplifier, passed through a band-pass filter to limit the noise, and digitized before being mixed with the reference signal from the oscillator. In the digital domain the mixer and low pass filter blocks together perform the operation of in-phase –quadrature or I-Q detection. The reference consists of two channels one in phase and the other quadrature , essentially two sinusoidal signals of the resonance frequency, differing in phase by 90 degrees. In the block 'mixer' these two reference signals multiply with the incoming digitized signal. The sum-frequency component generated in the multiplication process is filtered out using the low pass filters placed at the output of the multipliers. The difference frequency components are I and Q components of the detected input signal. The low pass filters also perform the job of limiting the band-width of the detected I and Q components. This detection scheme lets us detect not only the amplitude of the signal but also the phase of it. The detected signal is stored in the RAM, also implemented in the FPGA.

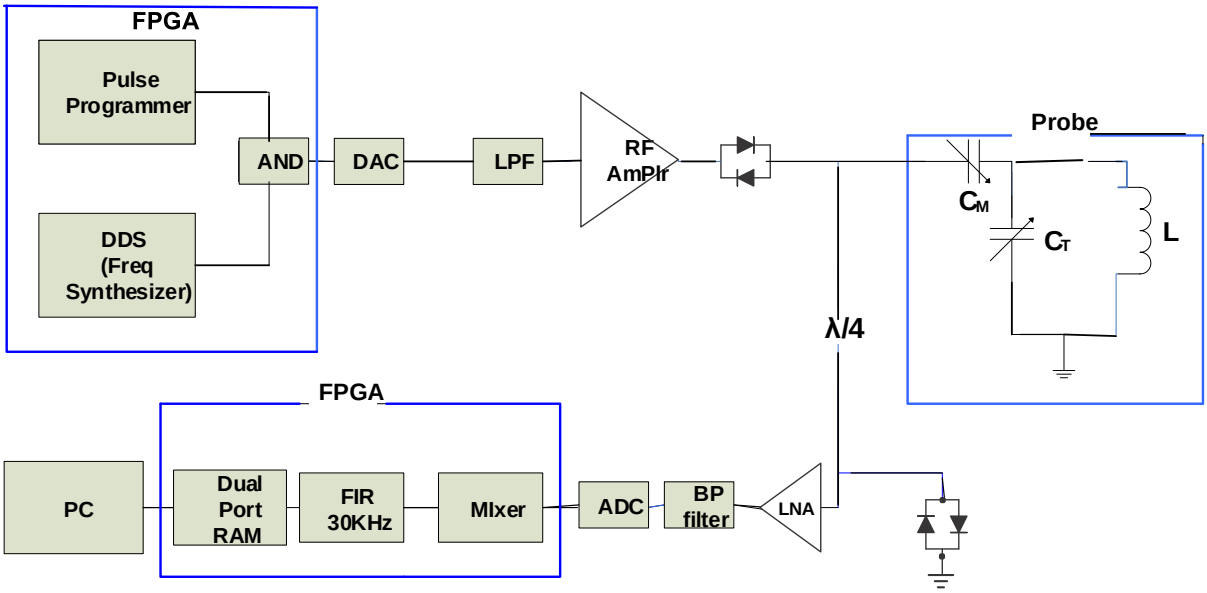

Fig 4.1. Schematic diagram of FPGA based NQR spectrometer

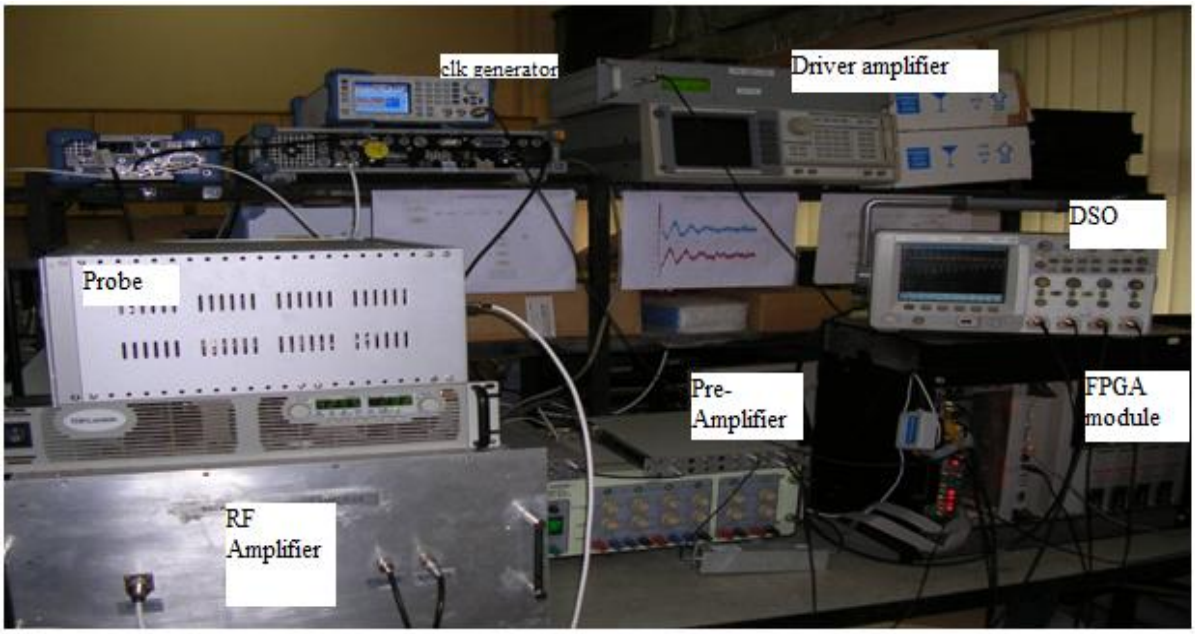

Fig 4.2 Photograph of the FPGA based NQR/NMR spectrometer developed in Electronics Division.

4.1 Specifications of the Instrument.

Specifications of the NQR instrument: Frequency between 0.5 – 6 MHz; pulse lengths between 1-500 μs; RF pulse power up to 200 watts and acquisition time of 50 ms. The developed spectrometer consists of:

- Transmitter, which consists of RF power amplifier to provide 13.5 MHz RF signal of power 200 W
- Probe which can be tuned to observe ^{14}N, ^{1}H , ^{2}H signals.
- Receiver, which consists of preamplifier (80dB gain), band pass filter (cut off frequency 4.64MHz, Band Width- 500 kHz), ADC and DAC
- FPGA module, which consists of pulse programmer (pulse length =1-500 μs, Acquisition time 0- 10s) DDS (0 -6MHz), gate, quadrature demodulator, FIR low pass filter (cut off 30 kHz).
- Computer controlled module, which is used for command/data transfer.

4.2 Transmitter Section

The transmitter section is designed to excite the nuclei using a high power RF pulse (hundred of watts), thus the transmitter of a proposed FPGA based NQR spectrometer is composed of RF Power Amplifier, Direct Digital Synthesizer, Pulse Programmer and Generator from which RF power amplifier was available in- house at ED.

4.2.1 RF Power Amplifier

The power amplification is carried out using a 500 W, 27 MHz, class AB RF power amplifier in two stages and is housed in two different instrumentation bins [51]. The total gain of the RF amplifier is 54 dB. The amplifier used is capable of continuous wave operation. Continuous or pulsed RF sinusoidal input to this amplifier comes from a driver stage which is

capable of producing 4 W. This driver amplifier is housed in a separate instrumentation bin. The instrumentation bin also houses the DC power supplies, control electronics board, micro controller card and display module on its front panel. The 500 W RF power is generated in the main power amplifier bin. In the main power amplifier, using a 4:1 splitter, 4 W RF power is split to get four 1 W drive signals to four power stages. N channel enhancement type MOSFET has been used in the power stages. Four 150 W power stages have been combined to get 500 W RF power using a 4:1 power combiner. The power amplifier stages are arranged so as to reduce the EMI between the stages. The output power is available through a directional coupler on the front panel on an N type connector. Control electronics have been developed to monitor various parameters of the RF amplifier and also to protect the amplifier against over temperature and over-drive. RF input to the amplifier is switched off if any of these conditions occur.

The forward and reflected powers from the directional coupler are routed to the front panel through the control electronics board. Electronics has also been developed to display the forward and reflected power and temperature on the front panel. The RF power amplifier can safely withstand a reflected power of 65 W. In the event of a heavy load mismatch condition at high RF output the forward power will be limited to 65 W so as to protect the RF devices. The unit is air cooled and 19" rack mountable. Two AC fans with air flow capacity of 280 CFM have been used for cooling purposes. It is observed that the temperature is less than 70 ^{o}C on the heat sink when measured very close to the power MOSFETs. The transistors are mounted directly on a copper heat spreader with thickness of 1 cm. The surface smoothness is important and special care has been given to it. The heat spreader is then attached to the main heat sink made of aluminum. Heat sink compound is used at all thermal interfaces and the recommended transistor mounting procedure has been followed.

4.2.1.1 Control electronics

The RF input signal from a signal generator is given to the pre-amplifier bin through the control electronics board. An RF switch is placed in the drive path to the low power stages on the board. It is made off in case of overdrive or over temperature. This will switch off the RF input signal to the pre amplifier. If the reflected power exceeds more than 65 W, the output of the main RF amplifier will be limited to 65 W using a limiter. A filter has been used after the limiter so as to remove the higher harmonics. The reflected power has to be brought down below 10 W so as to increase the forward power again.

4.2.1.2 Measurement of temperature, Forward and reflected power

Temperature of the heat sink is measured using a temperature sensor and the voltage is routed to the back panel on a BNC connector. This signal is also connected to the pre-amplifier bin on the back panel and is connected to the micro - controller board to display the temp. Extreme care has been taken to avoid RF pickups on this voltage signal since it is measured very close to the power devices.

The forward and reflected power pick up from the directional coupler is brought to the RF –DC control board. Sample of the forward and reflected power is brought to the front panel which can be used to calibrate the final RF output power, and also used for impedance matching purposes. An RF to DC converter gives DC equivalent of the forward and reflected power which is brought to a D type connector on the back panel. These signals are brought to the pre amplifier instrumentation bin and are given to micro controller board to display the forward and reflected power. The DC voltage equivalent of the reflected power is also routed to the control electronics board so as to protect the amplifier from excess reflected power.

4.2.2 Direct Digital Synthesizer

Direct Digital Synthesis (DDS) [52] is a method of producing an analog waveform usually a sine wave by generating a time varying signal in digital form and then performing a digital to analog conversion. Because operations within a DDS device are primarily digital, it offers fast switching between output frequencies, fine frequency resolution, and operation over a broad spectrum of frequencies.

The digital part of the phase tunable and fixed frequency DDS, denoted here as DDS, is built inside FPGA as a core module, while the non-digital parts, i.e., digital to analog conversion and low pass filter, are outside the FPGA. The output level of a digital to analog converter is updated in synchronism with a master clock. As a consequence of discrete change in the output voltage at clock rising edges, the output of a DDS circuitry contains signal components with the image frequencies in addition to the fundamental one. Thus, the output signal is passed through a low pass filter to select fundamental frequency.

The DDS is mainly composed of a phase accumulator, a means of phase to amplitude conversion which can be a Look up Table (LUT), or Coordinate Rotation Digital Computer (CORDIC) algorithm [53] and a digital to analog converter (DAC).

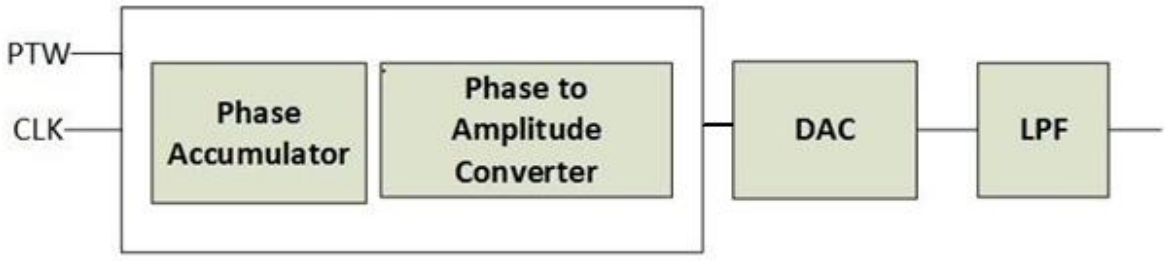

Fig 4.3. Block Diagram of Direct Digital Synthesizer.

The DDS circuitry shown in Fig 4.3 is basically a digital frequency divider function whose incremental resolution is determined by the frequency of the reference clock divided by the 2^n where n is number of bits in the tuning word. The phase accumulator is a variable-

modulus counter that increments the number stored in it each time it receives a clock pulse. When the counter overflows it wraps around, making the phase accumulator's output contiguous. Fig. 4.4 shows the block diagram of DDS implemented in FPGA.

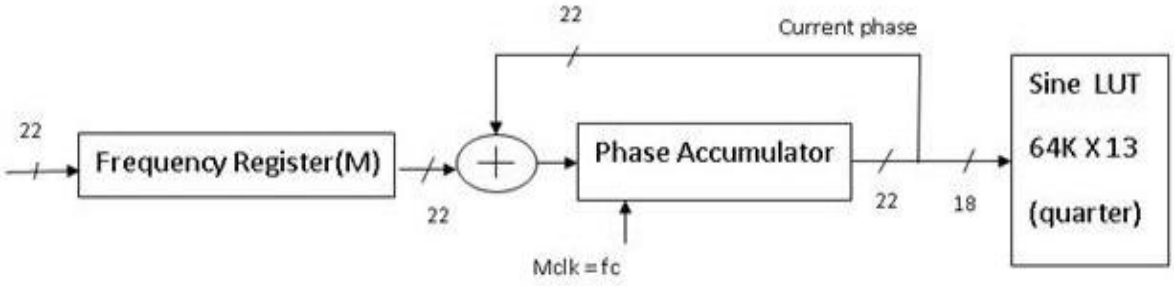

Fig 4.4 Block diagram of implemented DDS in FPGA

The phase tuning word sets the modulus of the counter that effectively determines the size of the increment (Δ Phase) that gets added to the value in the phase accumulator on the next clock pulse. The larger the added increment, the faster the accumulator overflows, which results in a higher output frequency. This unique algorithm uses a much reduced ROM look-up table and DSP techniques to perform this function. The relationship of the output frequency, reference clock, and tuning word of the DDS is determined by the formula:

$$F_{out} = \frac{M \; X \; F_c}{2^n} \qquad [4.1]$$

where $\boldsymbol{M}$ is Phase tuning word (PTW)

$\boldsymbol{F_{out}}$ is Output frequency of DDS

$\boldsymbol{F_c}$ is Internal reference clock frequency (CLK)

$\boldsymbol{n}$ is Length of phase accumulator

4.2.2.1 Implementation of LUT in FPGA

DDS generates a sine wave using phase accumulator and phase to amplitude converter that has full wave sine samples stored (LUT). The phase accumulator generates phase values for the sine wave while phase to amplitude converter uses the phase values as address for the LUT. In order to reduce the size of LUT the symmetry property of sine function is taken into consideration and only first quarter of the sine wave is generated i.e. the values of Sin (0) to Sin (π/2) are only generated. Fig 4.5 shows the four quadrants of the sine wave. The ROM has 16 address bits even though it holds only quarter sine wave. Hence for full sine wave ROM the address would be 18 bit. Two MSBs are required for deciding the quadrant in which the wave lies. Thus there should be 64K (65586) distinct sine values in this LUT representing sine values. For DDS with 14 bit output ranging from -8192 to +8192, these sine values are scaled up by 8192 to make them 14 bit integer values (1 sign bit + 13 data bit).

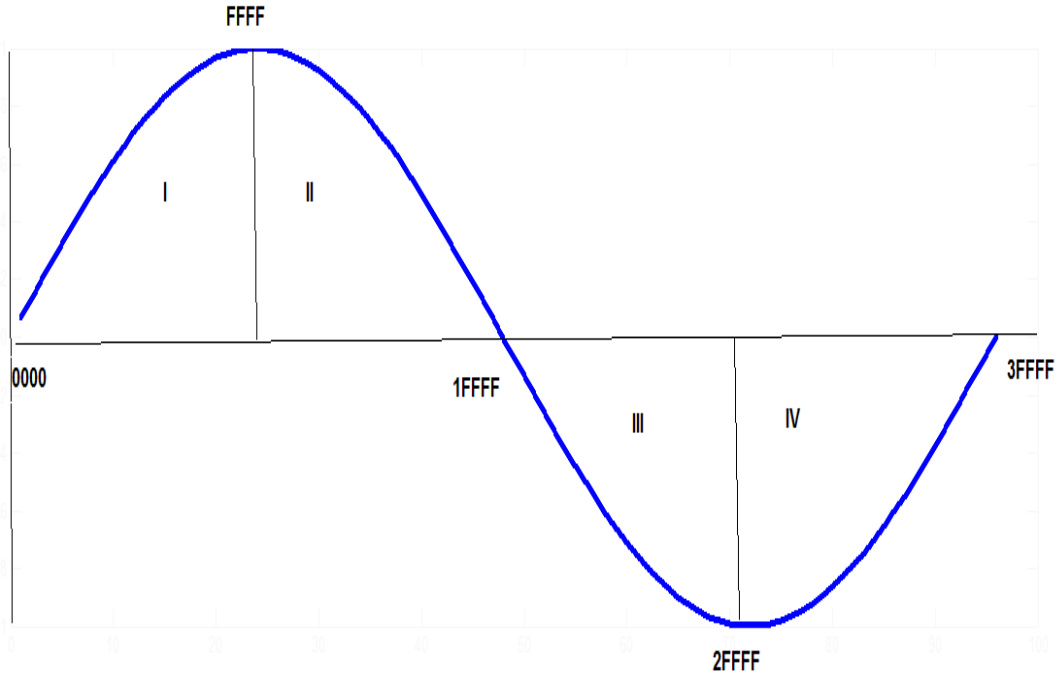

Fig 4.5 Four Quadrants of the Sine wave.

Table 4.1 : ROM addresses indicating the quadrant

Quadrant	A_{17} A_{16}	A_{15}…… A_0	Address	ROM Address required
1	0 0	0……0	00000	0000
	0 0	1……1	0FFFF	FFFF
2	0 1	0……0	10000	FFFF
	0 1	1……1	1FFFF	0000
3	1 0	0……0	20000	0000
	1 0	1……1	2FFFF	FFFF
4	1 1	0……0	30000	FFFF
	1 1	1……1	3FFFF	0000

In the table 4.1, it is clear that for two consecutive addresses (0FFFF and 10000, 1FFFF and 20000, 2FFFF and 30000) the same address of the ROM is accessed presenting same output values. In order to overcome this problem a register with a singular sample is introduced in the memory block. On inclusion of this single value register we have a full quadrant, which corresponds to 2^{16}+1 words. This singular register holds the peak value of sine function [53]. The modified table is

Table 4.2 Modified address to ROM

Quadrant	A_{17} A_{16}	A_{15}… A_0	Address	Address to ROM	Data From
I	0 0	0……0	00000	0000	ROM
	0 0	1……1	0FFFF	FFFF	ROM
II	0 1	0……0	10000*	0000	Register
	0 1	0……1	10001	FFFF	ROM
	0 1	1……1	1FFFF	0001	ROM
III	1 0	0……0	20000	0000	ROM
	1 0	1……1	2FFFF	FFFF	ROM
IV	1 1	0……0	30000*	0000	Register
	1 1	0……1	30001	FFFF	ROM
	1 1	1……1	3FFFF	0001	ROM
*During this addresses the address presented to ROM is insignificant because data from 'register' is selected. These addresses are the peaks or bottom peaks of sine wave.					

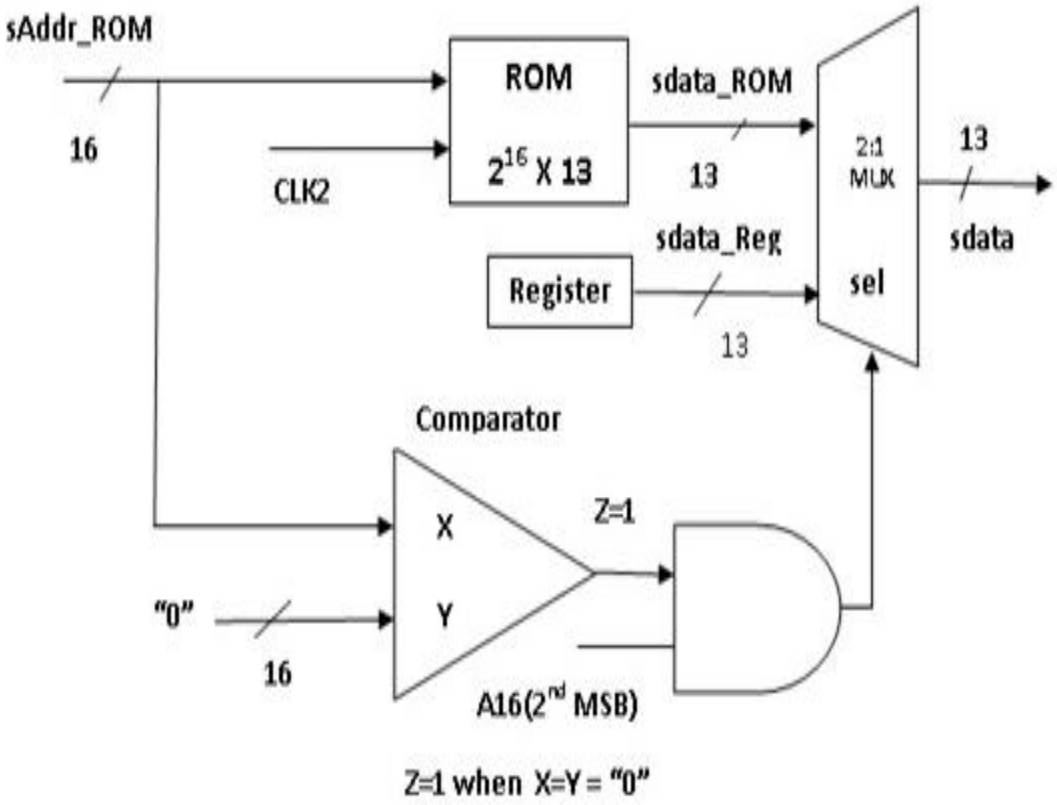

Fig 4.6. Implementation of LUT in FPGA

VHDL code has been written to produce two independent outputs 90^{o} out of phase, which are mandatory for quadrature detection [55]. Figure 4.6 shows implementation of LUT in FPGA.

4.2.2.2 Generation of quadrature outputs.

To reduce the ROM area the symmetry of sine function is taken into account and thus the quadrature outputs are obtained by using the same ROM. The designed quadrature DDS system is represented in Fig 4.7.

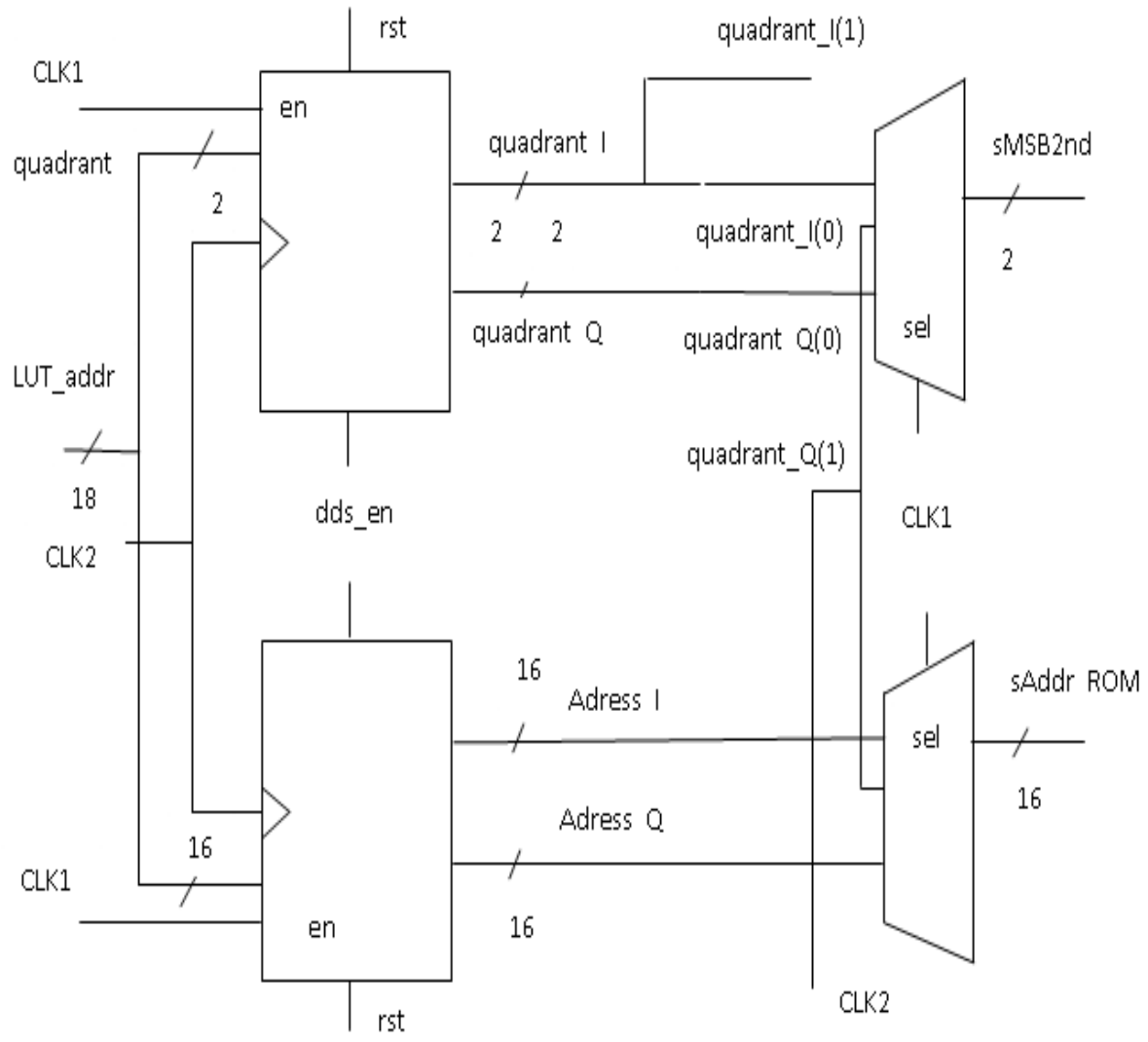

Fig 4.7 Quadrature DDS system in FPGA

All the communications are done from Labview to FPGA card through PCI bus, with f_o and f_c the value of M is calculated and sent to FPGA where phase accumulator adds this number to get the next value of sine wave. The quadrature outputs from DDS for $f_o = 1$ MHz and $f_c = 46$ MHz is shown if Fig 4.8 and 4.9

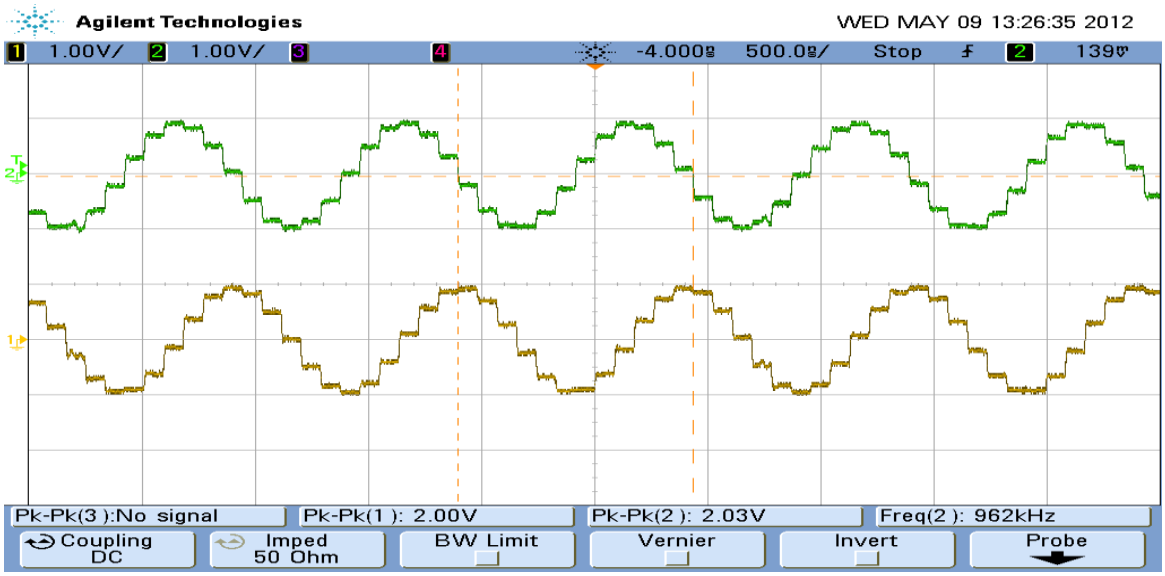

Fig 4.8 Output of DDS after DAC (--- I component, --- Q component).
Time base: 500ns/unit

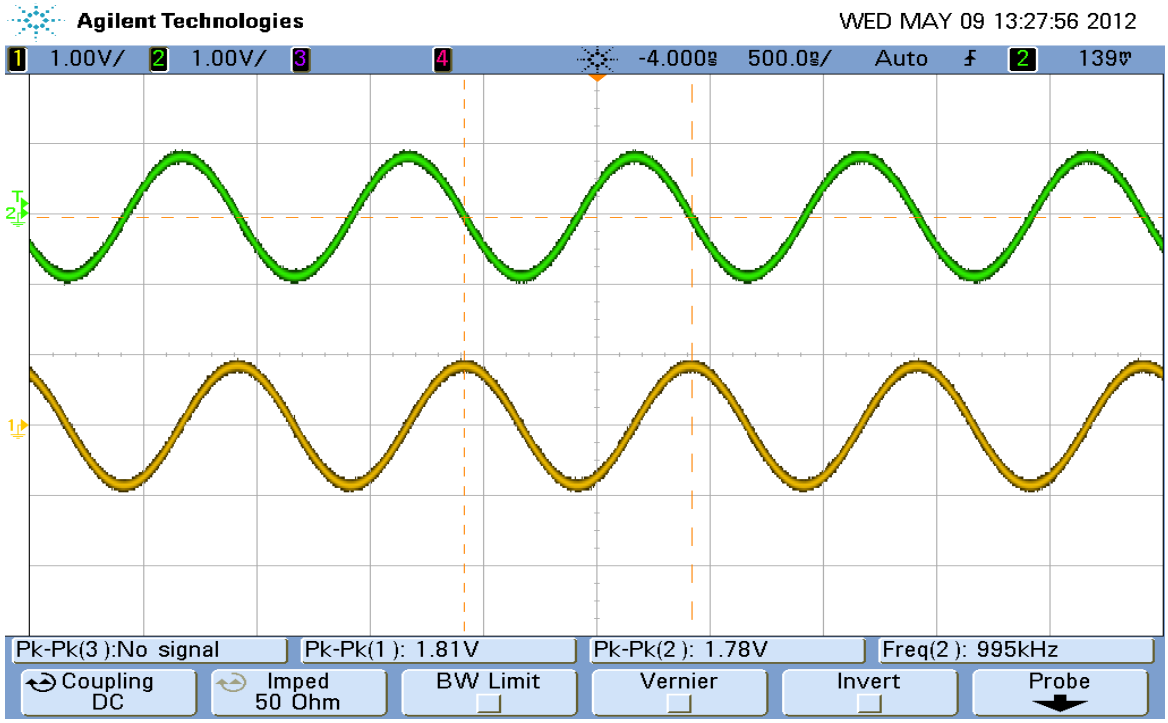

Fig 4.9 Output of DDS after LPF (--- I component, --- Q component).
Time base: 500ns/unit

The resolution of DDS in spectrometer designed is $fc/2^{22}$=10.96 Hz.

4.2.3 Programmable Pulse generator

The earlier pulse programmers used several tens of integrated circuits (ICs) on several circuit boards and enormous wire connections among them. Here finite state machine (FSM) is written for programmable pulse generator using state diagram editor of active HDL software which is converted to VHDL code that realizes the pulse programmer inside the FPGA. The function of pulse generator is to generate timing sequences for enabling transmitter, receiver, acquisition, and pulse-modulation of RF signal used for excitation. In addition pulse programmer also controls the phase of RF pulses as per the requirement for the observation of free induction decay (FID) and spin echo by triggering the DDS at appropriate phase points. Following are the timing signals that are generated by pulse programmer. They control various parts of the spectrometer.

1. Transmitter Enable.(1-200 µsec)
2. Receiver enable.(1 – 11 sec)
3. RF modulating Pulse.(1-100 µsec)
4. Acquisition Trigger (1 -10 sec)
5. RF Phase Control (0^o, 90^o, 180^o, 270^o)

Transmitter enable pulse is used to enable the RF power amplifier in between which RF pulses are sent to the probe. RF modulating pulse at resonance frequency is send to the probe for the exciting nuclei sitting in a probe. After the RF pulses the pulse programmer disables the transmitter and enables the receiver by receiver enable pulse. Now the receiver is ready to receive the signal for digital quadrature detection. The FSM of the pulse programmer is shown in Fig 4.10 and the pulses generated are shown in Fig 4.11.

4.2.3.1 FSM: Programmable pulse generator

FSM states: Reset_s, Idle_s, Start_s, Rd_ID_tw_s, Dly_tw_s, Check_N_s, Low_TxEn_s, Rise_RxEn_s, Rise_Acq_s, Low_Acq_s, Rise_TxEn_s,Low_RxEn_s, Dly_ID_s, RF_pulse_ON, Low_sStart_stp

Variables: vNum_pulses (Number of pulses in a sequence), vNum_ itern(Number of iterations), vID (initial delays) , vTw (pulse widths) , vval_Tst (time between start and Transmitter enable),vval_Tpt (time between pulse end to Transmitter disable), vval_Ttr (Transmitter disable to Receiver Enable), vval_Tra (Receiver Enable to Acquisition ON), vval_Tar(Acquisition OFF to Receiver disable), Start_stp (Start signal).These all the values are send to FPGA through application software. Algorithm of FSM is shown below.

Signals: sTxEn, sRxEn, sStart_stp, sRF_pulse, sAcq_ON, sdds_phase_0,sdds_phase_90

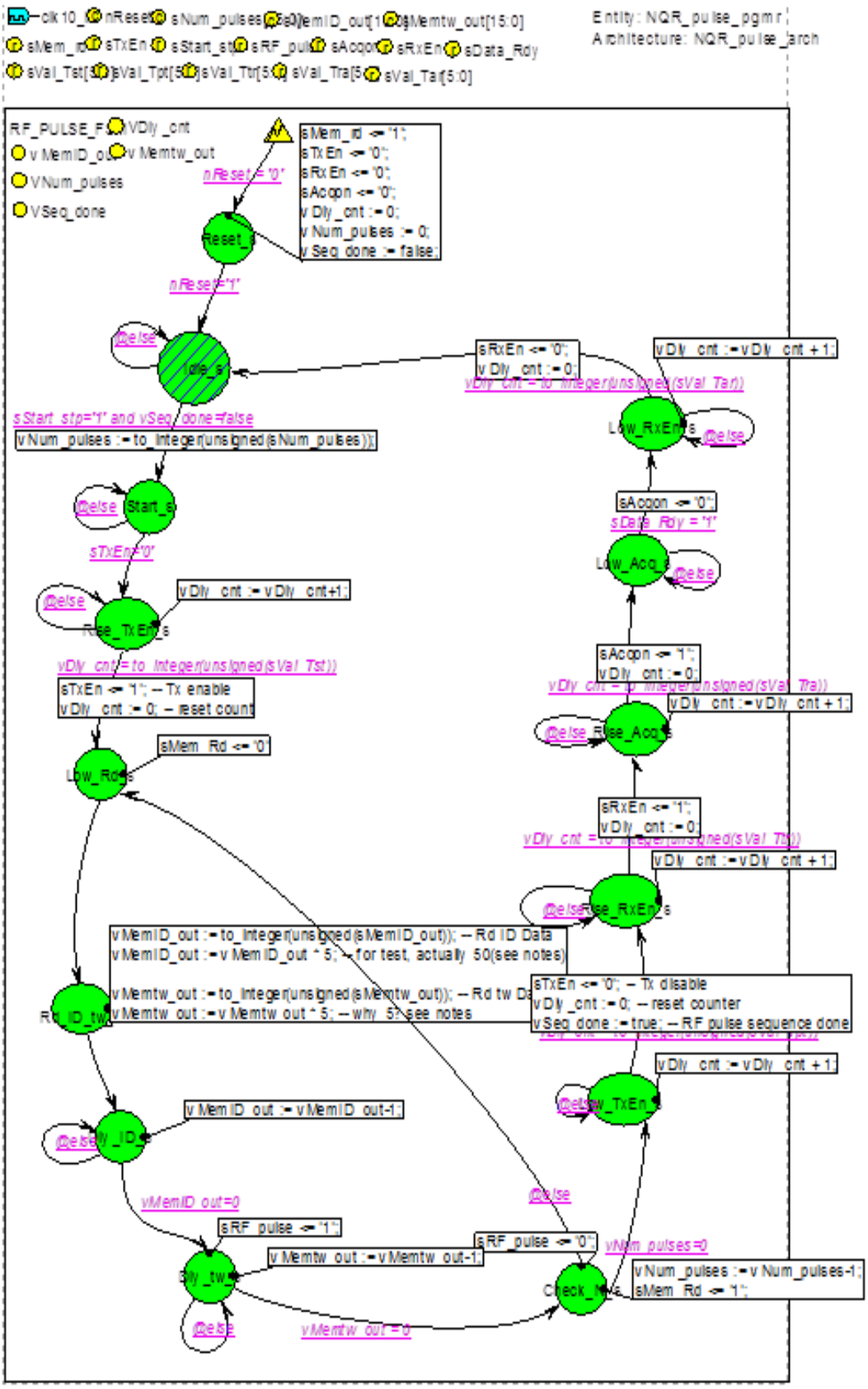

Fig 4.10 FSM of programmable pulse generator

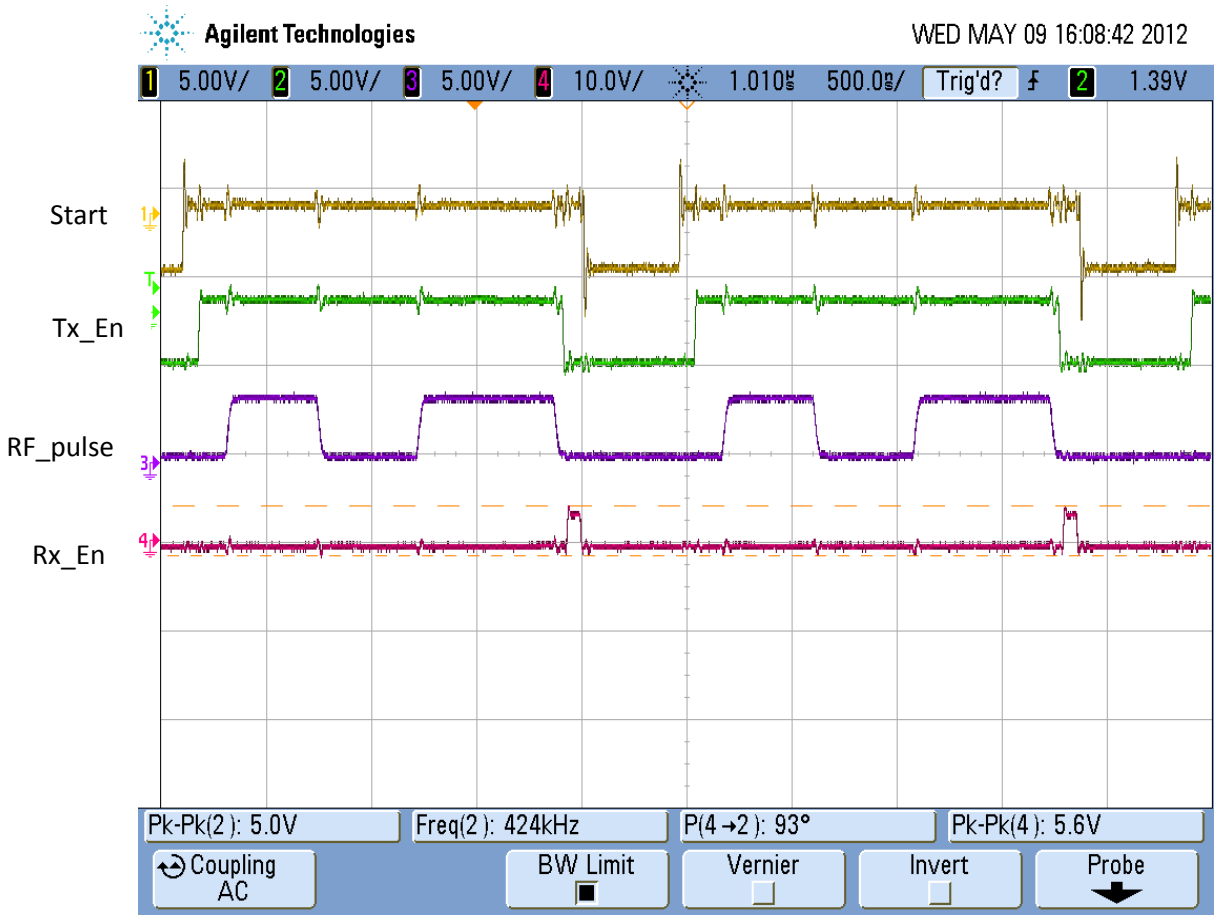

Fig 4.11. (--- Start), (---TxEn),(---RF_pulse),(--- RxEn).Time base: 500ns/unit

The DDS is programmed to generate an RF frequency (reference frequency). This signal is routed through the phase shifter which is controlled by the pulse programmer. The phase shift is to provide pulses along the different axes in the vector model. By convention,

i) phase shift of 0^o is an x-phase pulse,

ii) phase shift of 90^o is an y-phase pulse

iii) phase shift of 180^o is an -x-phase pulse

iv) phase shift of 270^o is an -y-phase pulse

RF modulating pulse can be one pulse sequence for observation of FID or a two pulse sequence for observation of spin Echo.VHDL code has been written for the pulses to be 90^{o} at x and 180^{o} at y. The two pulse sequence is shown in Fig 4.12.

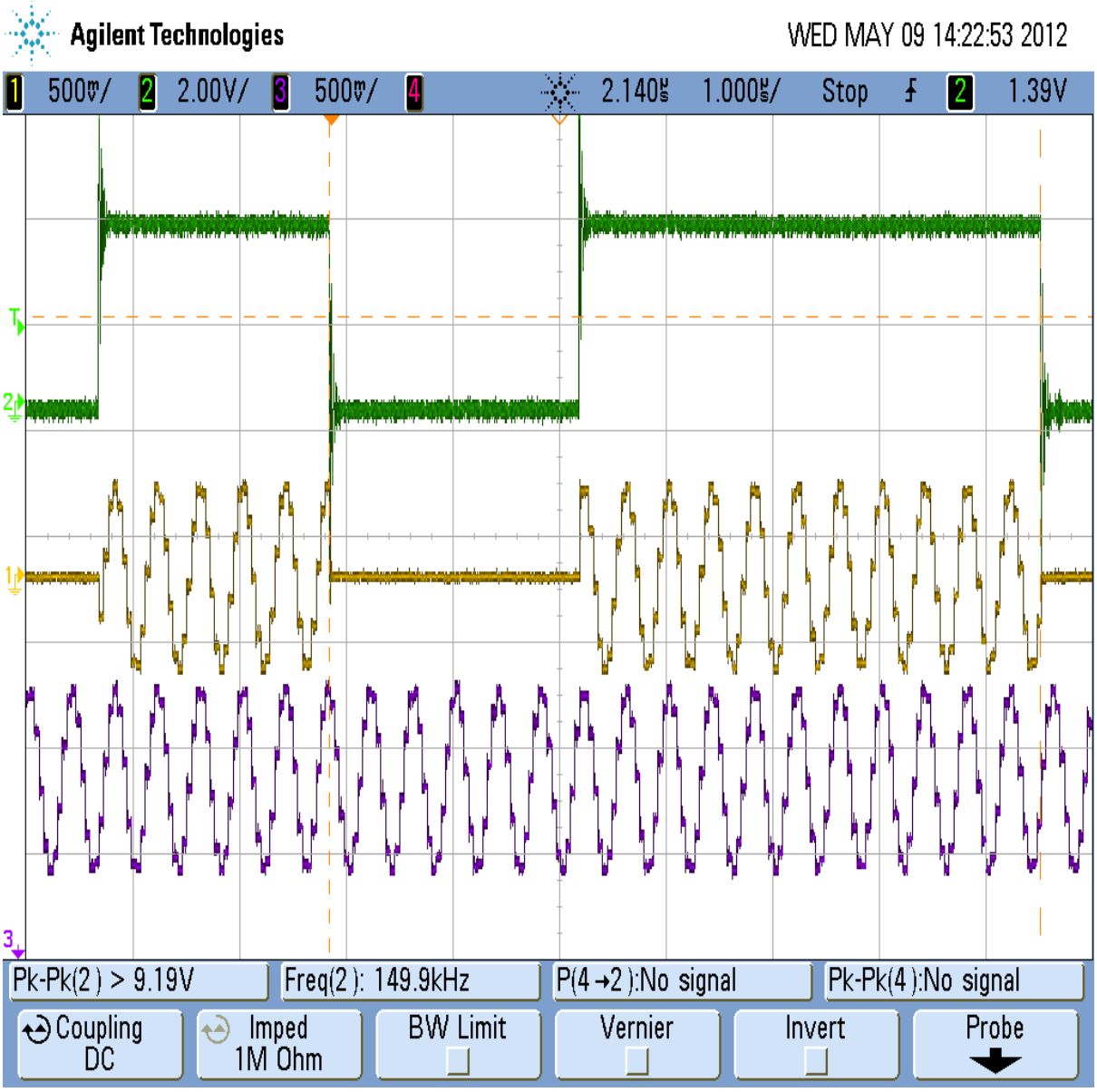

Fig 4.12 Two Pulse (90^{o}at x and 180^{o} at y) on Scope(--- Pulse), (---RF) (----RF pulse)
Time base: 1µs/unit

4.3 Crossed Diodes and Quarter Wave Impedance Transformer

The high power output of transmitter to the probe needs to be isolated from the sensitive receiver amplifier. This can be done by using RF switch. Thus the RF switch should have high isolation capability to attain high transmission power efficiency. Also, the sensitive receiver section needs to be protected from high transmission power.

In traditional NQR lab equipment, quarter-wave switches [57] along with cross diodes are ideal for realizing this function which is implemented for the current thesis. This is shown in Fig. 4.13a).

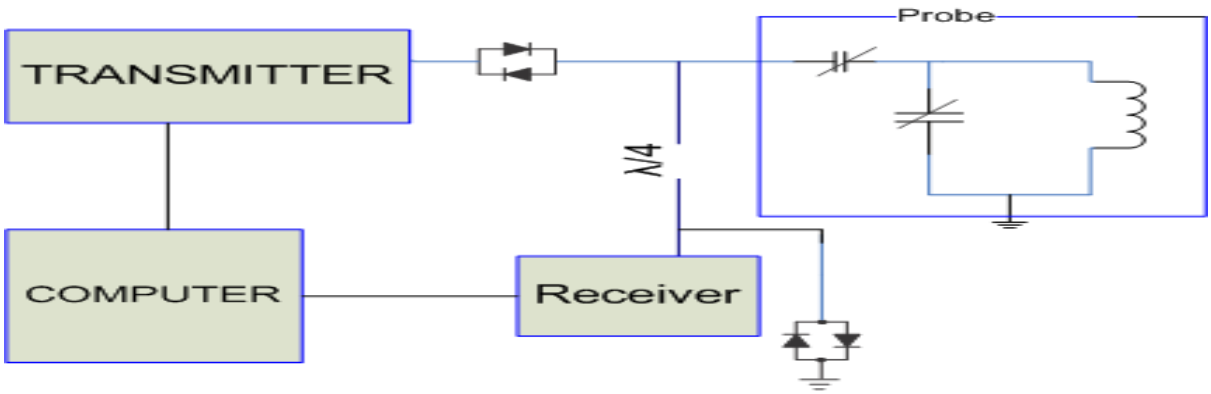

Fig 4.13 a) Block diagram of Spectrometer showing cross diodes

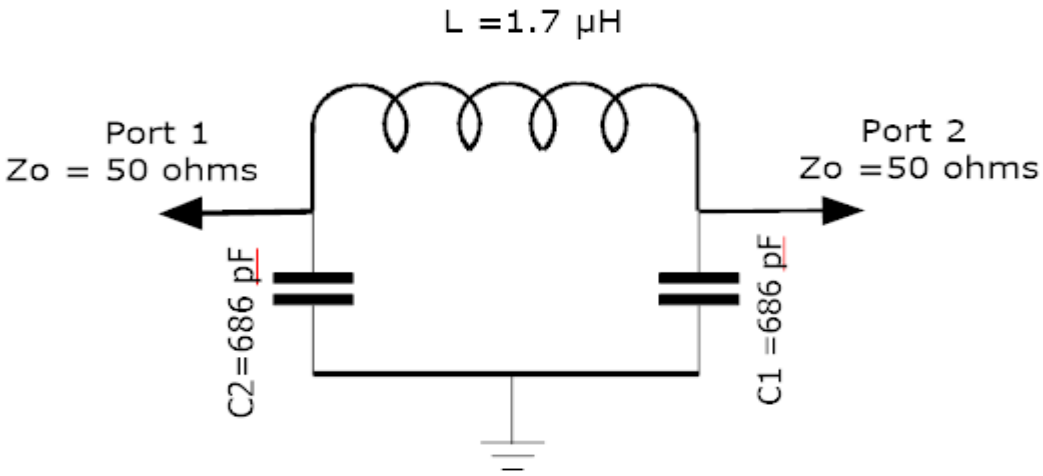

Figure 4.13 b) Equivalent of (λ/4) cable at 4.64 MHz

The quarter-wave switch is suitable for lab equipment. It has a very simple circuit

structure. Also, it cooperates with NQR systems automatically without any control circuit. Its low additive noise benefits detection accuracy. Though at high frequencies a suitable length of a co-axial cable like RG-58 itself can serve the purpose of a quarter wave line, but at the frequencies of our interest (viz. < 6 MHz), co-axial cables are inconvenient because of the long lengths so for portable field based NQR systems, it is not a practical choice.So 50 Ω compatible, quarter wave π-sections have been used for this spectrometer explained in Fukushima et al [58].

Between the RF power amplifier and the probe there is a pair of cross diodes which show high series impedance when the transmitter is off and a low impedance during the pulses. Thus between the pulses, the power amplifier and its associated noise is isolated from the probe circuit. The signal from the probe circuit passes through a quarter wave line to reach another pair of cross diodes which are shunted to ground at the input of pre-amplifier. The diode shorts the pre-amplifier end of the cable when transmitter is on, thus protecting the sensitive pre amplifier from high RF power out from the power amplifier. Between pulses, the voltage across the diodes is too small to turn them on, and they act like an open circuit, letting the NQR signal to pass to the preamplifier.

A quarter wave transmission line acts a transformer which transforms its output impedance Z_{output} according to the equation.

$$Z_{output} = \frac{Z_o^2}{Z_{input}} \qquad [4.2]$$

Where $Z_o = 50\ \Omega$ is the characteristic impedance of the transmission line and Z_{input} is input impedance of transformer. Thus, during the pulses, when the shunt diodes are acting as short, the input impedance of the transmission line is infinite acting as if the receiving circuit were completely disconnected from the probe.

The equivalent of (λ/4) cable for operating frequency as 4.64 MHz for $NaNO_2$ is a π network shown in Fig. 4.13b).

For different samples, different NQR frequencies demand different π sections which complicate the system design. A PIN diode based RF switch is used in [59].A PIN diode is a one kind of diode with an undoped, wide intrinsic semiconductor region between a P-type and N-type semiconductor region. These regions are normally heavily doped as they are used for Ohmic contacts. The wider intrinsic region is indifference to an ordinary p–n diode. This region makes the diode an inferior rectifier but it makes it appropriate for fast switches, attenuators, photo detectors and high voltage power electronics applications.

When the PIN diode is forward biased, the charge pool is loaded with free charges so that the PIN diode acts similarly to a regular diode. The PIN diode will introduce a PN conjunction voltage drop and a low additive resistance value. The resistance value depends on the DC bias current for the PIN diode. When the PIN diode is reverse biased, the charge pool is drained up. The I layer provides high isolation between P and N so that the capacitance between P and N terminals is very low(around a few pF). A more interesting characteristic of PIN diodes is that as charging and discharging I layer requires a certain amount of time (usually around tens of μS), high power AC signals can be switched on and off with a low power DC biasing control signal.PIN Diode Based RF Switches has been used in [60].

As compared to Quarter wave transformer the drawbacks of PIN diode switches are

1) It requires extra control and driving circuit to support PIN diodes.

2) It consumes power during the on-state as a DC bias current is needed to provide low signal attenuation.

Despite the drawbacks, the advantages of PIN diode switches are more remarkable.

1) It can be integrated in a compact volume.

2) It can be designed for range of frequencies for eg. (0.5 -6 MHz) i.e. the range of frequencies of the current spectrometer.

4.4 Probe

The probe circuit consists of the pickup coil and a pair of adjustable capacitors. The probe circuit is configured in such a way that with appropriate adjustment of the capacitors, the tuning is achieved over the desired frequency range with an input impedance of the probe circuit at 50.

By matching the impedance of the probe circuit to the characteristic impedance of the coaxial cables carrying the signal, all of the forward power generated by the power amplifier is transferred to the probe circuit, and signal generated by the probe circuit is efficiently transferred to the detection circuitry.

In the transmitting mode the circuit is matched to transmitter output impedance 50 ohm and in receiving mode it is matched to optimum input impedance of pre-amplifier.

The probe circuit used here is parallel tuned LC circuit impedance matched to 50 ohms with a series capacitor (Fig 4.14). In order to reduce the noise the probe circuit is shielded inside an aluminum box and is well grounded. The coil is made mechanically stable by binding its turns using a resin based adhesive (Araldite ®).

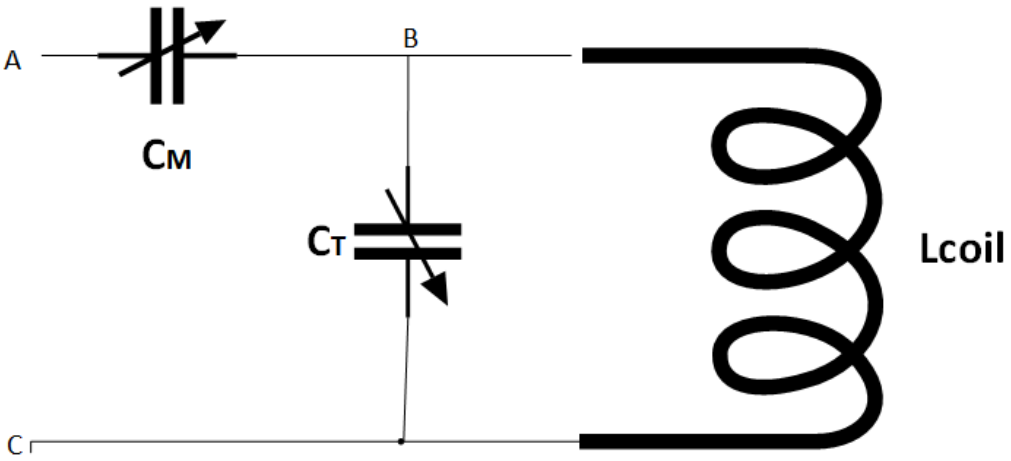

Fig 4.14 Probe

The capacitors are varied in order to tune the circuit to the resonance frequency and match the circuit to 50 ohms for maximum power transfer from the transmitter. For the circuit shown in Fig 4.9 the impedance between A and C equals

$$Z_{AC} = Z_{BC} + \frac{1}{j\omega C_M} = \frac{(R+j\omega L)/j\omega C_T}{R+j\omega L+1/j\omega C_T} + \frac{1}{j\omega C_M} \quad [4.3]$$

$$= \frac{R}{(1-\omega^2 LC_T)^2+(\omega C_T R)^2} + j\omega \frac{L(1-\omega^2 LC_T)-C_T R^2}{(1-\omega^2 LC_T)^2+(\omega C_T R)^2} + \frac{1}{j\omega C_M} \quad [4.4]$$

R is the resistance of coil at resonance frequency. Since the terms $C_T R^2$ and $(\omega C_T R)^2$ are very small and negligible compared to other additive terms in equation, Thus equation [4.4] can be simplified to

$$Z_{AC} = \frac{R}{(1-\omega^2 LC_T)^2} + j\omega\frac{L}{(1-\omega^2 LC_T)} + \frac{1}{j\omega C_M} \qquad [4.5]$$

In order to satisfy the matching condition the real part of eq.[4.5] must be set to characteristic impedance of the connecting coaxial cable which is 50Ω by adjusting C_T at fixed frequency:

$$\frac{R}{(1-\omega^2 LC_T)^2} = 50\Omega \qquad [4.6]$$

Thus $C_T = \frac{1-\sqrt{R/50}}{\omega^2 L}$ [4.7]

In order to obtain resonance at same frequency imaginary part of eq. [4.5] must be zero. Thus equating imaginary part of eq. [4.4] to zero, we get

$$C_M = \frac{\sqrt{R/50}}{\omega^2 L} \qquad [4.8]$$

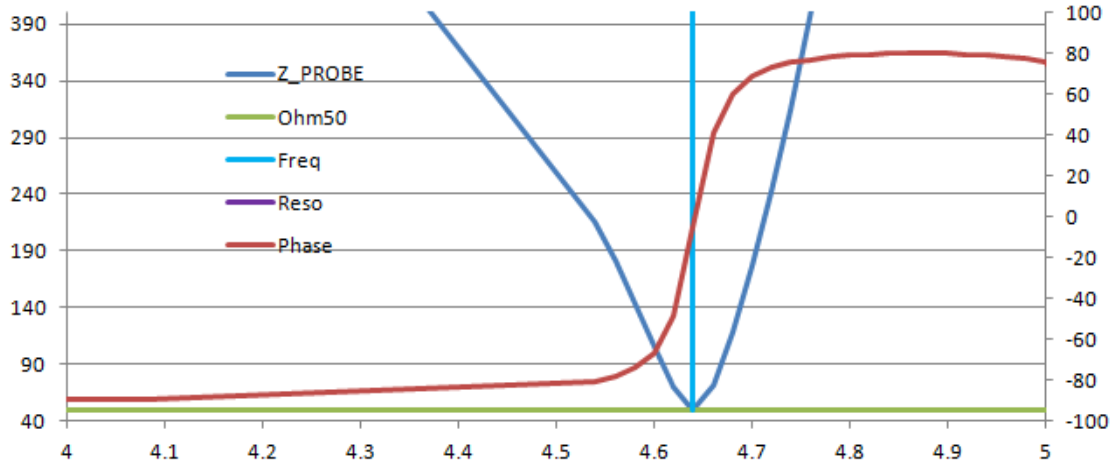

Fig 4.15 Impedance of Probe vs Frequency. Horizontal axis is Frequency in MHz, Vertical axis in left is Z_Probe in Ohms,Vertical axis in right is phase in degrees.

The tuning and matching are achieved by maximizing the forward power and minimizing the reflected power. The forward and reflected power is monitored using the directional coupler built in the transmitter. Fig 4.15 shows the plot of impedance of probe versus frequency.

4.4.1 Design of Coil

As part of probe module, the RF coil combines with matching network to form a resonant circuit, and works under the resonant state. Ideal coil should possess uniform RF field, good fill factor and high quality factor (Q ≥ 100). The amplitude of RF voltage which appears at the terminal of the tank circuit at resonance frequency is proportional to quality factor of the coil thus it is advisable to use coils with high Q factor. The quality factor is known as Q value and it represents the ratio of inductive reactance and equivalent loss resistance.

$$Q = \frac{2\pi f L}{R} \qquad [4.9]$$

Where f is the frequency, L is the inductance of the coil, and R is the total loss resistance. The Q value is higher, the loss of the circuit is smaller, the signal amplification is stronger, the frequency selectivity is better, and frequency stability of resonant circuits is higher. Since the Q and the bandwidth has inverse relation, a very high-Q (>100) means a very low bandwidth. Hence very high Q is not desirable when it could interfere with signal band. Thus the selection of Q value is the key of coil design. The range of the variable capacitors is one of the key constraints in the coil design. Several coils were wound and tested. The one that was finally used for this work was with length to diameter ratio of two has higher Q value [56], is made out of 17 AGW copper wire and has 32 turns of 20 mm diameter of length 40 mm.

Smith Software is used to find the range of inductance of coil with available capacitors C_T and C_M of (5 pF-125 pF). The capacitors used are high voltage (5kV) vacuum variable capacitors. According to inductance, the coil diameter and the length of turns, the turns of the coil winding were calculated by induction calculation software. The coil was designed

and made mechanical stable by potting its turns in resin based adhesive (Araldite ®). The inductance of the coil is 8 μH. The size of the coil and the tubes for keeping the sample were chosen in order to maximize the filling factor.

4.5 Receiver Section

The receiver design is extremely important since it directly determines the final spectrum quality. The NQR signal (along with attendant noise) is first amplified to a level of about several hundreds of mV. The signal is then passed to ADC. The ADC converts the signal from voltage to data points. This signal is then demodulated in FPGA using mixer with zero and ninety degree shifted reference signals which come as DDS outputs. The Receiver section is composed of Pre-Amplifier, Band Pass filter, ADC, Digital Demodulator, Finite Impulse Response (FIR) filter and Dual port RAM for data storage.

4.5.1 Digital Quadrature Detection (DQD)

DQD [60] [61] works on lock in amplification technique where signal is multiplied to I and Q components of reference signal (Fig 4.16). If signal is s(n) and I component of reference signal is $cos(\omega_o n)$ and Q component of reference signal is $sin(\omega_o n)$.

$$s_I(n) = s(n) * cos(\omega_o n) \quad [4.10]$$

$$s_Q(n) = s(n) * sin(\omega_o n) \quad [4.11]$$

If $s(n) = sin(\omega n)$

Then

$$s_I(n) = sin(\omega - \omega_o)n + sin(\omega + \omega_o)n \quad [4.12]$$

$$s_Q(n) = cos(\omega - \omega_o)n - cos(\omega + \omega_o)n \quad [4.13]$$

The lower frequency component is the desired signal. In the demodulation process the signal oscillating at frequency $(\omega - \omega_o)$ is of interest and component at $(\omega + \omega_o)$ are dropped off with low pass FIR filter.

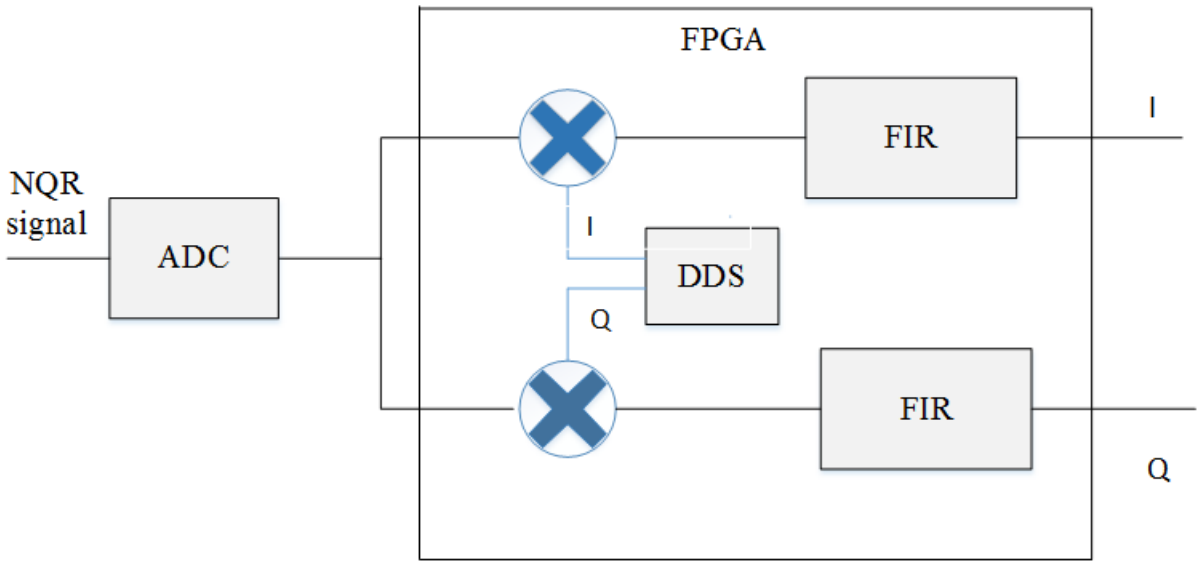

Fig 4.16 a) Digital Quadrature Detection

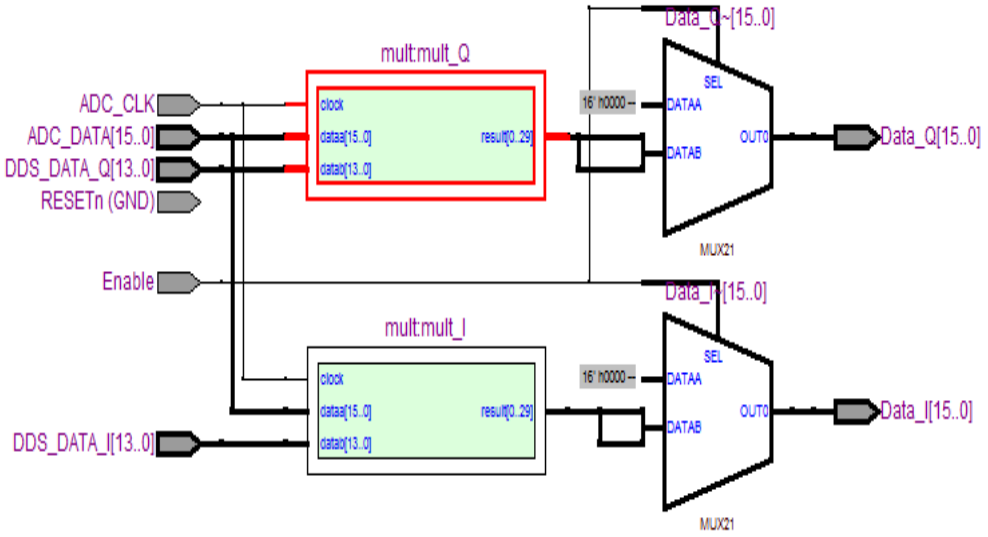

Fig 4.16 b) Demodulator implemented in FPGA

4.5.2 Finite Impulse Response Filter

An FIR filter of length M with input $x(n)$ and output $y(n)$ is described as

$$y(n) = \sum_{k=0}^{M-1} h(k)x(n-k) \quad [4.14]$$

Where $h(k)$ is the set of filter coefficients.Filter can be characterised by its system function

$$H(z) = \sum_{k=0}^{M-1} h(k)z^{-k} \quad [4.15]$$

Coefficients of desired frequency response is calculated as

$$h_d(n) = \frac{1}{2\pi}\int_{-\pi}^{\pi} H_d(\omega)e^{-j\omega n}d\omega \quad [4.16]$$

$$H_d(\omega) = \sum_{n=0}^{\infty} h_d(n)e^{-j\omega n} \quad [4.17]$$

The unit sample response $h_d(n)$ is infinite in duration and has to be truncated at M-1 to yield an FIR filter of length M. Truncation of $h_d(n)$ is same as multiplying by a rectangular window defined as

$$w(n) = 1, \quad n = 0, 1, \ldots \ldots M-1 \qquad [4.18]$$

$$0, \quad \text{otherwise}$$

Thus the unit sample response of FIR filter becomes

$$h(n) = h_d(n)w(n) \qquad [4.19]$$

$$= h_d(n), \quad n = 0, 1, \ldots \ldots M-1$$

$$0, \quad \text{otherwise}$$

The multiplication of window function $w(n)$ with $h_d(n)$ is equivalent to convolution of $H_d(\omega)$ and $W(\omega)$, Fourier transform of $w(n)$ i.e

$$W(\omega) = \sum_{n=0}^{M-1} w(n)\, e^{-j\omega n} \qquad [4.20]$$

Thus the convolution of $H_d(\omega)$ and $W(\omega)$ yields the frequency response of the FIR filter. i.e

$$H(\omega) = \frac{1}{2\pi} \int_{-\pi}^{\pi} H_d(v) W(\omega - v) \mathrm{d}\omega \qquad [4.21]$$

The Fourier transform of the rectangular window is

$$W(\omega) = \sum_{n=0}^{M-1} e^{-j\omega n}$$

$$= e^{-\frac{j\omega(M-1)}{2}} \frac{\sin \omega M/2}{\sin \omega/2}$$

$$|W(\omega)| = \frac{\sin \omega M/2}{\sin \omega/2} \qquad [4.22]$$

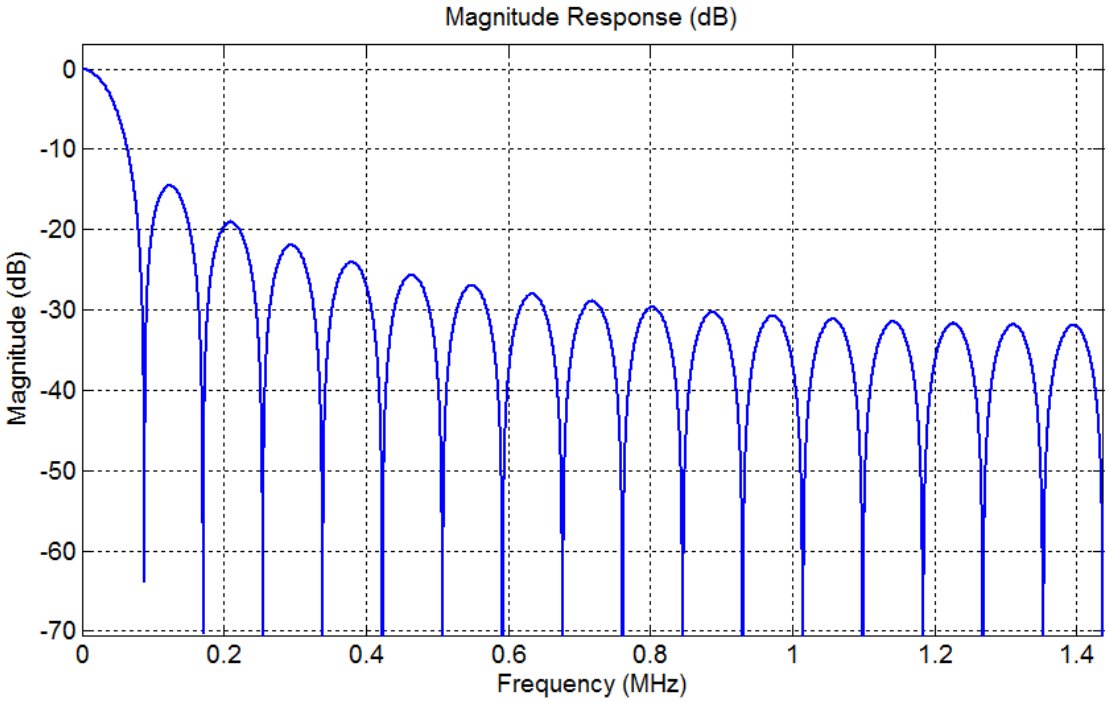

4.17 Magnitude response of rectangular window.

The magnitude response of rectangular window function is shown in Fig 4.17. The width of the main lobe is $4\pi/M$. Hence, as M increases, the main lobe width becomes narrower, However the side lobes of $|W(\omega)|$ are relatively high and remain unaffected by increase in M. Though the width of each side lobe decreases with increase in M, the height of each side lobe increases with increase in M such that the area under each sidelobe remains invariant to changes in M. As M is increased $W(\omega)$ becomes narrower and the smoothing provided by $W(\omega)$ is reduced. The larger side lobes of $W(\omega)$ result in undesirable ringing effects in the FIR filter frequency response $H(\omega)$. These undesirable effects are best alleviated by use of windows that do not contain abrupt discontinuities in their time domain characteristics, and have low side lobes in their frequency domain characteristics. Table 4.3 below lists several window functions that possess desirable frequency response characteristics of the windows.

Table 4.3 Window Functions

Name of Window	Time- domain sequence W(n), $0 \leq n \leq M-1$
Hamming	$0.54 - 0.46Cos(2\pi n/M - 1)$
Hanning	$0.5 - 0.5Cos(2\pi n/M - 1)$
Blackman	$0.42 - 0.5Cos(2\pi n/M - 1) + 0.08Cos(4\pi n/M - 1)$

The frequency response characteristic of the Hanning, Hamming and Blackman windows is shown in Fig 4.18. All of these window functions have significant lower side lobes compared with the rectangular window. Also for the same value of M, the width of main lobe is also wider for these windows as compared to the rectangular window, as a result the transition region in the FIR filter response is wider. Table 4.4 summarizes these important frequency domain features of the various window functions.

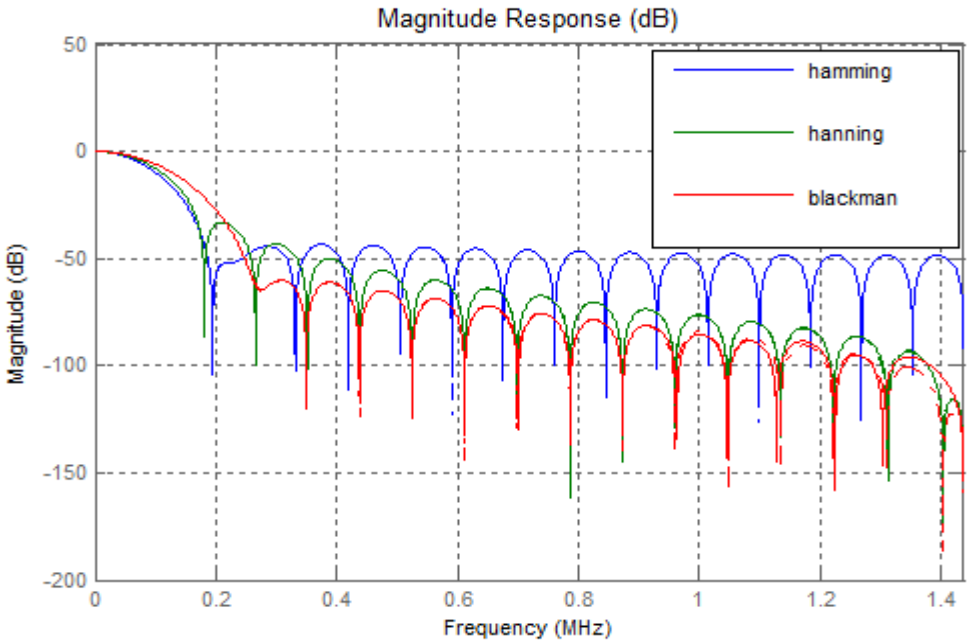

Fig 4.18 Frequency Response for Hamming, Hanning and Blackman window for M =33, Fc = 30 kHz and Fs =2.875 MHz

Table 4.4 Frequency Domain characteristics of some window functions.

Window Type	Approximate Transition width of main lobe	Peak side lobe(dB)
Rectangular	4π/M	-13
Hanning	8π/M	-32
Hamming	8π/M	-43
Blackman	12π/M	-58

4.5.2.1 FIR filter designed for NQR spectrometer.

Digital demodulator outputs I and Q components separately at rate of 23 MHz. The rate of data storage will be determined by spectral width of the NQR signal under interest which is at most few kHz. The oversampled data points can be used for digital filtering to get rid of frequency components lying outside the spectral width. Thus FIR filter with cut off frequency of 30 kHz can be designed but with sampling frequency of 23 MHz, the number of delay elements, multipliers and adders required will be more and thus needs more memory in FPGA. Thus sampling frequency can be decreased first by down sampling the digital demodulator outputs which is to be fed to FIR filters. Sampling leads to periodicity in frequency domain and the overlap of replicated signals in frequency domain (i.e. aliasing) is avoided if $F_s \geq 2 * F_m$(Nyquist Theorem). Anti-alias filter is required prior to down sampling to avoid aliasing as shown in Fig 4.19.

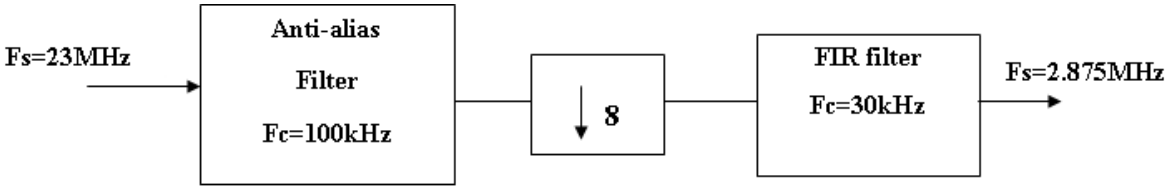

Fig 4.19 Block Diagram of FIR filter with down sampling

Here hamming window is used to design FIR filter as its peak side lobe is less as compared to hanning window and transition bandwidth is less as compared to Blackman window. The HDL code is written for FIR filter for various cut off frequencies. (shown in Fig 4.20)

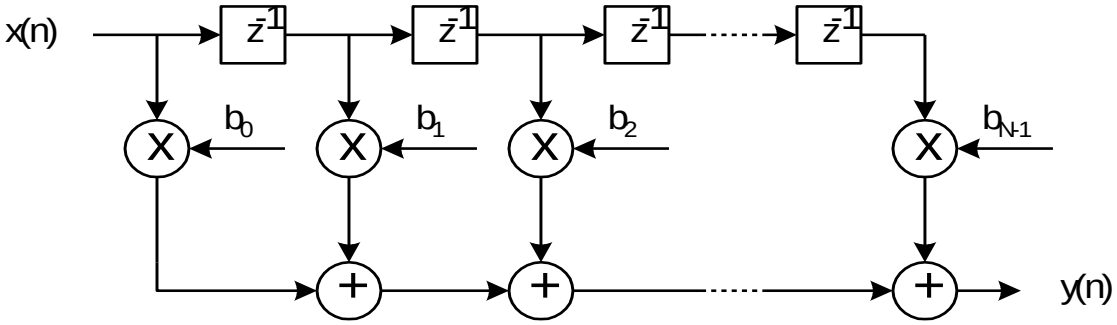

Fig 4.20 FIR filter implemented in FPGA.

The two filters implemented in FPGA as shown in Fig 4.19 are 100 kHz filter(anti-alias Filter) with $M = 33$ and $F_s = 23\,MHz$ and other one with $F_c = 30kHz$,$F_s = 2.875MHz$ and $M = 33$. The frequency response of the two filters is shown in Fig 4.21

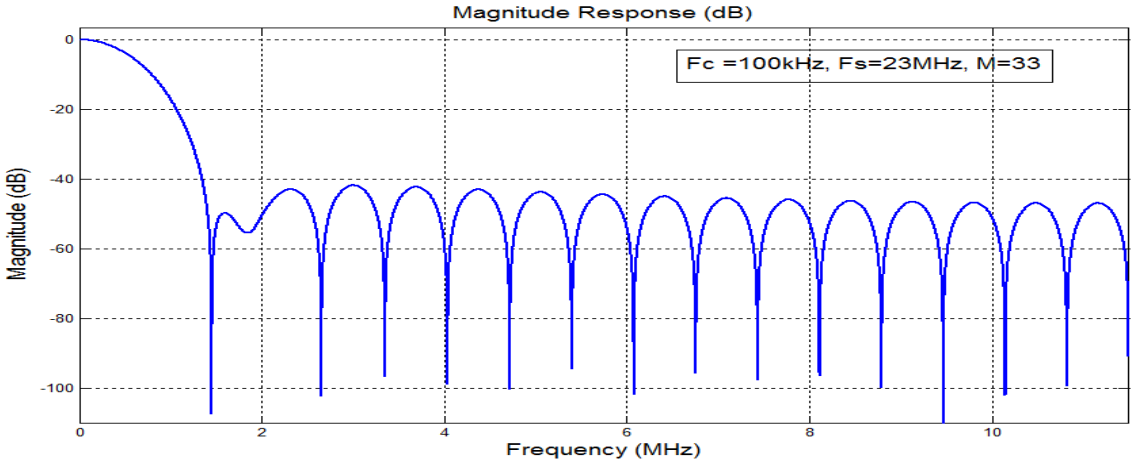

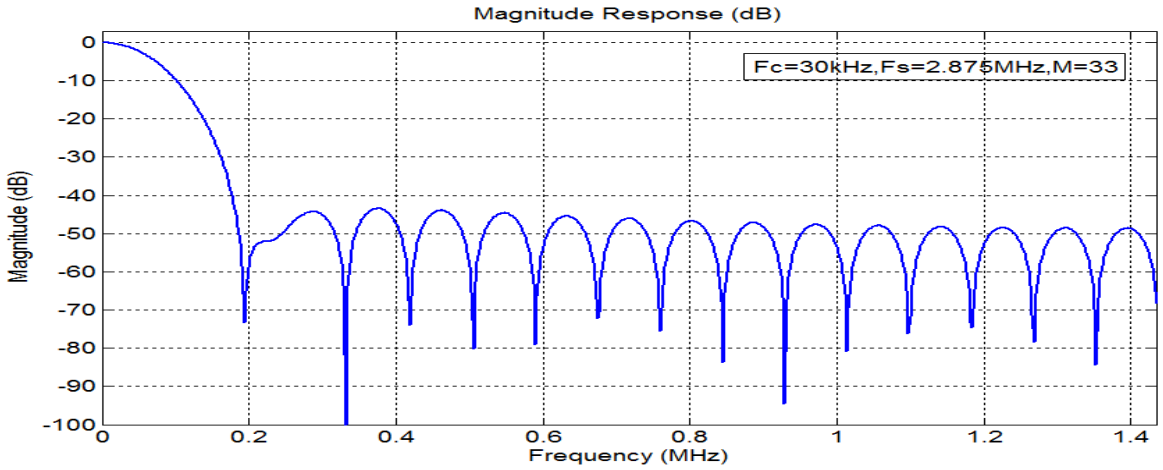

Fig4.21 Frequency response of FIR filters with M=33 a) Fc=100 kHz Fs=23 MHz b) Fc=30 kHz Fs=2.875 MHz

4.5.3 Data Acquisition and Signal Accumulator.

The signal intensity of ^{14}N NQR seldom exceeds the thermal noise signal therefore it can only be detected with high degree of reliability after multiple acquisitions. A memory module for storing the NQR signal is also prepared inside the FPGA using Dual Port RAM (DPRAM) module created by Quartus®- II Megawizard ™ plugin Manager. In the current NQR spectrometer, up to 16384 data points can be stored for each of the in-phase and quadrature signals at the rate of clock frequency =2.875 MHz, thus the signal of 5.7 ms duration can be stored .

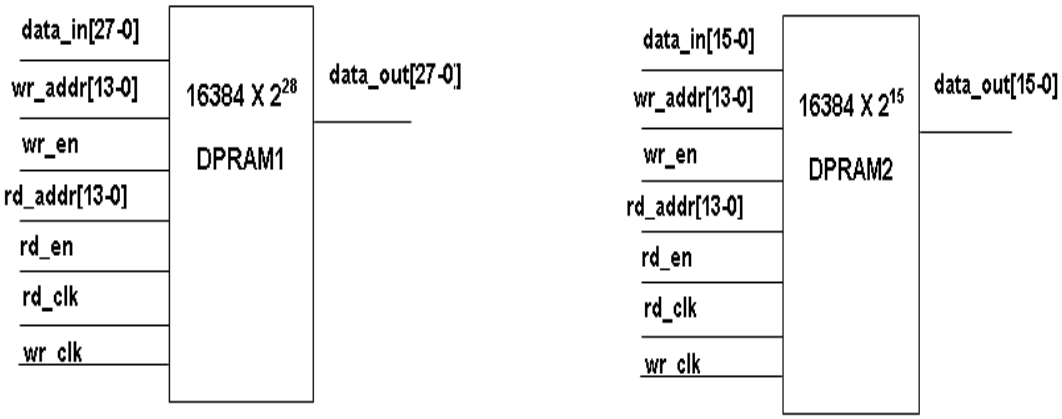

Fig 4.22 DPRAM implemented in FPGA.

Two Dual port RAMs were created from Megawizard. First one is used to store the additions of the multiple acquisitions and second one the average of the acquisitions. The provision is made for averaging up to 4096 signals and simultaneously storing the data in first DPRAM, thus the size of first DPRAM is (16384 X 2^{28}). The FIR outputs are stored and also accumulated in DPRAM1 so the rd_clk (Read Clock) and wr_clk (Write clock) has to be same as rate of output of FIR. When accumulation is over the data is divided by no. of signals and sent to DPRAM2 with wr_clk as same as the rate of FIR output. Then the averaged data is sent to PC at rd_clk =23 MHz. The block Diagram of DPRAMs is shown in Fig 4.22.

4.5.4 Pre-Amplifier

NQR signal is expected to be order of -100 dBm [62] so it needs to be amplified considerably before it can be observed on an oscilloscope. Three stages, each of which contains two amplifiers i.e. (BMC 1124 which is broadband RF amplifier of gain 14 dB with Noise figure of 6 dB.) are connected in series as preamplifier with total gain of 84 dB and noise figure of 6.74 dB to achieve necessary level of amplification of signal. The part of receiver which is outside FPGA is shown in Fig 4.23.

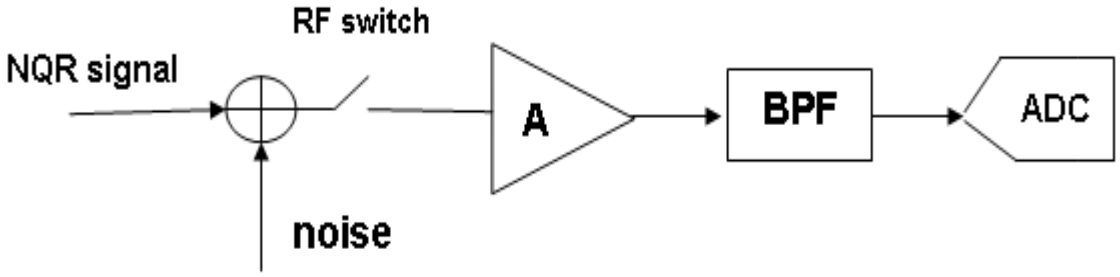

Fig 4.23 Receiver

The NQR signal comes to receiver through RF switch which is controlled by pulse programmer and generator in transmitter section. When RF pulse is ON, the RF switch is

OFF and thus receiver is disconnected by RF switch and protected when RF pulse is send to probe i.e. when transmitter is ON. When RF pulse ends, RF switch is closed and thus NQR signal is sent to the receiver. The amplifier was tested without RF switch and band pass filter, the gain obtained was 85 dB. Gain with only RF switch connected 83.9 dB, with both switch and band pass filter connected the gain was 82.12 dB. Thus the loss in RF switch is 1.10 dBm and loss in BP filter is 1.78 dBm.

The amplifier was tested with the whole NQR system and the minimum value which amplifier can detect is -100 dBm signal and as there is provision of averaging the signal for 4096 times, which increased the SNR by 36dB and thus it can detect the signal of -136 dBm at the input of receiver.

4.5.5 Band Pass Filter

At the end of the preamplifier a band pass filter centered at NQR signal frequency is cascaded to further reduce the noise and improve signal to noise ratio. Filter was simulated using Genesys software with centre frequency 4.64 MHz and bandwidth 500 kHz is shown in Fig. 4.24.

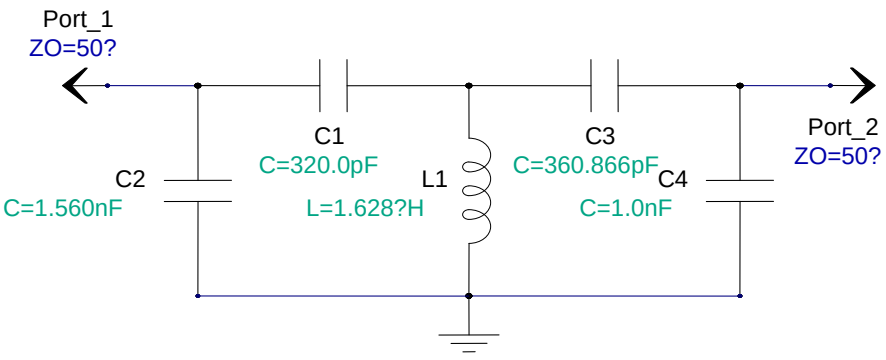

Fig 4.24 Band Pass filter

4.6 Application Software

The application software used in this work is CVI through which all communication to FPGA is done via PCI bus. GUI developed in CVI for present work is shown in Fig.4.25

Applications for pulse programmer, DDS, data acquisition, coherent averaging are written here. The programs can be referred in Appendix B. All the inputs like intial delays (ID_0, ID_1), time width (TW_0,TW_1), time from start to transmitter on(Tst), Time from transmitter off to receiver on (Ttr), time for acquisition(T_Acqon), time from receiver on to acquisition on(Tra),time from acquisition off to receiver off (Tar). Time to repeat the sequence(Next_seq) can be changed from application side. Similarly the frequency to the DDS can be changed during the experiment. Number of Averages for coherent averaging, filter bandwidth for FIR filter, number of pulses to observe FID or spin echo is also given from application side.

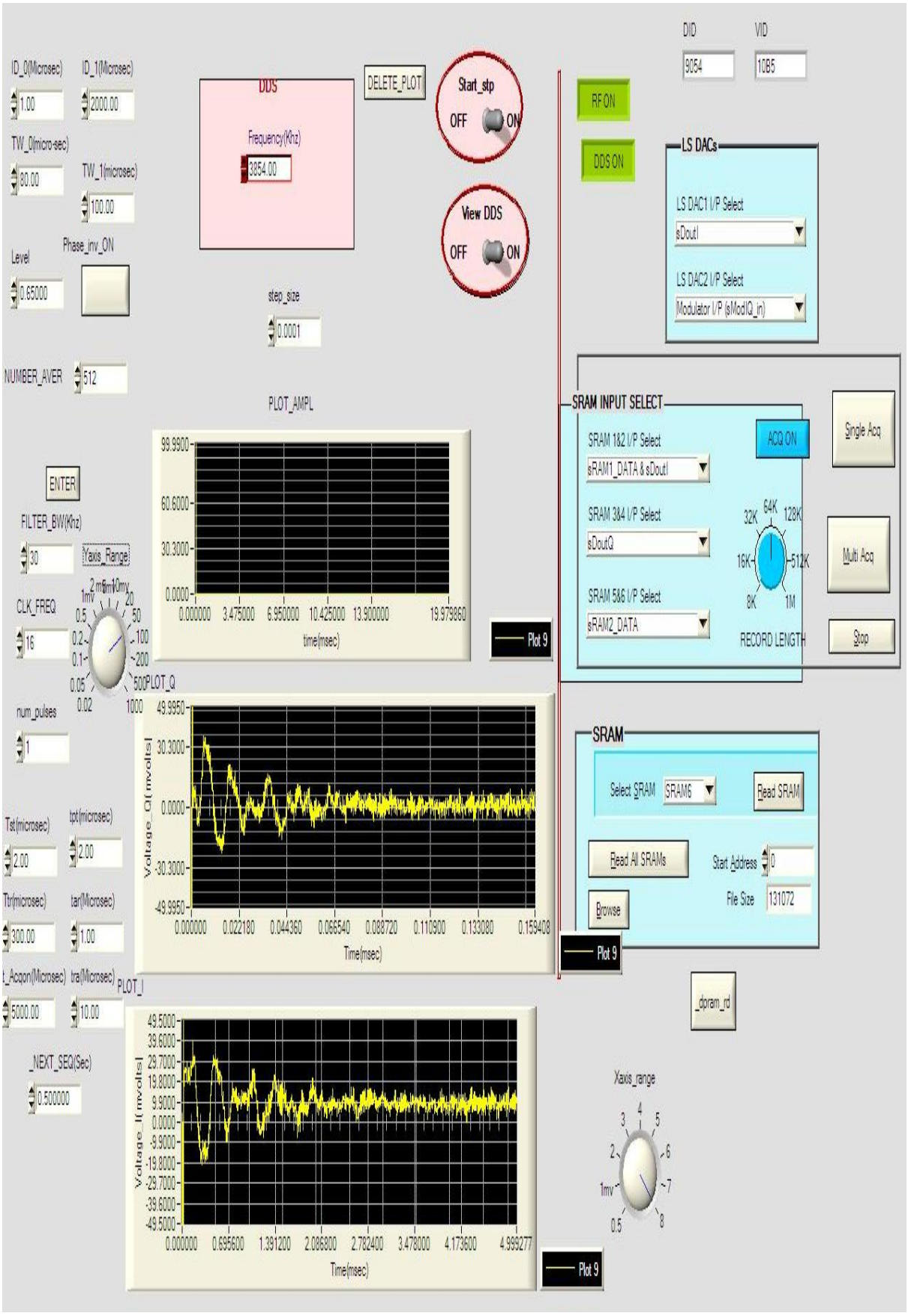

Fig 4.25 Application and GUI developed in CVI for NQR/NMR spectrometer.

4.7 Troubles and Rectifications

As the design of spectrometer was over the transmitter and receiver were tested separately as follows.

Receiver: The gain of the preamplifier was tested with a known small (5 micro volts) signal to obtain gain times the input. Then the tuned probe is connected through the preamplifier to the rest of the receiver circuit and a small voltage is induced using separate coil (6 mm diameter) and function generator. The output of receiver was observed. These two tests made sure that receiver is working and also it is sensitive to detect weak signals.

Transmitter: An RF pulse was applied to the sample coil through cross diodes and quarter wave transformer and single turn coil of 6 mm diameter was used to catch the signal to observe the signal on scope. This test made sure that power is actually going in the sample of coil.

The sample of $NaNO_2$ was used to observe ^{14}N NQR signal. But initially with power of 200 W, L =8 μH, C_T =115 pF C_M= 18pF sparking was observed. Though the capacitors are high voltage vacuum variable capacitors, the voltage could reach up to Q times the applied voltage i.e. (100 volts (200 watts)) which is approximately 6000 V which is a above capacitors rating. The voltage at capacitors was reduced by reducing the RF power. It was required to increase the pulse length to a value that is comparable to the T_2^* (0.7 ms) of the $NaNO_2$. Thus the power was reduced to 120 W then to maximize the strength of ^{14}N NQR $\pi/2$ pulse length was obtained by using a single turn 6 mm diameter probe to calculate the field generated in the sample coil. The B_1 of 40.63 G was obtained with the experiment and calculations and from equation no. [2.6] $\pi/2$ pulse width was calculated as 20 μs. Thus with power of 120 W and τ = 20 μs the experiment was started by scanning the frequency from 4.6 MHz to 4.7 MHz at the intervals of 10 kHz.

4.9. Comparison of the current thesis with one of the similar NQR based Detection system.

The system [59] is an customized IC based low-power compact NQR based explosive detection system which also consists of a transmitter section, an NQR probe , a receiver section and auxiliary modules similar to the system " FPGA based NQR system" developed as a part of this thesis. It also has an RFI probe to mitigate RFI. This system is an IC based system where all the front-end circuits, including LNA, pre-amplifier, analog adaptive filter are integrated on a customized IC with a microcontroller unit (MCU) circuit. The MCU is used for the coordination and timing sequence control of the system. In the TX section, Class-D type switching voltage power amplifier is used to provide high power efficiency during the transmitting period. More importantly, the Class-D power amplifier has very low standby power consumption during the receiving period, which is proven to be the most significant power saving advantage compared to traditional Class-AB power amplifiers used in the current thesis.

The receiver section consists of LNAs, an adaptive filter for RFI mitigation and an advanced DSP platform for NQR signal processing. The LNA is an infinite input impedance power matching scheme, which improves noise figure and simplifies the circuit structure. A continuous time least mean square adaptive filter is employed to mitigate RFI in analog domain.

Between transmitter and receiver, a power multiplexing scheme is used in order to use a single probe for both transmitting and receiving. A PIN diode based RF switch is used here in place of traditional quarter impedance transformer to provide high isolation during transmitting and low signal attenuation during receiving.

For the NQR signal processing, a DSP based data processing platform is to provide not only powerful and versatile signal processing capability, but also low volume and low power consumption.

The best spectrometers those are commercially available for eg. developed by **Jecmag, Bruker, JEOL, Varian/ Agilent** are expensive, not usually capable of operating at low frequencies and are also not specifically designed for NQR. So the NQR spectrometer developed as part of the thesis cannot be compared to these spectrometers. All NQR systems which are developed are laboratory based systems (also discussed in Chapter 1). The table 4 comparison between some of the laboratory based systems with the system developed as a part of the thesis based on general requirements for the NQR detection systems.

Table 4.5 Comparision between various laboratory based NQR detection systems.

General Requirements	Takeda[21]	Ferrari[20]	Begus[22]	Zhang [83]	System developed as part of this thesis
Programmable RF sequence signal source	DDS	DDS	Software Defined Radio(SDR)	Digital oscillator and control	DDS
Power amplifier with a high power level	-	-	Op-amp Based amplifier	Class D	Class AB
Power multiplexing	λ/4–RF switch	λ/4 –RF switch	-	PIN diode RF switch	λ/4–RF switch with lumped circuit
Power matching for LNA	50 Ω	50 Ω	-	Infinite input impedance	50Ω
RFI mitigation	-	-	-	Analog Adaptive filter	ALE ,Wavelet Transform
Digital Processing and Acquisition	FPGA	DSP	SDR	DSP	FPGA, Lab view
Signal processing chain circuit implementation	FPGA	Discrete off the shelf components	Customized IC	Customized IC	FPGA

Chapter 5

NMR and NQR signal Detection

As discussed in chapter 2 there are two popular methods of observing NQR/NMR signals i.e. FID using a single pulse excitation and spin echo using a double pulse excitation. The choice of the sequence depends mainly on the relaxation time (T_2^*) of the sample. For a long relaxation time of milliseconds as in the case for ^{14}N signal from $NaNO_2$, a single pulse sequence is appropriate and for a short relaxation time of microseconds as in the case NMR of ^{1}H and ^{2}H double pulse sequence is used to observe a spin echo.

The stable nitrogen ^{14}N has natural abundance of 93.6% and nuclear spin I = 1 with its associated nuclear electric quadruple moment of 0.0193e barns (where e is the electronic charge) [63]. The ^{14}N NQR transitions in various solids fall in the frequency range 0 to 6 MHz [64]. Hence ^{14}N was chosen for the design. ^{14}N NQR signal from sample of 20 g of $NaNO_2$ was observed at a frequency of 4.64 MHz. With the addition of permanent magnets ^{1}H and ^{2}H, NMR signals from H_2O and D_2O were detected. Observation of Proton NMR is easy as the strength of this signal is strong as compared to ^{14}N NQR signals therefore to standardize our spectrometer, we have observed ^{1}H NMR.

5.1 ^{14}N NQR signal from $NaNO_2$

The test of developed NQR/NMR spectrometer started with ^{14}N NQR signal of Sodium Nitrite. The coil which is used here is of value L=6 μH, made out of 17 AGW copper wire and has 32 turns of 40mm length and 20mm diameter. The probe is tuned and matched to 50 ohms with C_T = 162 pF and C_M = 33 pF. Here 20g of $NaNO_2$ is placed inside the solenoidal coil. RF excitation pulse length of 20 μs and power of 120 W was used for

excitation. The pulse length is selected such that it is a $\pi/2$ pulse, to get maximum amplitude of FID.

First, the power was kept constant and pulse width was increased. Then pulse width was kept constant and the power was increased. The resultant value of 20 μs as pulse width and power of 120 W was obtained which matches with equation [2.6 and 2.7] approximately. The entire cycle is repeated after every 0.5 s (large compared to the T_1 of 0.1 s) [65]. After RF pulse, the receiver records 5 ms of NQR signal. The detection cycle is repeated for averaging the NQR signal for 1024 times. The signal strength is at the expected level of 6 μV. The ^{14}N NQR signal from $NaNO_2$ shown in Figure 5.1.The observation frequency is 4.64 MHz where as the signal is off resonant by about 2500 Hz resulting in oscillatory FID. T_2^* was calculated to be 700μs.

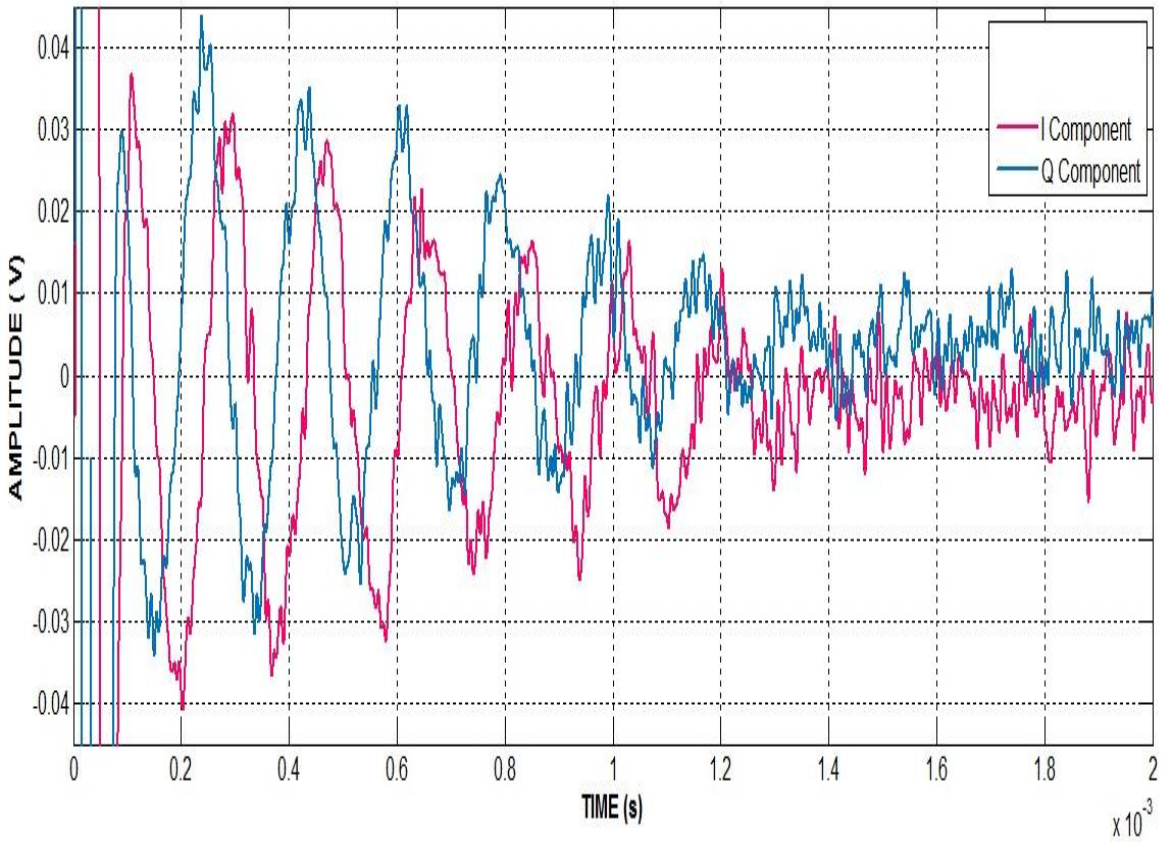

Fig 5.1 ^{14}N NQR signal from $NaNO_2$

5.2 ^{1}H NMR signal from H_2O

The NQR spectrometer was modified to NMR spectrometer by placing the coil in a permanent magnet. Here sample in a coil was placed between poles of a horse shoe magnet of magnetic field 1.35 kG and as the T2* of proton is around 100 μs, FID will merge into ringing so two pulse excitation was used to observe spin echo. The probe is modified to coil of 4.5 μH with C_T = 178.3 pF and C_M= 37.3 pF. A small quantity of ferric nitrate is added in order to reduce the T_1(14s) of pure water.

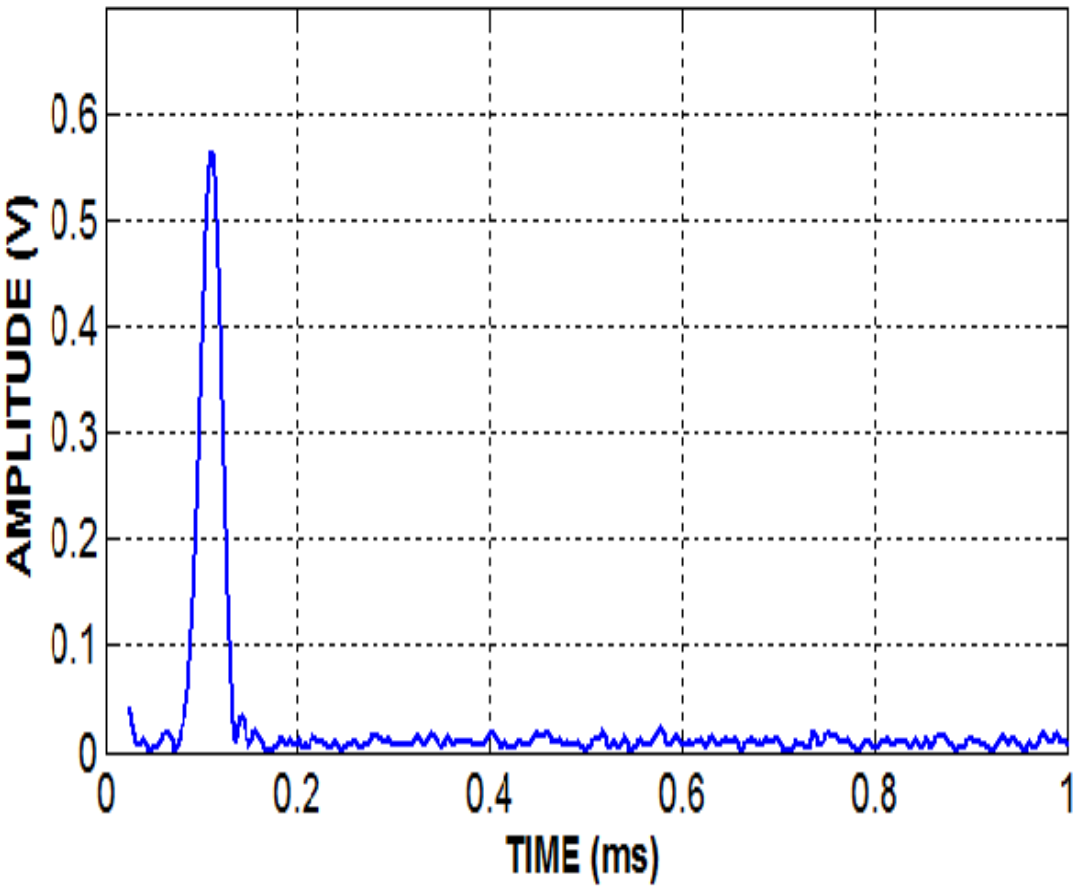

Figure.5.2. ^{1}H NMR signal from H_2O .

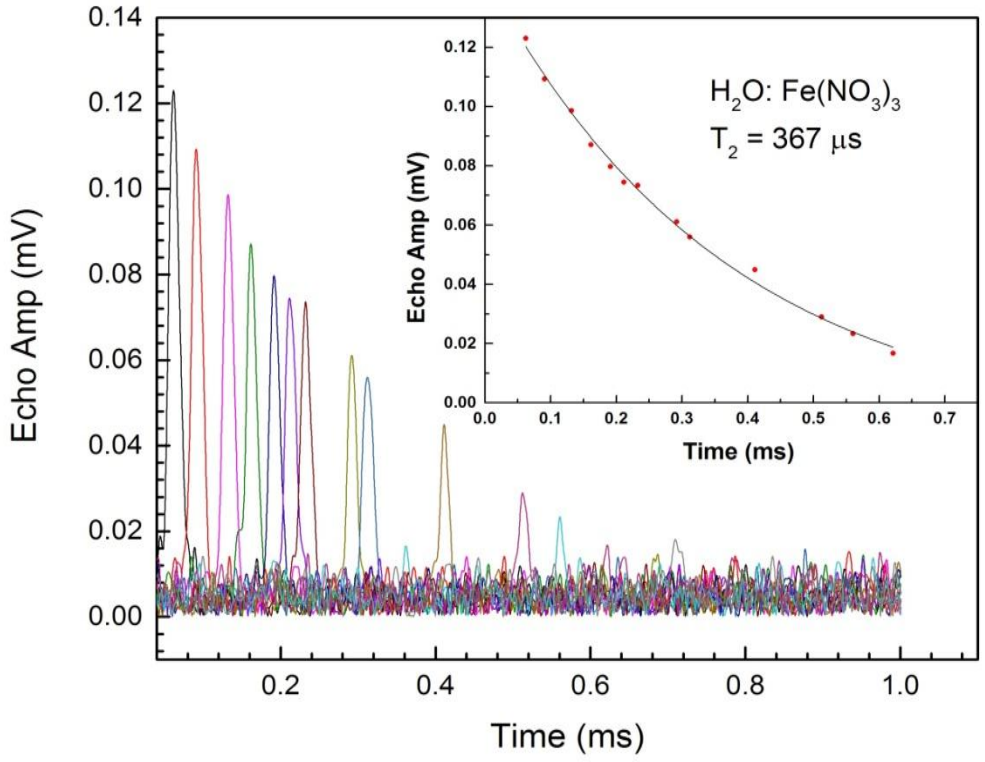

Fig 5.3 T_2 measurement of NMR signal of ^1H in H_2O.

Fig 5.2 shows the spin echo (^1H from H_2O:$FeNO_3$). The observation frequency is 5.765 MHz as per equation 2.1. We used two RF pulses with pulse widths, $t_1 = 5\ \mu s$, $t_2 = 10\ \mu s$, and spacing between pulses as $\tau = 200\ \mu s$, RF excitation power was about 70 W. The power and pulse width was selected (from equation 2.6 and 2.7) such that t_1 is a $\pi/2$ pulse. The entire cycle was repeated every 0.5 s. The signal strength was 50 µV. The trace shown in Figure 5.2 is the signal after averaging for 256 times. The two pulse experiment was performed for measuring T_2 by varying the spacing between the pulses. Figure 5.3 shows that T_2 for ^1H in water is 367 µs.

5.3 ^{2}H NMR signal from D_2O

The γ for deuterium is $41.065\ X\ 10^6$ rad/Tesla, hence the magnet used for observing proton cannot be used with same setup, thus the magnet with a magnetic field of 5.85 kG was used here to observe the spin echo of deuterium from D_2O. The probe was modified here with 30 guage, 75 turns, length = 25mm, diameter=10mm coil of value 18.5 µH with C_T =64.6 pF and C_M =25.5 pF. The deuterium signal is shown in Figure 5.4. The observation frequency is 3.855 MHz

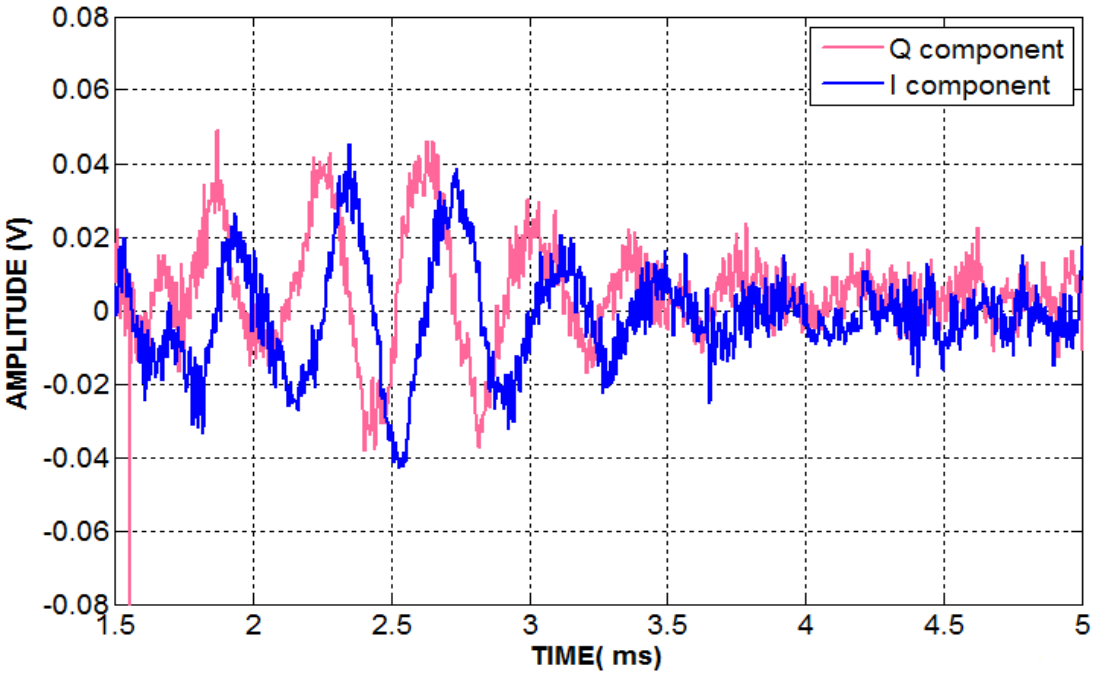

Fig 5.4: ^{2}H NMR signal from D_2O.

The spin echo was observed using two pulse sequence with $t_1 = 5$ µsec,$t_2 =$ 10 µs,$\tau = 2.5\,ms$. RF excitation power was about 200 W. The widths of RF pulses for echo observation were calculated from eq. 2.6 and 2.7 such that t_1 is π/2 pulse. The sequence was repeated for 128 times to observe the sequence.T_2^* of ^{2}H form D_2O was calculated as 1 ms.

Chapter 6

Post processing of NQR signals

In field, the time required to detect the NQR signal is an important parameter. While, the main challenge for NQR techniques is the extremely poor signal to noise ratio (SNR), variations in the other parameters like temperature could also influence the signal strength and position. Under such conditions, improving SNR by averaging response to repetitive excitations could prove futile. The rate at which RF pulse has to be repeated depends on physical parameters of nuclear relaxation, which are, T_1 and T_2. In practice we can apply a pulse sequence of length T_2 and repeat the pulse sequence every T_1. For most of explosives the relaxation times are very long (100 ms - 1s) which lead to long detection times [1].

The signal shown in Figure 5.1 is ^{14}N NQR signal observed from $NaNO_2$. The SNR of the NQR signal after one pulse was low (-12dB) so the SNR was improved by accumulation of 1024 times.

As we cannot shorten the relaxation times, much effort has been put into increasing the sensitivity of receiver and improving signal detection technique. To improve SNR per unit time several other techniques have been used i.e. FIR filter [66], wavelet transform [67], and adaptive filter [68]. FIR filter is generally based on prior knowledge of signal. Adaptive filter algorithms are used in this work as these do not need prior knowledge of signal and also parameters of adaptive filter changes to meet the optimization parameters.

6.1 Wavelet De-noising

Wavelet, filter bank and multi-resolution are used independently in field of signal processing [69]. Wavelet decomposes the signal into different frequency bands and de-noising is done in each frequency band. The efficiency of Wavelet Transform over Fourier Transform is compared by G.V. Mozzhukhin and S.V. Molchanov [70] and they proved that Wavelet Transform is better than Fourier Transform for NQR response in terms of removing noise. They showed result of Donoho–Johnstone method for selecting threshold value for de-noising. De-noising is performed on every detailed coefficient.

Nagendra H has shown that how non-stationary ECG signal is represented in time and frequency domain together by Wavelet Transform [71]. Soft and hard thresholding can be used for Wavelet Transform de-noising [72, 73]. Four different thresholding methods, Minimax Criterion, Sqtwolog Criterion, Rigrsure and Heursure are compared by Neema [74].

Fourier transform filters, which can remove noise effectively, could fail when noise shares the same frequency band with signal. Wavelet transform is a powerful tool in such cases because it provides multi-resolution analysis of same signal.

The basic idea behind wavelet transform based signal processing is to analyze same signal with different scale. Wavelet is function which satisfies certain mathematical requirement [75]. Wavelet function has two different parameters: dilation and translation. By changing dilation parameter same signal can be presented and analyzed at different resolution. If large window is taken in time domain then it gives small frequency information (low frequency signals) and small window is taken in time domain gives more information (high frequency signals) in frequency domain. By changing the translation parameter signal can be shifted left or right within same dilation parameter [76]. If dilation parameter is changing in power of 2 and translation parameter is changing in integer then it is called as

Daubechies Wavelet Family. The main wavelet function in which these changes are done called “Mother Wavelet Function” and derived functions called “Child Wavelet Function”. If *s* is dilation parameter and *l* is translation parameter then Mother Wavelet Function is given by Eq. 6.1,

$$\Psi(s,l) = 2^{-\frac{s}{2}}\Psi(2^{-s}t - l) \qquad [6.1]$$

This mother wavelet function is convolved with signal to perform wavelet transform on signal.

In wavelet transform signal is decomposed into low frequency and high frequency components, where low frequency components are basically signal part, called as approximation coefficient and high frequency components are noise part, called detailed coefficient. Wavelet de-noising is carried out by soft & hard thresholding on wavelet transform coefficients. There are mainly three steps involved in wavelet thresholding.

- Decomposition: Signal is decomposed in approximation and detailed coefficients. The approximation coefficients are still further decomposed into next level of approximation and detailed coefficients. This process is repeated till desired level N is achieved.
- Detailing: For each level 1 to N, a threshold value is determined and thresholding is done on each detailed coefficients. It removes the noise content at each levels of detailed coefficient.
- Reconstruction: Filtered signal is reconstructed with modified detailed coefficients and approximant coefficient. Thus reconstructed signal is filtered at different frequency scales.

6.2 Adaptive filters

An adaptive filter is a self-modifying digital filter that adjusts its coefficients in order to minimize an error function. This error function, also referred to as the cost function, is a distance measurement between the reference or desired signal and the output of the adaptive filter [74].

The basic configuration of an adaptive filter, operating in the discrete-time domain is shown in Fig 6.1. In such a scheme, the reference signal is denoted by $x(n)$, the primary signal $d(n)$ represents the desired output signal (that usually includes some noise component), $y(n)$ is the output of the adaptive filter, and the error signal is defined as

$$e(n) = d(n) - y(n). \qquad [6.2]$$

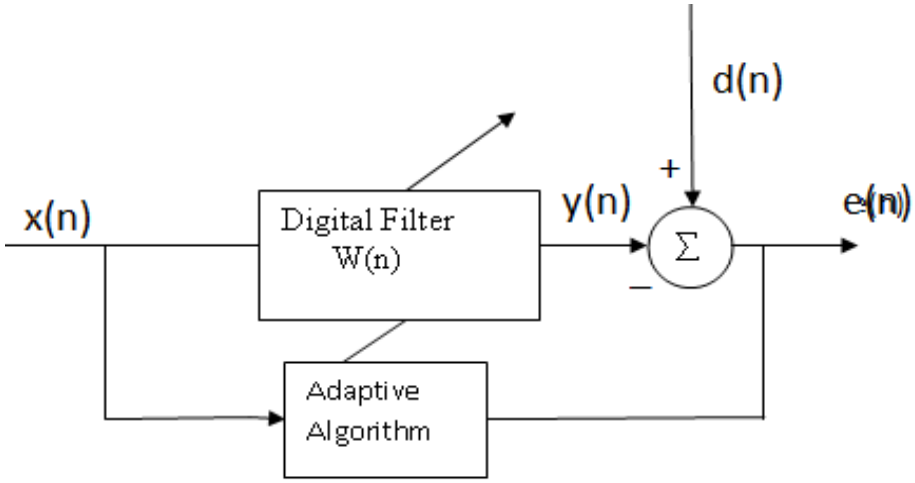

Fig 6.1 Adaptive Filter

The error signal is used by the adaptation algorithm to update the adaptive filter coefficient vector $\boldsymbol{w}(n)$ according to some performance criterion. In general, the whole adaptation process aims at minimizing error signal, forcing the adaptive filter output signal to approximate the reference signal in a statistical sense.

6.2.1 Adaptive Noise Cancellation

Adaptive Noise Cancellation (ANC) and Adaptive Line Enhancement (ALE) are two adaptive filtering systems with similar mechanisms but slightly different designs [74]. The ANC has two sensors as shown in Fig 6.2 to receive target signal and noise separately. The primary signal $d(n)$ is signal and noise No together and reference signal $x(n)$ is noise N_I which is uncorrelated to signal but correlated to noise No.

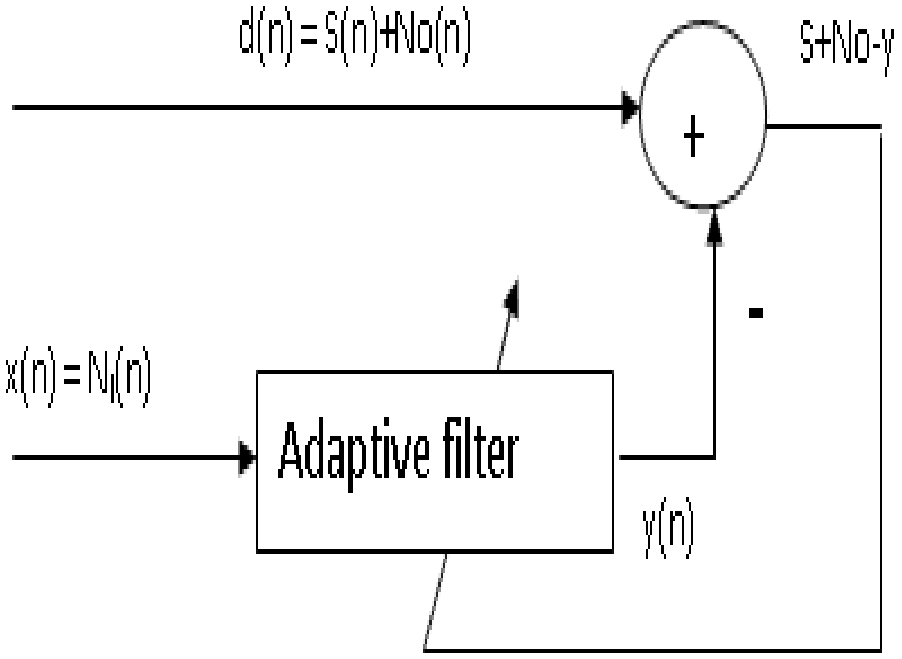

Fig 6.2 Adaptive Noise Cancellation

The reference signal pass through the adaptive filter and output $y(n)$ is produced as close a replica as possible of $N_o(n)$. The filter readjusts its coefficients continuously to minimize the error between $N_o(n)$ and $y(n)$ during this process. The output $y(n)$ is subtracted from the primary input to produce the system output $e = S + No - y$, which is filtered signal. The error signal $e(n)$ provides the system control signal and updates the adaptive filter coefficients, which minimizes the residual noise.

6.2.2 Adaptive Line Enhancer

The ALE shown in Fig 6.3 is a simplified form of ANC [75]. ANC has two inputs namely, the primary signal $d(n)$ (signal + noise) and a reference signal $x(n)$ (noise) while ALE needs only the primary signal. The second input is generated by delaying the primary signal suitably.

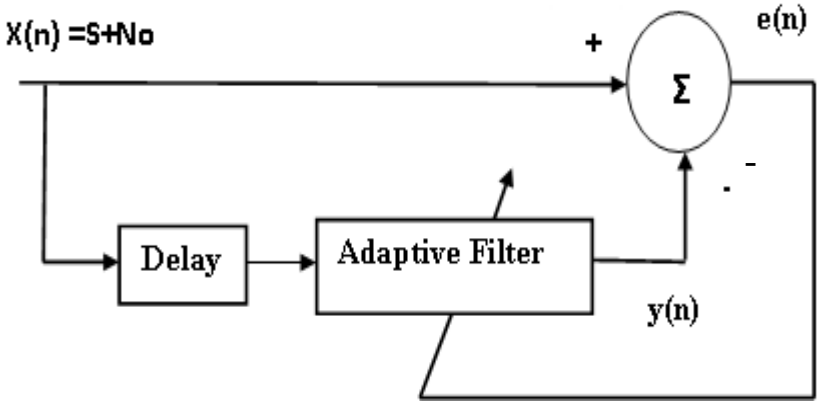

Fig 6.3. Adaptive Line Enhancer

The process depends on the fact that the correlation time (or correlation length = τ_d) of broadband noise is shorter than the narrowband signal. So by suitably delaying the primary signal one can generate the second signal that is still correlated to the signal and not correlated to the noise. The adaptive filter responds by forming a transfer function equivalent to that of narrowband filter centered at frequency of narrowband signal. The output $y(n)$ of the adaptive filter in the ALE is an estimate of the noise free input signal. Delay Δ is selected such that Δ is longer than $\tau_d(BB)$ i.e correlation length of broadband noise and smaller than τ_d (NB) correlation length of narrowband signal, beyond these lags, the respective correlations die out quickly.

$$\text{i.e. } \tau_d\,(BB) < Delay\,(\Delta) < \tau_d(NB) \qquad [6.3]$$

6.2.3 Adaptive Filter Structure

The adaptive transversal FIR structure, whose input–output relationship is described by:

$$y(n) = w_0\ x(n) + w_1 x(n-1) + \cdots\ +\ w_N x(n-N)$$

$$= \sum_{k=0}^{N} w_k x(n-k)$$

$$= w^T x(n). \qquad [6.4]$$

Where, N is the filter order and $x(n)$ and w are vectors composed by the input signal samples and the filter coefficients, respectively; that is

$$x(n) = [x(n)\ x(n-1)x(n-2) \ldots\ldots\ldots\ldots x(n-N)]^{\ T},$$

$$w = [w_0\ w_1 \ldots\ldots w_N]^T.$$

6.2.3.1 Adaptive Algorithm

Adaptation of the filter coefficients follows a minimization procedure of a particular objective or cost function. This function is commonly defined as a norm of the error signal $e(n)$. The most commonly employed norms are the mean-square error (MSE) which is described below [77].

The MSE is defined as

$$\xi\ (n) = E[e^2(n)] = E[|d(n) - y(n)|^2] \qquad [6.5]$$

Writing the output signal $y(n)$ as given in Equation (6.2), one obtains,

$$\xi\ (n) = E[e^2(n)] = E[|d(n) - w^T x(n)|^2]$$

$$= E[d^2(n)] - 2w^T E[d(n)x^T(n)] + w^T E[x(n)x^T(n)]w$$

$$= E[d^2(n)] - 2w^T \boldsymbol{p} + w^T \boldsymbol{R} w \qquad [6.6]$$

where $\boldsymbol{R}$ and $\boldsymbol{p}$ are the input-signal correlation matrix and the cross-correlation vector between the reference signal and the input signal, respectively, and are defined as

$$\boldsymbol{p} = E[d(n)x^T(n)],$$

$$\boldsymbol{R} = E[x(n)x^T(n)].$$

From Equation (6.5), the gradient vector of the MSE function with respect to the adaptive filter coefficient vector is given

$$\nabla_w \xi(n) = -2\mathbf{p} + 2\mathbf{R}\mathrm{w} \qquad [6.7]$$

The wiener solution w_0, that minimizes the MSE cost function, is obtained by equating the gradient vector in Equation (6.6) to zero.

$$w_0 = \boldsymbol{R}^{-1}\boldsymbol{p} \qquad [6.8]$$

The MSE is a cost function that requires knowledge of the error function $e(n)$ at all time n. Thus, the MSE cannot be determined precisely in practice and is commonly approximated by other cost functions. The simpler form to estimate the MSE function is to work with the Instantaneous Square Error (ISE) [74] given by

$$\xi(n) = e^2(n)$$

$$\nabla_w \xi(n) = 2\mathrm{e(n)}\nabla_w e(n)$$

$$= 2\mathrm{e(n)}\nabla_w [d(n) - w^T x(n)]$$

$$= -2\mathrm{e(n)}x(n) \qquad [6.9]$$

6.2.3.2 LMS AND Normalized-LMS Algorithms

Determining the Wiener solution for the MSE problem requires inversion of matrix ***R***, which makes Equation (6.7) hard to implement in real time. One can then estimate the Wiener solution, in a computationally efficient manner, iteratively adjusting the coefficient vector w at each time instant n, in such a manner that the resulting sequence $w(n)$ converges to the desired w_0 solution, possibly in a sufficiently small number of iterations.

The steepest-descent scheme searches for the minimum of a given function following the opposite direction of the associated gradient vector. A factor $\mu/2$, where μ is convergence factor, adjusts the step size between consecutive coefficient vector estimates, yielding the following updating procedure:

$$w(n) = w(n-1) - \frac{\mu}{2} \nabla_w \xi(n) \qquad [6.10]$$

This iterative procedure is illustrated in Fig 6.4 for the one-dimensional coefficient vector

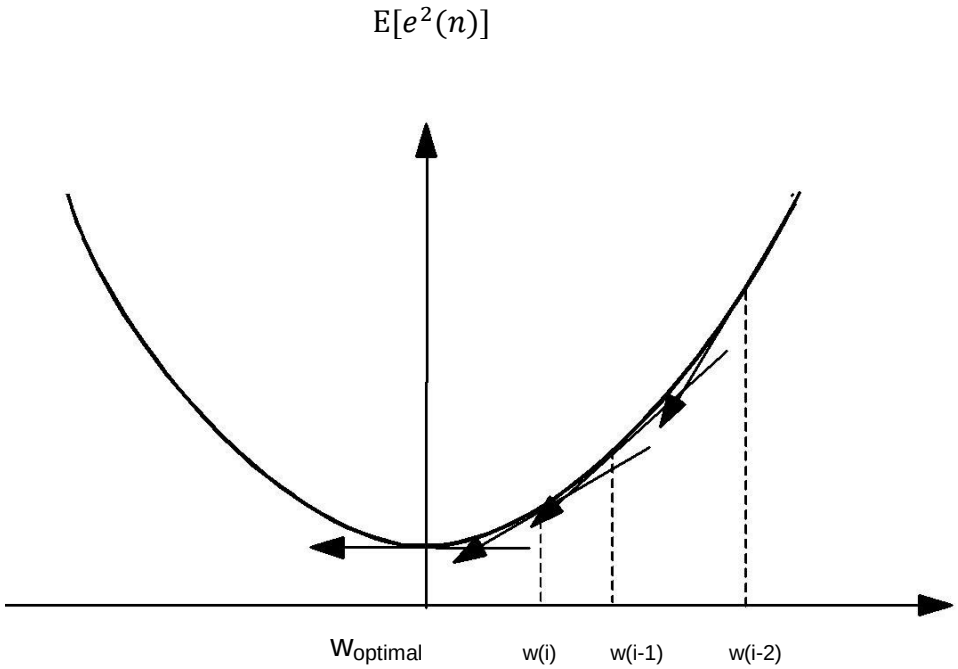

Fig 6.4 Steepest Descent Method

The wiener solution requires knowledge of the autocorrelation matrix $\boldsymbol{R}$ and the cross-correlation vector $\boldsymbol{p}$, that requires access to the complete second-order statistics of signals $x(n)$ and $d(n)$, what makes equation (6.8) unsuitable for most practical applications. A rather simpler approach is to approximate the MSE by the Immediate Square Error (ISE) function, using the gradient vector of the latter, given in Equation (6.8), to adjust the coefficient vector in equation (6.9). The resulting algorithm is the LMS algorithm is given by

$$w(n) = w(n-1) + \mu e(n)x(n) \quad [6.11]$$

$$e(n) = d(n) - w^T(n-1)x(n) \quad [6.12]$$

An approximation for the upper bound of this parameter is given in [74] and may be stated as

$$0 < \mu < 2/\lambda_{max} \quad [6.13]$$

Where λ_{max} is the maximum Eigen value of input signal $x(n)$. Maximum convergence is achieved when

$$\mu = 2/(\lambda_{max} + \lambda_{min}) \quad [6.14]$$

The LMS algorithm [74] is very popular and has been widely used due to its extreme simplicity. Its convergence speed, however, is highly dependent on the condition number ρ of the input-signal autocorrelation matrix, defined as the ratio between the maximum and minimum Eigen values of this matrix. The Normalized LMS (NLMS) algorithm normalizes the convergence factor such that the relation

$$w^T(n)x(n) = d(n) = w^T(n-1)x(n) + \mu e(n)x^T(n)x(n) \quad [6.15]$$

is always satisfied. This results in variable step size parameter given by

$$\mu(n) = 1/x^T(n)x(n) \qquad [6.16]$$

In practice this factor is modified to

$$\mu(n) = \mu'/(\varepsilon + x^T(n)x(n))$$

$$0 < \mu' < 2 \qquad [6.17]$$

6.3 Performance of ALE under different parameters such as SNR of input signal and value of delay.

The structure of an adaptive line enhancer is illustrated in Fig 6.3. The input signal composed of a harmonic signal $S(n)$ plus broadband background noise $N_o(n)$ is input to two channels. One is treated as the expected signal to an adaptive filter. The other goes through a delay Δ and then acts as a reference input signal to the adaptive filter. The adaptive filter will adjust its coefficients according to the principle of least mean square error between its output and the expected signal. After the optimum processing of the adaptive iteration, the output $y(n)$ of the ALE system will suppress the wide band noise, and enhance the harmonic signal, which is called the adaptive line enhancer.

6.3.1 The optimal weights of an Adaptive filter.

According to Fig 6.3 input signal $x(n) = S(n) + No(n)$ where No is wideband background noise and $S(n)$ is harmonic signal.

$$S(n) = Ae^{j\omega nT} \qquad [6.18]$$

where A is the amplitude of the signal, ω is the frequency of the signal $S(n)$ and T is the sampling time of the signal $S(n)$.

For Adaptive Transverse Filter structure, the following vectors are defined.

$$X(n) = [x(n), x(n-1) \dots \dots \dots . x(n-L+1)]^T \quad , \qquad [6.19]$$

$$W(n) = [\, w^n(0)\, w^n(1),\, w^n(2) \dots \dots \dots \dots w^n(L-1)]^{\,T} \, , \qquad [6.20]$$

$$\boldsymbol{q} = \left[\, 1, e^{-j\omega} \quad , e^{-j2\omega} , \dots \dots \dots . e^{-jL\omega}\right]^T \, , \qquad [6.21]$$

$$S(n) = Ae^{j\omega nT} . \boldsymbol{q} \, , \qquad [6.22]$$

$$S(n-\Delta) = Ae^{j\omega(n-\Delta)T} . \boldsymbol{q} \quad , \qquad [6.23]$$

where $x(n)$ is the input vector, $w(n)$ is the weight vector of the adaptive filter and $\boldsymbol{q}$ is the factor vector of the adaptive filter. $S(n)$ is the vector of simple harmonic signal, L is the length of the adaptive filter.

The autocorrelation matrix of the simple harmonic signal is given by:

$$R_{ss} = E(S(n).S(n)^T) = A^2 \boldsymbol{q}.\boldsymbol{q}^T \, . \qquad [6.24]$$

and autocorrelation matrix of white noise $N_o(n)$ is

$$R_{nn} = S_n^2 \quad . I_{,} \qquad [6.25]$$

where S_n^2 is the power of noise N_o and I is the unit matrix.

Considering the independence of signal $S(n)$ with noise $N_o(n)$ the autocorrelation matrix R_{xx} of the filter input is given below.

$$R_{xx} = E[x(n).x(n)^T] = E[x(n-\Delta).x(n-\Delta)^T], \quad [6.26]$$

$$R_{xx} = R_{ss} + R_{nn}. \quad [6.27]$$

Similarly cross correlation matrix of the input $x(n-\Delta)$ with $x(n)$ is expressed as:

$$R_{xd} = E[x(n).x(n-\Delta)^T]$$
$$= A^2 e^{j\omega\Delta T}\boldsymbol{q}. \quad [6.28]$$

According to principle of LMS, the weight vector of the adaptive filter will converge to solution of Weiner Hopf equation when adaptive iterative process reaches its steady optimum [74].

$$w_{opt}(n) = R_{xx}^{-1}R_{xd} \quad [6.29]$$

Thus from above equations

$$w_{opt}(n) = \frac{A^2}{S_n^2+LA^2} e^{j\omega\Delta T}\,\boldsymbol{q} \quad [6.30]$$

Through introduction of SNR, the optimal weight is given by:

$$w_{opt}(n) = \frac{SNR}{1+LSNR} e^{j\omega\Delta T}\,\boldsymbol{q} \quad [6.31]$$

6.3.2 The steady state frequency response function of ALE.

When the Adaptive filter reaches its optimum coefficients [74], in accordance to least mean square, the weight vector $w(n)$ will converge to $w_{opt}(n)$ and the output of ALE is given by:

$$y(n) = x^T(n-\Delta).w_{opt}(n) \quad . \qquad [6.32]$$

By using Z Transform of above equation:

$$Y(z) = X(z)z^{-\Delta}W_{opt}\ (z)\ . \qquad [6.33]$$

So the transfer function of ALE is given by:

$$\frac{Y(z)}{X(z)} = H(z) = z^{-\Delta}W_{opt}(z). \qquad [6.34]$$

If the input signal has a frequency of ωo, then the z-transformation of optimum weight vector of ALE with filter length L can be written as

$$Wopt(z) = \frac{SNR}{1+L\ SNR} z_o^{\Delta} \sum_{l=1}^{l=L} \left(\frac{Z}{z_o}\right)^{-l} \qquad [6.35]$$

Thus

$$H(z) = \frac{SNR}{1+L\ SNR} \left(\frac{z}{z_o}\right)^{-\Delta} \sum_{l=1}^{l=L} \left(\frac{Z}{z_o}\right)^{-l} \qquad [6.36]$$

Transforming equation into frequency domain

$$H(\omega) = \frac{SNR}{1+L\ SNR} e^{-j(\omega-\omega o)\Delta T} \frac{1-e^{-j(\omega-\omega o)LT}}{1-e^{-j(\omega-\omega o)T}} \qquad [6.37]$$

At $\omega = \omega o$ $\qquad$ $\mathrm{H}(\omega o) = \frac{L\ SNR}{1+L\ SNR}$ $\qquad$ [6.38]

Equation 6.36 shows that the transfer function depends on characteristic frequency ωo of input, indicating that ALE is capable of adapting to the frequency variation of the input.

6.3.3 The Influence of the Filter Length

It is clear from equation (6.37) that the number of coefficients (L) in the FIR filter has an influence on the response of ALE. The value of L specifies how accurately a bandpass filter can be modeled by the ALE. In addition to this, it affects the convergence rate considerably. For instance, when L is large, the gain of ALE is high but the computation time of the whole system will increase which may slow down the convergence rate. When, it is small, this time the computation time will be decreased and the convergence rate will be faster, but the gain of ALE will be smaller [78].

6.3.4 The Influence of the Input SNR

The gain of the ALE with SNR and L can be computed by using equations [6.36] and [6.36].The influence of input SNR can be explained by three cases [79].

1. High SNR (SNR > 0 dB). When the power of the broadband signal (noise) is less than that of narrowband signal, the gain value of the optimal filter becomes one. In this case, the broadband signal will be suppressed to a minimum value according to the LMS algorithm and the narrowband signal will pass through the ALE. In such a case, the output signal power can be written as

$$E[\,y(n).y^T(n)] = E\{\left[w_{opt}^T\,(n)x(n-\Delta)\right]\left[w_{opt}\,(n)x^T(n-\Delta)\right] \quad [6.39]$$

$$= w_{opt}^T\,R_{xx}w_{opt}$$

Where w_{opt} is given by

$$w_{opt}(n) = \frac{A^2}{S_n^2 + LA^2} e^{j\omega\Delta T} \quad [6.40]$$

where S_n^2 is the power of the noise and R_{xx} is autocorrelation of the filter input

i.e $$R_{xx} = R_{ss} + R_{nn}$$

where R_{ss} is auto-correlation matrix of signal $s(n)$ and R_{nn} is auto-correlation matrix of the of noise $No(n)$.

Thus $$E[\, y(n)y^T(n)] = L\,(\frac{A^2}{LA^2 + S_n^2})^2(A^2 + \frac{S_n^2}{L}) \quad [6.41]$$

Equation 6.40 shows that when x(n) passes through the ALE, the power of Signal S remains the same, while the noise power decreases to 1/L of its original power.

ii) Medium SNR (-10 dB < SNR < 0). The gain of the optimal filter is between 0 and 1 i.e. the narrowband signal can partially pass through the ALE.

iii) Low SNR (SNR < -10 dB). The gain value of the optimal filter becomes zero. In this case, the ALE cannot suppress the broadband signal or equivalently, the narrowband signal cannot be enhanced by the ALE. As a consequence of this, the broadband signal causes a large value of the mean error at the ALE output.

6.4 Simulation Results

The simulations with ANC, ALE and wavelet transform are explained here with NQR signal model and real time NQR signal.

6.4.1 NQR Signal Model

NQR signal is often measured as FID which is response after single excitation pulse. As discussed in chapter 2 the noise corrupted FID signal Xo is modeled as linear combination of signal So with strength A and background noise Wo as shown in equation [6.41].

$$Xo\ (t)\ = A\ So(t)\ +\ Wo\ (t) \qquad [6.42]$$

$$So(t)\ =\ e^{-t/T_2^*}\ cos(2 * pi * fc * t) \qquad [6.43]$$

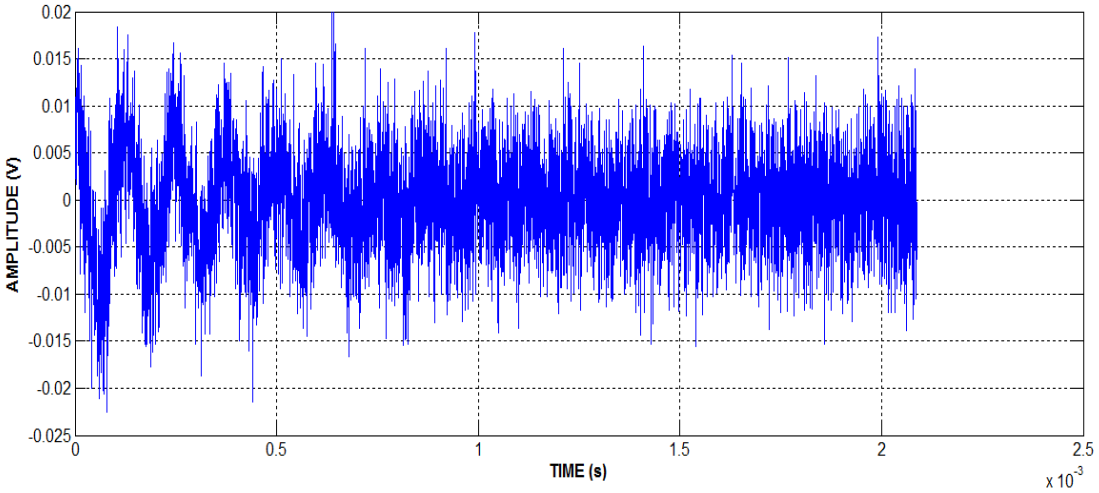

Fig 6.5 Simulated Noise corrupted FID

For ^{14}N detection from $NaNO_2$, T_2^* of FID response with resonance frequency of 4.642 MHz is 0.5 ms. The amplitude of the FID envelope is assumed to be 10 mV, sampling frequency 2.875MHz. The noise is modeled as having normal distribution with mean zero and σ =0.005. The simulated noise corrupted FID signal is shown in Fig 6.5.

6.4.2 Simulations

ANC and ALE configurations simulated are shown in fig 6.6 and 6.7 respectively. The algorithm implemented was least mean square with length of filter L = 256.

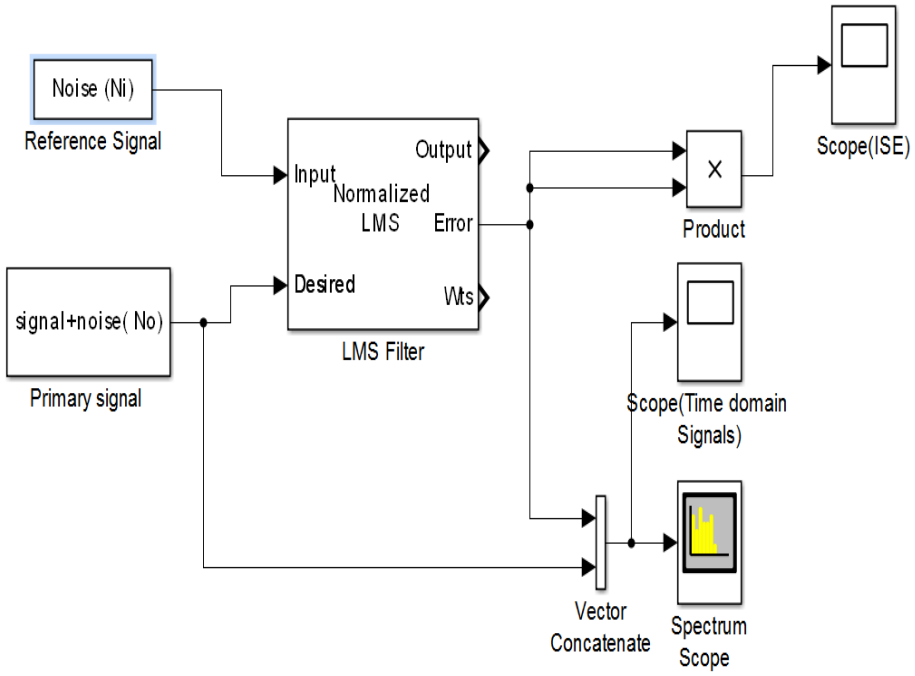

Fig 6.6 Adaptive Noise Canceller implementation

ANC(Fig 6.2) implemented is shown in Fig 6.6, in which the primary signal is signal (S) and noise (N_o) together and reference signal is noise N_I which is correlated to noise (N_o) but uncorrelated to signal (S). Noise (N_I) is passed through the adaptive filter and output y is produced as close a replica as possible of N_o. The filter adjusts its coefficients to minimize the error between the output and primary signal which is the filtered signal (i.e $S + No - y$) i.e. observed in scope as time domain signal as well as frequency domain signal(in Spectrum Scope)

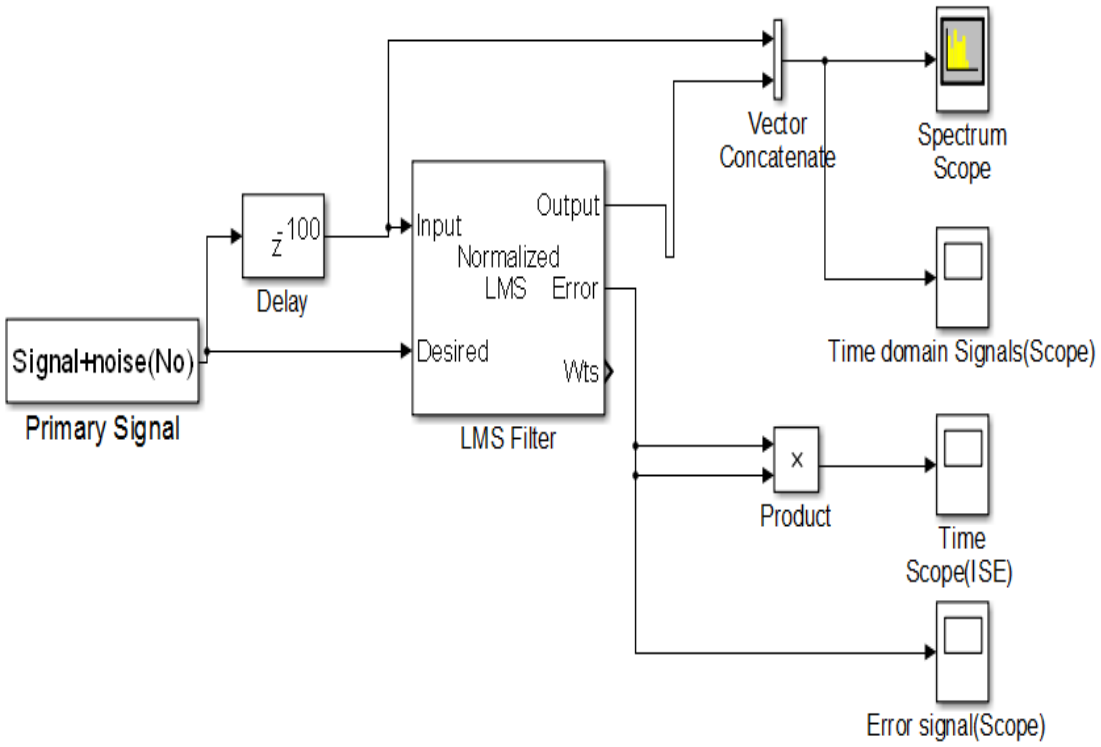

Fig 6.7 Adaptive Line Enhancer implemented in Simulink® .

ALE (Fig 6.3) implemented is shown in Fig 6.7 in which the primary signal is signal (S) and noise (N_o). The input signal is generated by delaying the primary signal. The delay is selected by eq. [6.2]. The input signal is passed through the filter. The adaptive filter will adjust its coefficients such that it forms a narrowband filter centered at frequency of narrowband signal. The output is the filtered signal (S). The error is difference between the output and primary signal i.e. only noise component. The performance of ALE with SNR of input signal and delay has been studied, and the results are shown for NQR signal model and real time NQR signal in the following sections.

6.4.3 Influence of Input SNR.

The SNR is defined as ratio of signal power to noise power. At the input side of ALE filter the SNR of the NQR signal model is known but at the output the signal and noise cannot be separated so SNR is not known at the output. Following is the algorithm implemented to find SNR at the output. Let,

$$S_I = 10 * Log_{10}(var(clean\ signal\ at\ input)), \text{ and}$$

$$N_I = 10 * Log_{10}(var(noise\ signal\ at\ input)). \text{ Then}$$

$$SNR_I\ in\ dB = S_I - N_I.$$

1. When clean signal is sent to filter. Let the Output be $Y_2(dB)$.
2. When noisy signal is sent to filter Let the Output be $Y_1(dB)$.
3. Therefore, the residual noise No = $Y_1 - Y_2\ (dB)$.
4. $S_o = Y_2$
5. SNR at output of ALE in dB $= S_o - N_o$

Using above algorithm with NQR signal model (with random noise) with different SNRs (-26 dB to 4 dB) was applied at input of ALE, and output SNR were calculated. Fig 6.8 shows the time domain and frequency domain signals of input and output signals of ALE for input SNR of -20dB. The input signal is NQR signal model from equation [6.41] where noise is modelled as having normal distribution with mean zero and $\sigma = 0.025$.

.

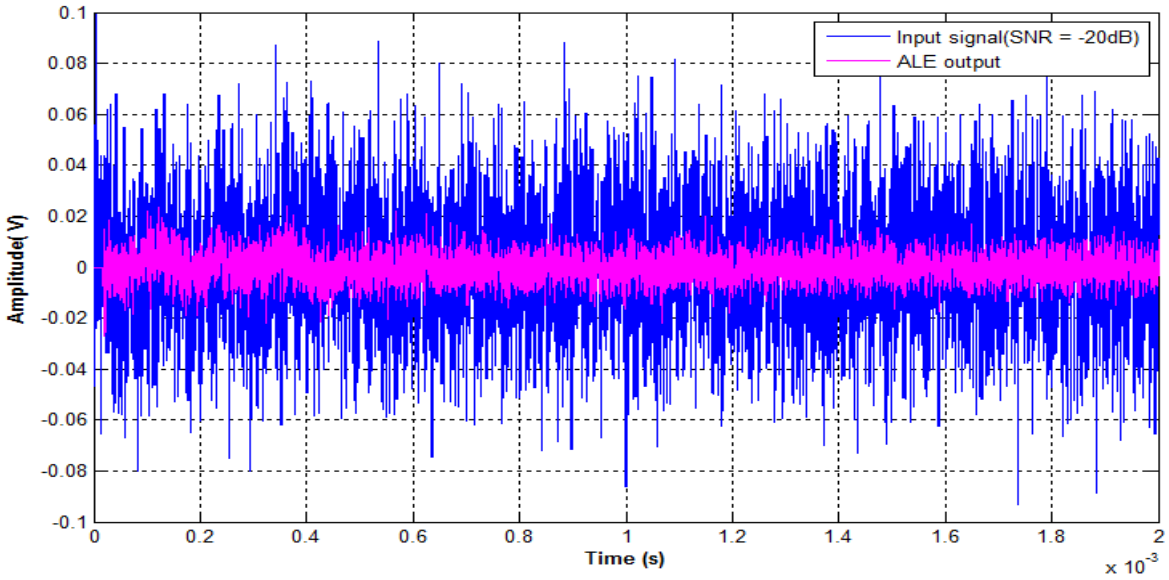

a)

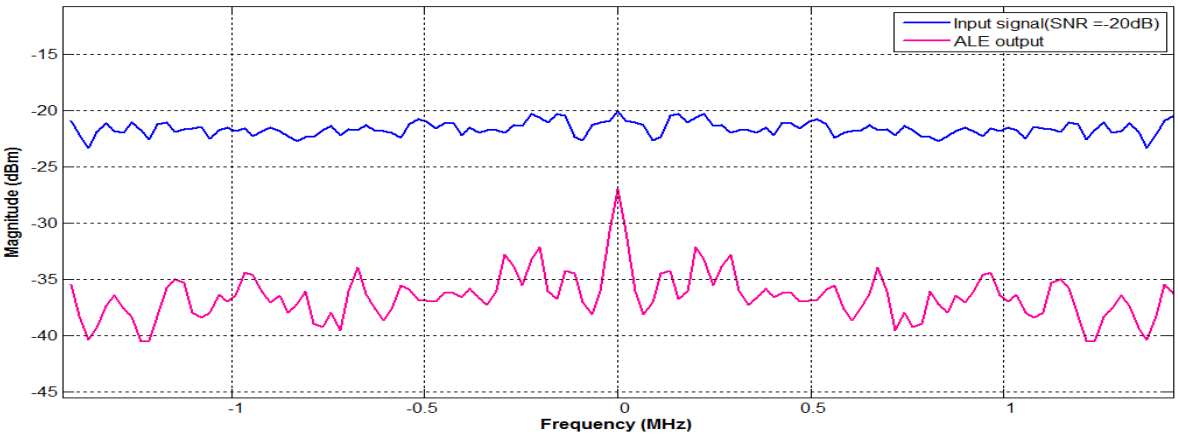

b)

Fig 6.8 a) Time domain signal of NQR signal model (SNR = -20dB) and output of ALE

b) Spectrum of NQR signal model (SNR =-20dB) and output of ALE.

Fig 6.9 shows the time domain and frequency domain signals of input and output signals of ALE for input SNR of -6 dB. The input signal is NQR signal model where noise as having normal distribution with mean zero and σ =0.005.

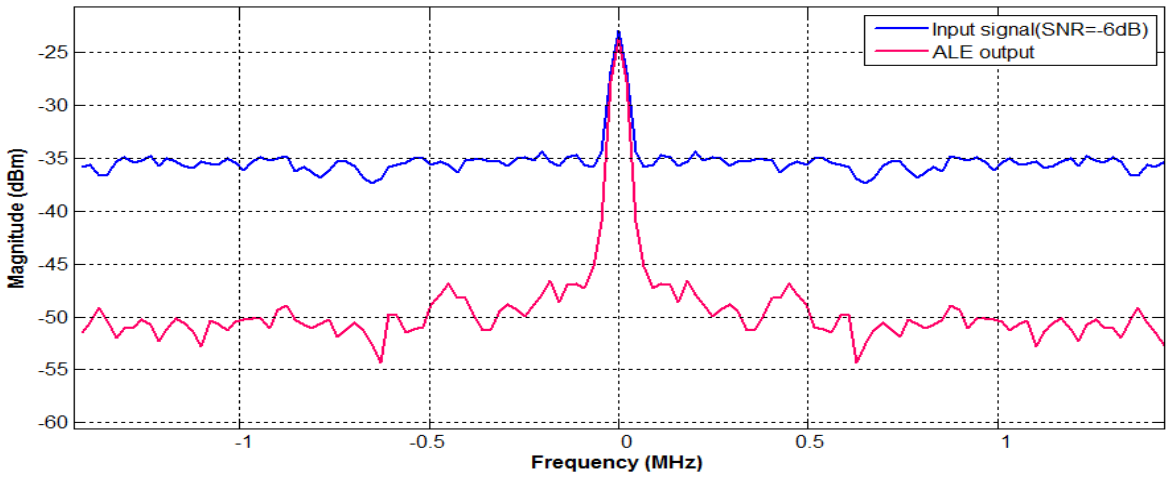

a)

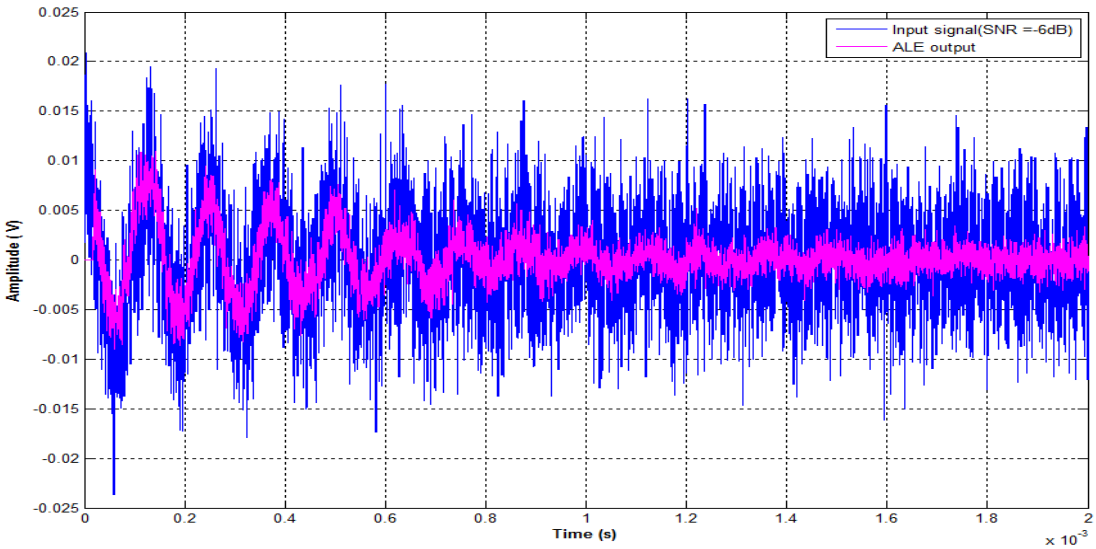

b)

Fig 6.9 a) Time domain signal of NQR signal model (SNR = -6 dB) and output of ALE

b) Spectrum of NQR signal model (SNR = -6 dB) and output of ALE.

This process was repeated for different input SNRs from which plots of two input SNRs are shown in Fig. 6.8 and 6.9 and it was observed that the performance of ALE is not good for the input SNR value less than -6dB. However, when SNR value is increased, the performance of the ALE increases considerably.

6.4.3 Influence of Delay

The steady state frequency response indicates that the delay Δ can only change the phase property of ALE. As discussed in previous section that delay Δ in ALE filter is selected such that Δ is longer than τ_d(BB) i.e. correlation length of broadband noise and smaller than τ_d (NB) correlation length of narrowband signal, beyond these lags, the respective correlations die out quickly. The function of delay Δ is to de-correlate the noise component between the the two channels of ALE and to correlate the signal component of the two channels. As NQR signal model bandwidth is 8 kHz with random noise. The SNR is -6dB. So τ_d(BB) will be zero and τ_d (NB) = Fs/fm. Here Fs= 2.875MHz and fm = 8 kHz, thus τ_d (NB) = 350.

$$0 < \Delta < 350 \qquad [6.44]$$

Simulations were carried out by varying the value of Δ from 1 to 400. The output SNR was calculated for different delays. Fig. 6.10 shows the spectrum of input and output signals of ALE for Δ= 25,100,200. It is observed that with increase in delay the output SNR decreases. Simulations were also repeated for pink noise (1/f) of bandwidth 30 kHz added to NQR signal model (SNR =-6dB). Delay Δ is calculated as per the bandwidth of pink noise with Fs= 2.875MHz. i.e. Δ=Fs/30kHz =95 and so according to eq.[6.3]

$$95 < \Delta < 350 \qquad [6.45]$$

It is observed that for input signal with pink noise output SNR is highest at Δ = 100 and then it decreases with increase in delay (Fig. 6.11).

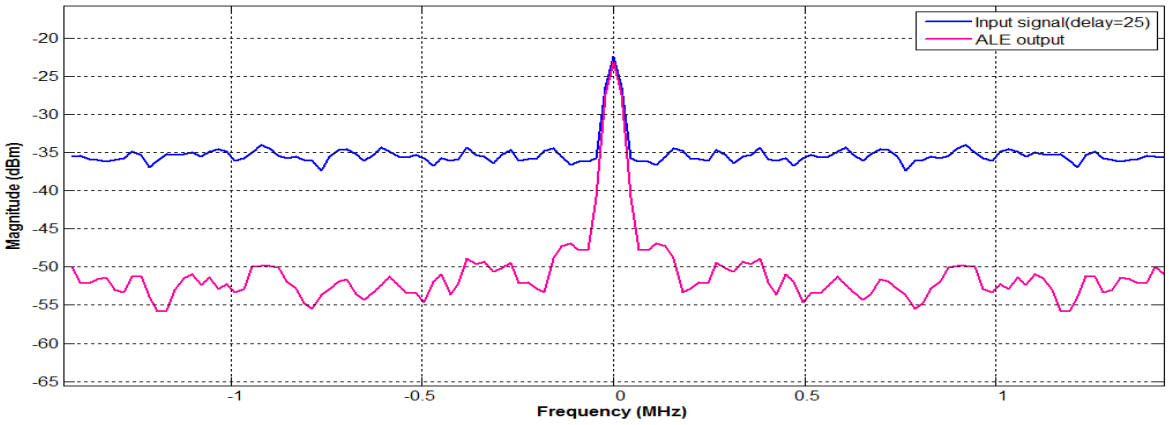

a)

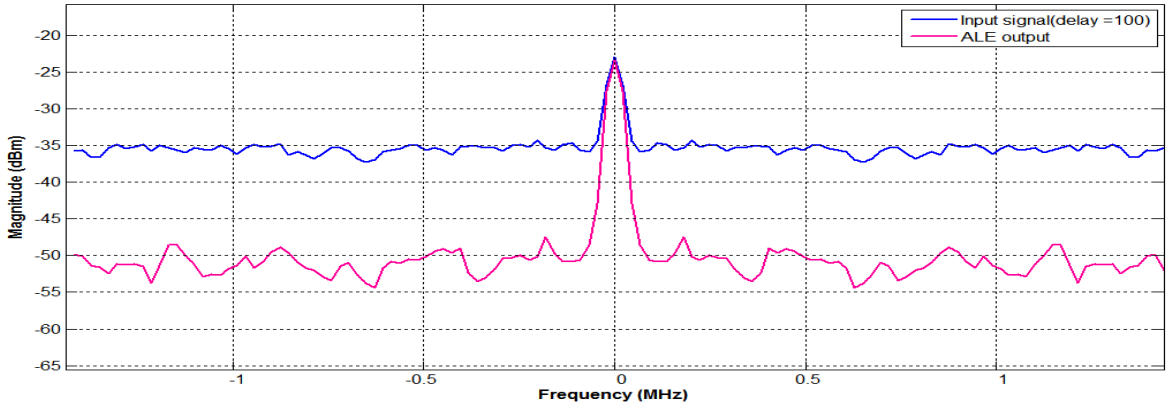

b)

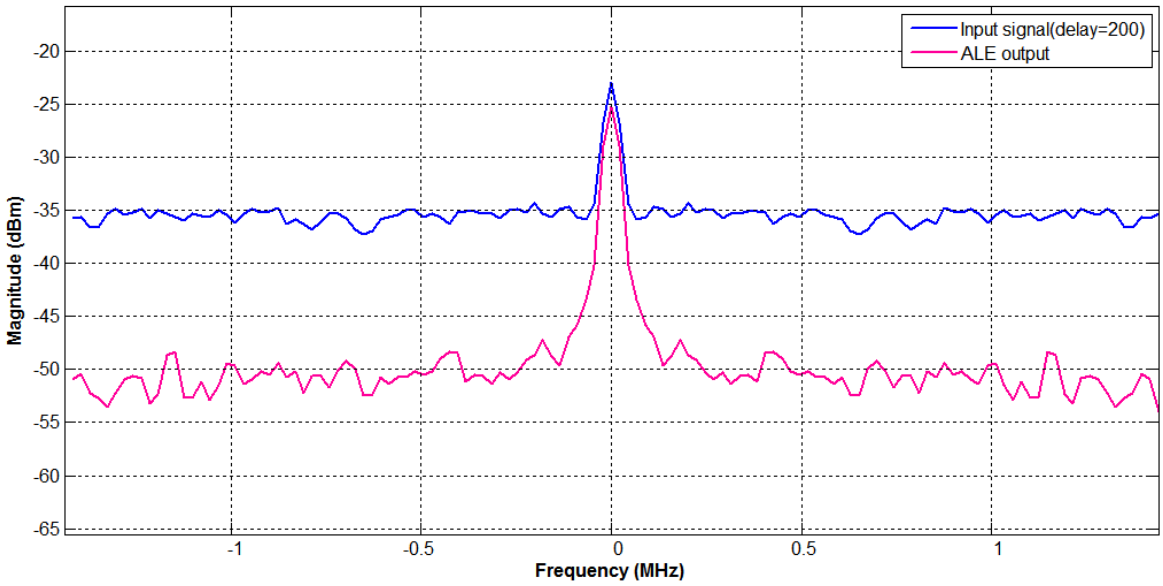

c)

Fig 6.10 Spectrum of NQR signal model and output signal of ALE with delay a) Δ= 25 b) Δ=100 c) Δ= 200

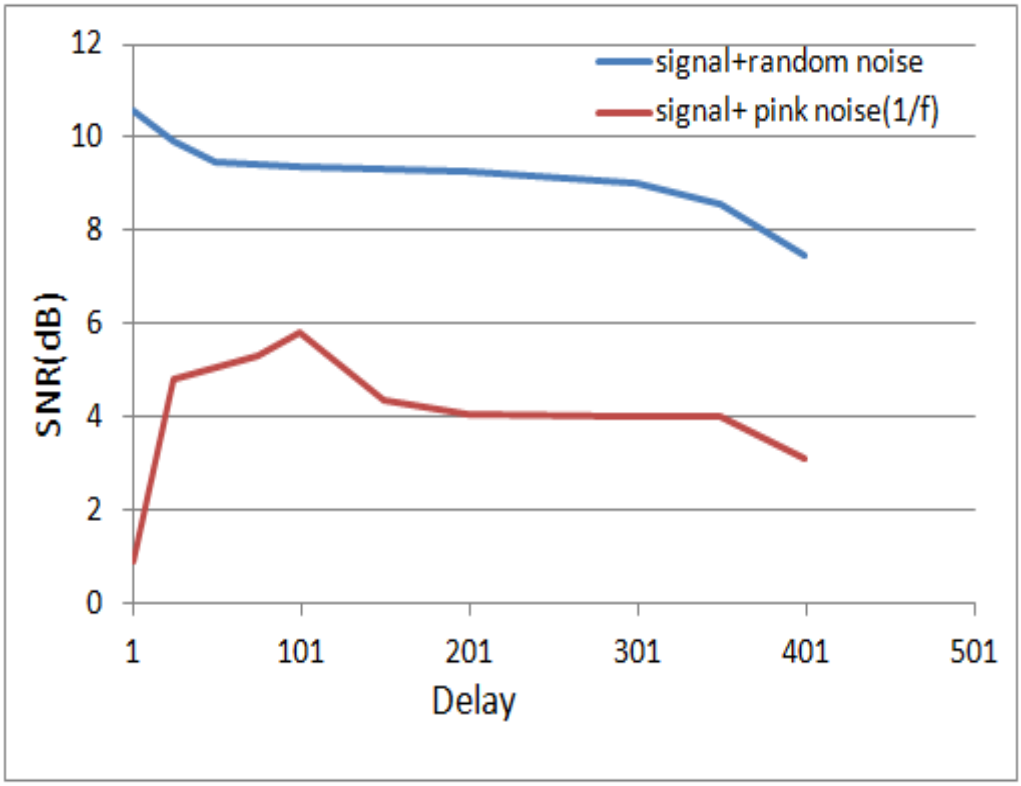

Fig 6.11 Output SNR Vs Delay.

The performance of ALE depends on SNR of the input signal and delay. It was observed that the performance of ALE is good when input SNR is greater or equal to -6dB. Various inputs with different SNR were applied to ALE, of which frequency domain signals are shown in Fig 6.8 and 6.9, and thus the performance of ALE with delay was studied using input signal with random and pink noise (SNR = -6dB) for different value of delays. The SNR of the output signal Vs Delay is shown in Fig. 6.11 and it can be observed that for input signal with random noise the output SNR decreases as the delay increases. However when the input signal is with pink noise the SNR decreases after delay = 100 which is also shown by Eq. [6.45].

6.4.5 Simulation using Adaptive Noise Canceller

The reference input in ANC(Fig 6.2), is simulated noise corrupted FID shown in Fig 6.5 The input signal is only noise (N_I).The output of adaptive filter is estimated by adaptive filter weights to be close to N_o, so that only NQR signal is obtained as the error signal $e(n)$. The result is shown in Fig 6.12 and Fig 6.13. Also SNR of the output signal is 7dB which shows that there is SNR improvement of approximately 13 dB.

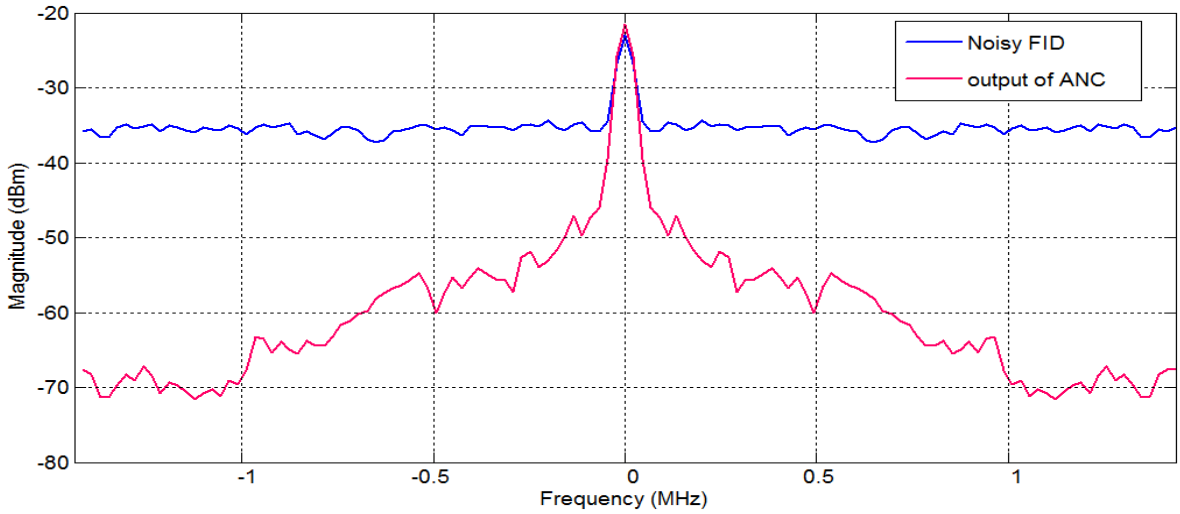

Fig 6.12 Spectrum of Simulated Noise corrupted FID and output of ANC

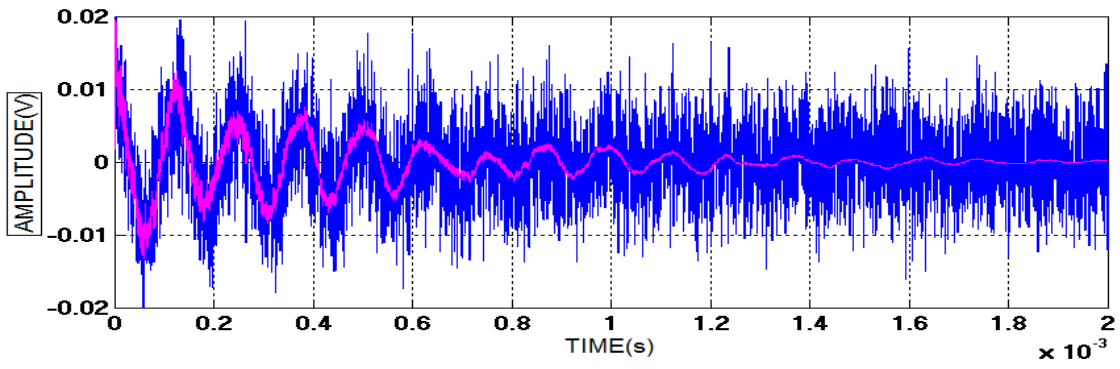

Fig 6.13 (---) Simulated Noise Corrupted FID and (---) output of ANC .

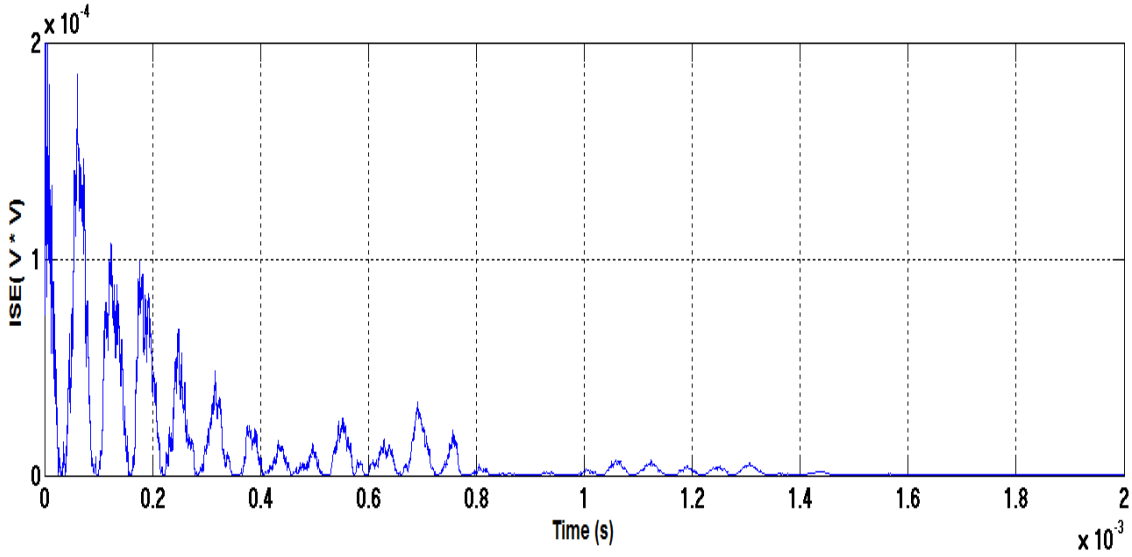

Fig 6.14 ISE for Simulated FID input to ANC

The instantaneous square error above shows that it converges at about 1 msec.

6.4.6 Simulation using Adaptive Line Enhancer

While in ALE the reference signal is a delayed version of primary signal. The simulated noise corrupted FID is given as reference signal and its delay is given as primary input signal . The delay is given such that it decorrelates the noise components. The signal is correlated so the error signal will be noise component only. This error is employed to update the filter weights such that ALE output is close to FID. Fig 6.15 and 6.16 shows the spectrum and time domain of input as well as output of ALE. The SNR of the signal at the output of ALE is 11 dB which show that there is SNR improvement of approximately 17 dB.

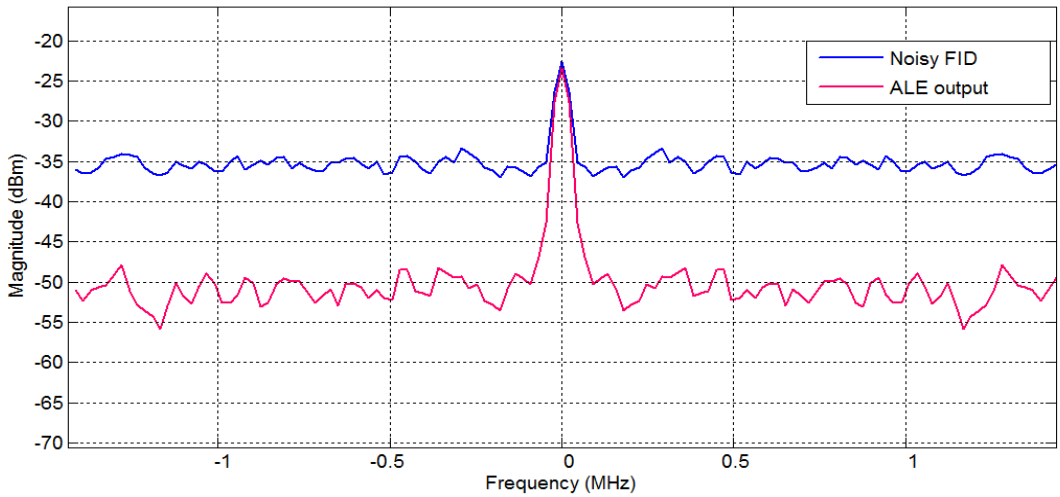

Fig 6.15 Spectrum of Simulated Noise corrupted FID and output of ALE

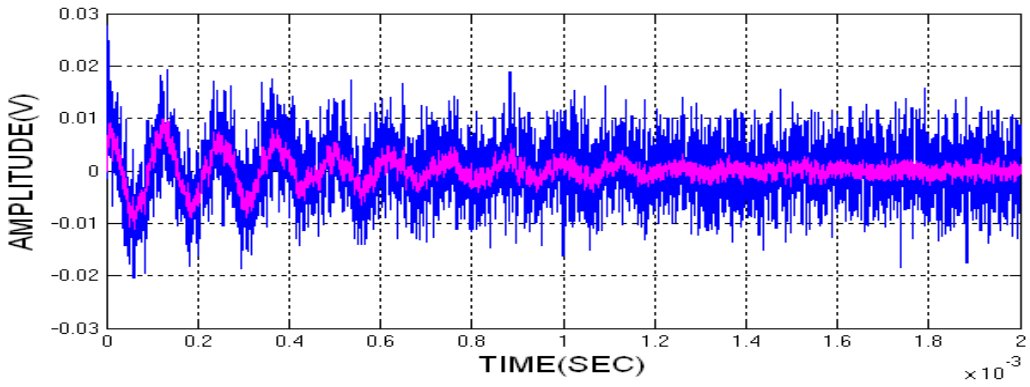

Fig 6.16 (---) Simulated Noise Corrupted FID and (---) output of ALE.

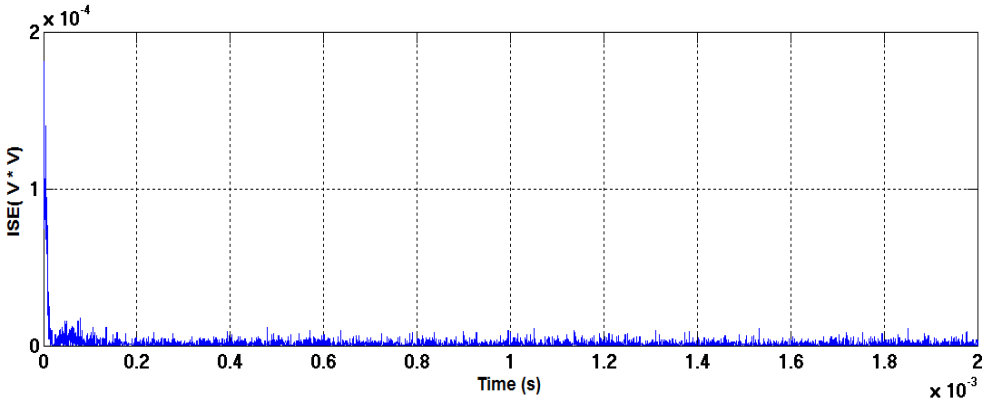

Fig 6.17 ISE for Simulated FID input to ALE

6.4.7 Wavelet Transform applied to simulated NQR signal

The use of different wavelet basis would give different results from the analysed signal, and there are no defined criteria's to describe the selection of optimum wavelet family. Selection is mostly done by trial and error. Another important parameter is the choice of threshold estimation value for signal de-noising. Four common threshold techniques have been used in literature, which are heursure, rigrsure, minimaxi and sqtwolog. It is shown in [74] and [80] that huersure gave better performance as compared to other thresholding methods. So heursure thresholding is used for the present work.

Three steps explained in section 6.1 are performed on synthesized NQR signal and decomposition of signal is done to level 5 with different wavelet type like Daubechies, Bi-Orthonormal, Coiflets and Symlets. The improvement in SNR for all the wavelets is shown in Table 6.1 which shows that 'Coif5' wavelet gives the best performance in terms of SNR improvement.

Table 6.1.Performance of different wavelets in terms of SNR improvement

Sr. No.	Wavelet	Output SNR (dB)
1	db5	13
2	Sym5	12
3	Bior5	11.5
4	Coif5	13.5

The thresholding is done on individual detailed coefficient and finally modified detailed coefficients are added with approximation coefficient to produce filtered signal.The filtered signal in time and frequency domain using 'Coif5' wavelet and heursure thresholding technique is shown in Fig. 6.18 and 6.19, respectively. The SNR of the filtered signal is 13dB. Thus SNR improvement in this case is 19dB.

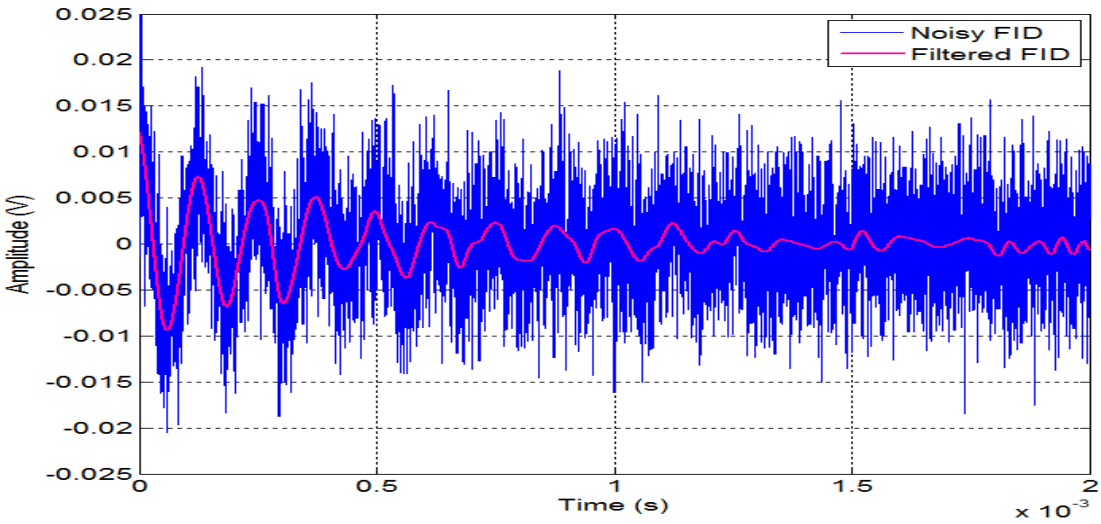

Fig 6.18 Simulated Noisy FID and wavelet transform ouput.

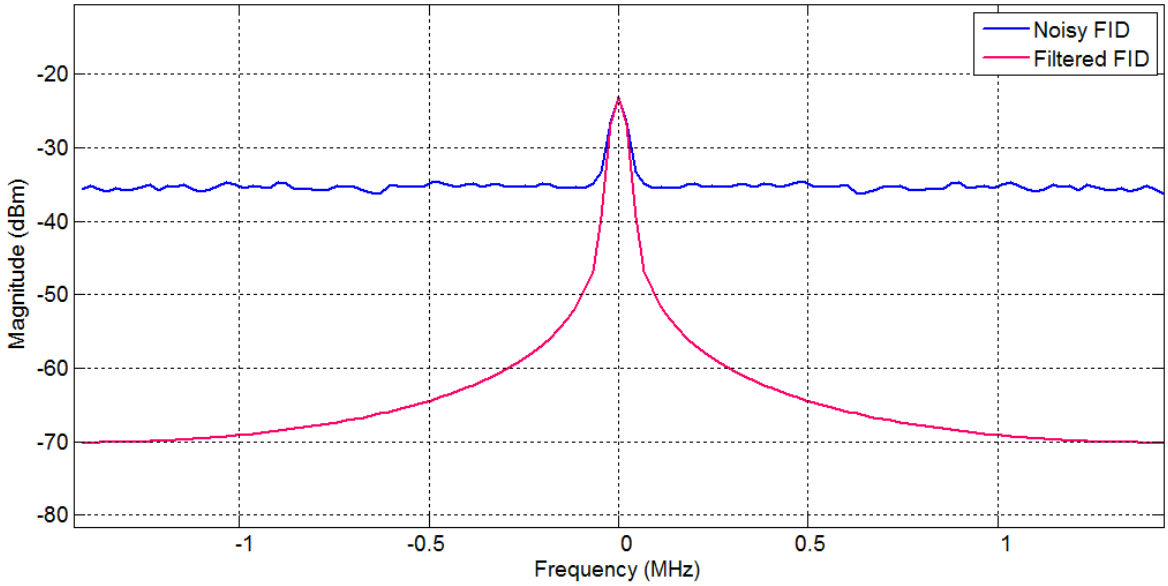

Fig 6.19 Power spectrum of Noisy FID and filtered signal for wavelet transform

6.4.8 Adaptive filtering algorithms and wavelet transform applied to real NQR signal

The real time ^{14}N NQR signal from $NaNO_2$ acquired from our NQR spectrometer is shown in Fig 6.20. Due to low SNR of single FID i.e. approx -12dB it is enhanced by accumulation of 256 FIDs to approx. 12dB (The signal to noise ratio increases by $\sqrt{n}$ when the signal is averaged by n times). As the noise in case of NQR signal cannot be acquired

independently, the simulation is shown for ALE only. The NQR signal is applied at reference input and its delayed version is applied to input of ALE. As the NQR signal is acquired after 30 kHz filter. The delay is decided by this filter (Equation 6.2). The delay is taken as 100. The simulation results for real time data are shown for ALE in Fig. 6.20 and 6.21. The SNR at the output of ALE is calculated as 18 dB which shows that there is SNR improvement of about 6 dB. The instantaneous square error is shown in Fig 6.22.

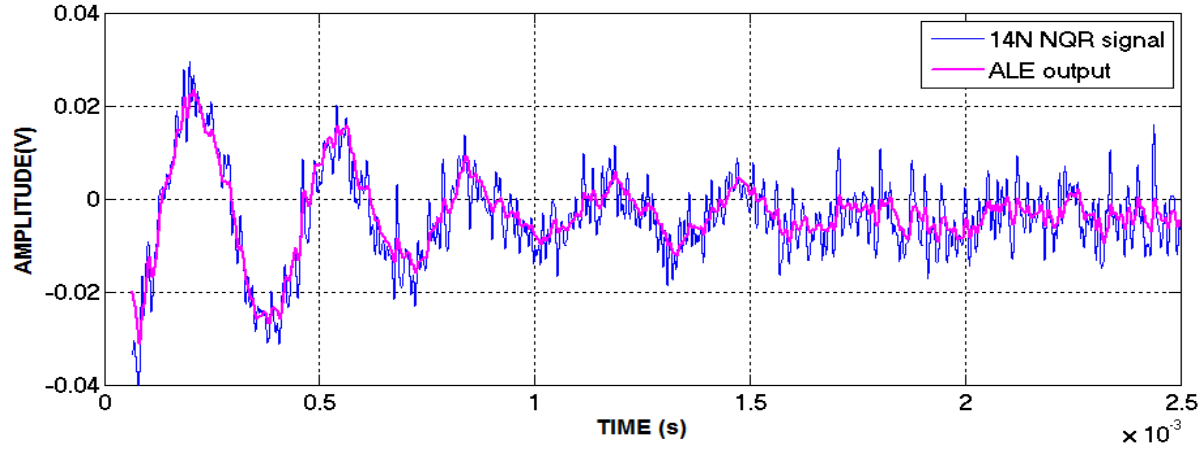

Fig 6.20. Real time NQR signal at input and output of ALE

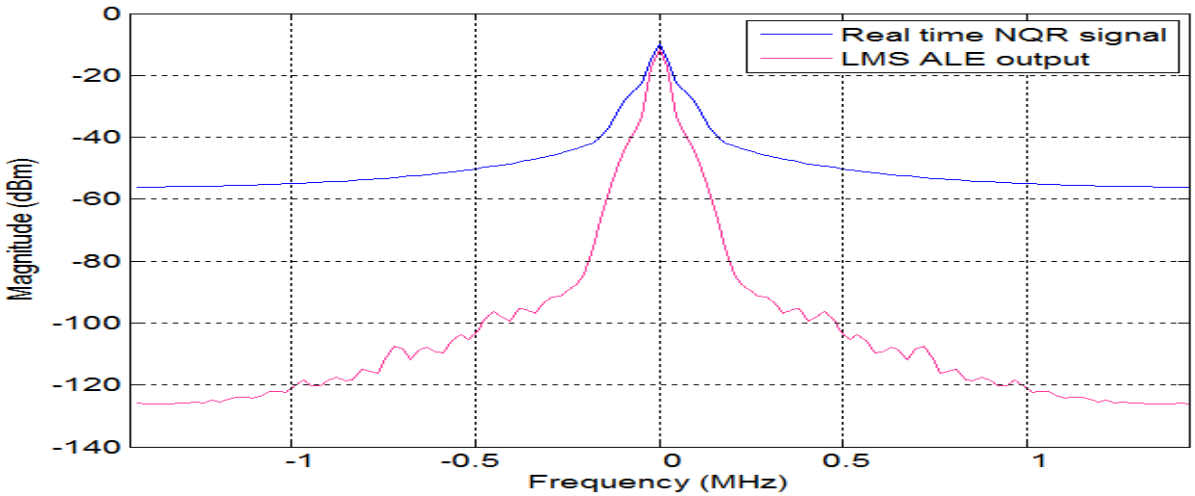

Fig 6.21 Power spectrum of real time NQR signal and output of ALE

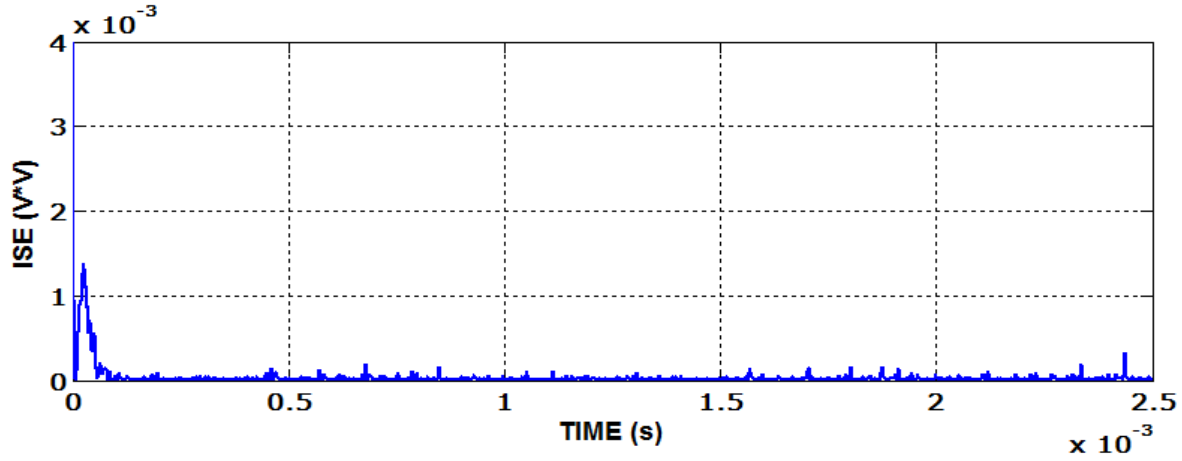

Fig 6.22 ISE for real time NQR as input to ALE

The steps explained in section 6.1 are performed on Real time NQR signal using 'coif5' wavelet.The filtered signal in time and frequency domain is shown in Fig.6.23 and 6.24 respectively. The SNR of the output signal in this case is 20dB thus there is SNR improvement of 8dB. Thus it can be seen that with both the methods i.e ALE and Wavelet Transform improvement in SNR is almost same.

The signal to noise ratio increases by n when the signal is averaged by n times. Thus a signal which is already averaged by 256 times will increase by 6dB when it is further averaged by 768 times. Also, in our experiment to observe ^{14}N NQR signal form $NaNO_2$ we repeated the pulse after very 0.5 seconds, therefore the time taken by averaging is 6.4min which can be obtained by ALE in few ms.

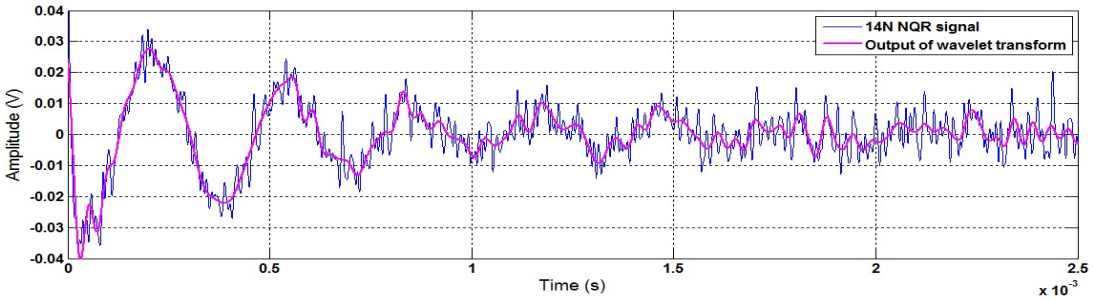

Fig 6.23 Real time NQR signal and output of wavelet transform

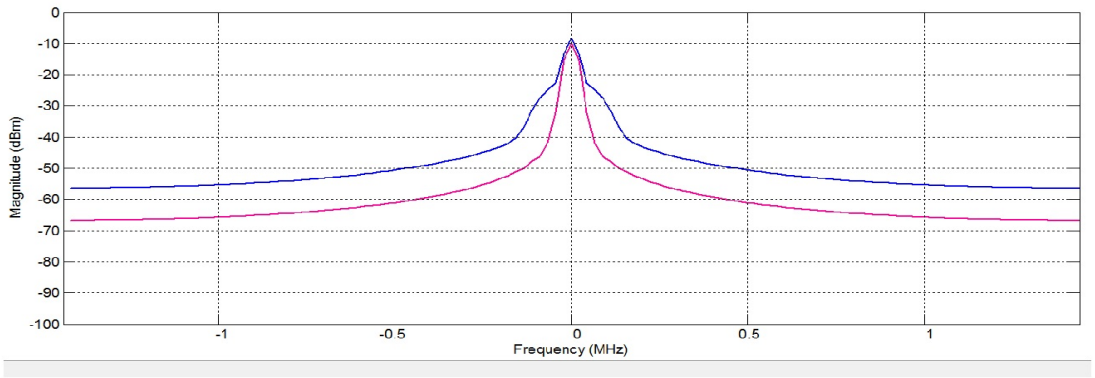

Fig 6.24 Power spectrum of (---)Real time NQR signal and (---)wavelet transform output

6.5 Summary

In this chapter NQR signal processing based on adaptive filters and wavelet transform is presented. Also the performance analysis of ALE is done based on input SNR and delay. Both wavelet transform and ALE gave almost same SNR improvement with NQR signal model as well as real time NQR signal. Both are faster and better detection methods as compared to averaging. But incorporating ALE in FPGA is easier as compared to wavelet transform.

Chapter 7

Summary and Future works.

There have been significant improvements in NMR instrumentation in the past few years. Also in many cases these instruments have been used for both NMR and NQR studies. However the best spectrometers that are commercially available are expensive and also not usually capable of operating at low frequencies and are also not specifically designed for NQR. Thus there is lot of scope of research still to apply as modern circuitry and signal processing technique towards production of pulsed spectrometer for low frequency NQR and NMR applications targeting specific applications like explosives and drug detection and quantitative analysis.

A FPGA based NQR spectrometer was designed in Electronics Division (ED), BARC.A single FPGA chip is used to perform the digital tasks required for NQR spectrometer including pulse programmer, direct digital synthesizer, digital receiver composed of quadrature demodulator, a low pass Finite Impulse Response filter and PC interface for data transfer. The compact digital module is highly sensitive and is suitable for applications like mine detection and non-invasive compound identification etc. Also, the analog peripheral components such as pre-amplifier, cross diodes and quarter wave transformer and probe were designed and developed as part of the current research. RF power amplifier was available in-house at ED. By adding a permanent magnet of uniform field one could carry out NMR as well which, can be a very useful tool for quantitative analysis of trace elements like Tritium and deuterium etc. The ^{14}N NQR transitions in various solids fall in the frequency range 0 to 6 MHz. Hence ^{14}N was chosen for the design. ^{14}N NQR signal from sample of 20 g of $NaNO_2$ was observed at a frequency of 4.64 MHz. With the addition of permanent magnets ^{1}H and ^{2}H, NMR signal from H_2O and D_2O was detected. Observation

of proton NMR is easier than observing Deuterium and ^{14}N NQR as the strength of this signal is much stronger. For this reason we have observed ^{1}H NMR as the process of standardizing the instrument.

The low SNR in NQR spectrometer has been observed to present certain challenges pertaining to high interferences in the detection of signal. To improve SNR, many repetitions of the experiments were done and NQR signal after each pulse was acquired. The rate at which RF pulse has to be repeated depends on physical parameters of nuclear relaxation i.e relaxation times. For most of explosives the relaxation times are very long (100ms -1s) which lead to long detection times. The results shown for ^{14}N NQR signal from $NaNO_2$ in chapter 5 are after averaging of 1024 times which took 8.5 minutes to be observed on scope.

As relaxation times cannot be shortened, the other option to improve the SNR is by improving the signal detection technique. To improve SNR per unit time, techniques like FIR filter, wavelet transform and adaptive filter have been used. Suitability of adaptive filter algorithms, since they do not require previous knowledge of the signal, is studied in this work.

Adaptive filter algorithms such as ANC and ALE and wavelet de-noising were applied to NQR signal model as well as real time signal and it was observed that ALE and wavelet transform are better and faster detection method as compared to averaging technique. For further research, this NQR/NMR spectrometer can be further developed into a miniature spectrometer through the integration of RF amplifier, reciever module and FPGA module on one board. In this manner, the explosive detection and mine detection mechanisms of NQR/NMR experiments can be enhanced and result in more productive performance.

Future Work

The prototype of NQR/NMR spectrometer using FPGA, high speed ADCs, DACs, RF power amplifier, pre amplifier, cross diodes, quarter wave transformer, and band pass filter has been designed and described as a part of this thesis. The system was designed and developed using available components in ED, BARC. There are many aspects of the system that can be optimized to improve the integration and reduce the cost and power consumption. Some of them can be listed as follows:

1) Compact class-D type switching power amplifier [81] can be used as RF power amplifier in transmitter section to provide high power efficiency (90%) during transmitting period. Also these amplifiers have very low standby power consumption (in mW) during receiving period thus it will have power saving and reduced size advantage as compared to Class-AB power amplifier which is used in current work.
2) Probe which in present work is constructed as resonance circuit is to be tuned and matched to comparatively narrow bands frequently while scanning over whole NQR spectrum. Commercial NQR/NMR probe heads employ stepper motor for setting mechanical tunable capacitors in standard resonators. These probe heads can provide high Q and thus high SNR but are large in size and not convenient to be used for field applications. The solution to this is a new concept which is no- tune, no-match wideband concept for the transmitter pulse with an electronically tunable receiver employing varactar diodes [82].
3) High Q factor of the probe is required for high efficiency during the transmission period. After RF pulse, the dissipation time of the residual excitation power in the NQR probe is also proportional to the Q. Thus a high-Q NQR probe will have long ringing time and as the FID signal appears after RF pulse, the residual power needs to be decayed immediately. Otherwise FID signal is interfered with the ringing signal.

Thus, a Q damping circuit is required to switch the Q factor to a lower value to reduce ringing time [83]. This will help in increasing SNR and reducing the detection time in field applications.

4) This spectrometer can further be developed into a miniature spectrometer by combination of RF amplifier, receiver module and FPGA module on one board and thus enhances opportunities for Extensive NQR/NMR applications like explosive detection, mine detection etc.

.

REFERENCES

[1] A. N. Garrowway, M. L. Buess, J. B. Miller, B. H. Suits, A. D. Hibbs, G. A. Barrall, R.Matthews and L. J. Burnett, “Remote sensing by nuclear quadrupole resonance," IEEE Transactions on Geoscience and Remote Sensing”, vol. 39, no. 6, pp. 1108-1118, 2001.

[2] Zhu Shengyun, Li Xing, Lu Zhongcheng, Wang Guobao, & Shu Weiguo (2010). “Application of Nuclear Quadrupole Resonance to Detection of Explosives and Research Activities at CIAE”. International Atomic Energy Agency (IAEA): IAEA.

[3] Latosińska, J.N. (2007). “Applications of nuclear quadrupole resonance spectroscopy in drug development”, Expert Opinion on Drug Discovery, 2(2):225-48. doi: 10.1517/17460441.2.2.225.

[4] Gudmundson E Jakobson A and Stolea P, “ NQR based Explosive detection-An Overview”, 9th Interntional symposium on signal Circuits and systems(ISSCS 2009)Iasi ,Romania July 2009.

[5] V S Grechishkin, N Ya Sinyavskii, “Nuclear Quadrupole resonance as an explosive and narcotic detection technique”, Instruments and methods of investigation, Physics-pp 393-406, 1997.

[6] Bryan H. Suits, “Nuclear Quadruple Resonance spectroscopy”, Handbook of Applied solid state soectroscopy, 2006

[7] Jamie Barras, Darragh Murnane, Kaspar Althoefer, Sulaf Assi, Michael D. Rowe, Iain J. F. Poplett, Georgia Kyriakidou, and John A. S. Smith, “ Nitrogen-14 Nuclear Quadrupole Resonance Spectroscopy: A Promising Analytical Methodology for

Medicines Authentication and Counterfeit Antimalarial Analysis" , *Anal. Chem.*, 2013, *85* (5), pp 2746–2753.

[8] Hideo Itozaki and Go ota, "NQR for Explosive Detection." International journal of Smart sensing and intelligent systems. Vol 3 sept 2008

[9] H. G. Dehmelt and H. Kruger, "Pure quadrupole resonance in solids",Naturwissensch aften, vol. 37, pp. 111, 1950.

[10] W. L. Rollwitz, J.D. King, and G. A. Matzkanin, "Fundamentals of nuclear magnetic resonance for the detection and identification of explosives," Proceedings of New Concepts Symposium and Workshop on detection and Identification of Explosives, 1978.

[11] J. A. S. Smith, "Nuclear quadrupole resonance spectroscopy. General principles", Journal of Chemical Education, vol. 48, no. 1, pp. 39-49, 1971 .

[12] Hideo Itozaki and Go ota, "NQR for Explosive Detection.", International journal of Smart sensing and intelligent systems.Vol 3 sept 2008

[13] J.C. Harding , Jr., J. A. Wade, " A Pulsed NQR FFT Spectrometer for Nitrogen 14", Journal of magnetic resonance ,36,2133(1979).

[14] S.S.Prasad and S.K.Sanyal, "A Novel Direct Digital Synthesis Technique to Generate Low Frequency Acoustic Signal for underwater signal processing using Digital signal processor," Proc. of Symposium on Ocean Electronics-2005,Cochin, India, pp. 170-175, Dec 2005.

[15] Kazuyuki Takeda, " A highly integrated FPGA based nuclear magnetic resonance spectrometer," Review of scientific instruments 78, 033103, 2007

[16] Shengyun Zhu, "Detection of Explosives by ^{14}N Nuclear Quadrupole resonance technique", Patent in 1993.

[17] G.L.Peterson, P.J.Bray, R.A,Marino, " A new pulsed Nuclear Quadrupole resonanc e spectrometer" .,Xllth International Symposium on Nuclear Quadrupole Resonance, Zürich, July 19-23,1993.

[18] T. N. Rudakov, A. V. Belyakov and V. T. Mikhaltsevich, "A low-frequency instrument for remote nuclear quadrupole resonance experiments", Measurement Science and Technology, vol. 8, no. 4, pp. 444-448, 1997

[19] J. L. Schiano and M. D. Ginsberg, "A Pulsed Spectrometer Designed for Feedback NQR", XVth International symposium on Nuclear Quadrupole Interactions,Leipzig, Germany, July 25 - 30, 1999.

[20] Nicolas Hiblot, Denis Grandclaude, Se´bastien Leclerc, "A fully homemade ^{14}N quadrupole resonance spectrometer". Article in Comptes Rendus Chimie·April2008

[21] Kazuyuki Takeda ,"OPENCORE NMR: Open-source core modules for implementing an integrated FPGA-based NMR spectrometer", Journal of Magnetic Resonance 192 (2008) 218–229

[22] Samo Begus, Vozko Jazbinsek , Janez Pirnat, Zvonko Trontolej, "A miniaturized NQR spectrometer for a multi-channel NQR-based detection device", Journal of Magnetic Resonance 247 (2014) 22–30

[23] J.L. Schiano, A.J. Blauch and M.D. Ginsberg. "Optimization of NQR pulse parameters using feedback control". XVth International Symposium on Nuclear Quadrupole Interactions. Leipzig, Germany. July 25-30, 1999.

[24] J.L.Schiano, T.Routhier, A.J. Blauch and M.D. Ginsberg. "Feedback optimization of pulse width in the SORC sequence". Journal of magnetic resonance.Vol. 140 No 1,pp . 84-90. Sep.,1999. ISSN: 1090-7807.DOI: 0.1006/jmre.1999.1824.

[25] Y. Tan, S.L. Tantum and L. M. Collins, “Landmine detection with nuclear quadrupole resonance," Proceedings of IEEE International Geoscience and Remote Sensing Symposium, vol. 3, pp. 1575-1578, 2002.

[26] Y.Tan, S.L. Tantum,and L.M Collins, “Cramer-Rao lower bound for estimating quadrupole resonance signals in non-Gaussian noise”, IEEE Signal Processing Letters, vol. 11, pp. 490-493, May 2004.

[27] Y.Tan, S.L. Tantum,and L.M Collins, “Kalman filtering for enhanced landmine detection using quadrupole resonane” ,IEEE transaction on Geoscience and Remote Sensing, vol 43, pp 1507-1516,july 2015

[28] G. Liu, Y. Jiang, H. Xiong, J. Li, and G. A. Barrall, “Radio frequency interference suppression for landmine detection by quadrupole resonance”, EURASIP, Journal on Applied Signal Processing, vol. 2006, pp. 1-14, 2006

[29] J. Stegenga, “Humanitarian de-mining: Detection algorithms for NQR signals”. M.S. Thesis, University of Twente (Netherland), January 2004.

[30] Jakobsson, M. Mossberg, M. D. Rowe, and J. A. S. Smith, “Exploiting temperature dependency in the detection of NQR signals”, ICASSP, Detection, Estimation, Classification Theory and Applications I, pp. 653-656, 2005.

[31] Jakobsson, M. Mossberg, M. Rowe and J. A. S. Smith, “Exploiting temperature dependency in the detection of NQR signals”, IEEE Transactions on Signal Processing, vol. 54, no. 5, pp. 1610-1616, 2006

[32] S. D. Somasundaram, A. Jakobsson, J. A. S. Smith, and K. Althoefer, “Exploiting spin echo decay in the detection of nuclear quadrupole resonance signals”, IEEE Transactions on Geosciences and Remote Sensing, vol. 45, no. 4, pp. 925-933, 2007

[33] S. D. Somasundaram, A. Jakobsson, M. D. Rowe, J. A. S. Smith, N. R. Butt, and K.Althoefer, “Robust detection of stochastic nuclear quadrupole resonance signals”, IEEE Transactions on Signal Processing, vol. 56, no. 9, pp. 4221-4229, 2008

[34] N. R. Butt, A. Jakobsson, S. D. Somasundaram, and J. A. S. Smith, “Robust multichannel detection of mixtures using nuclear quadrupole resonance”, IEEE Transactions on Signal Processing, vol. 56, no. 10, pp. 5042-5050, 2008.

[35] S. D. Somasundaram, A. Jakobsson, and E. Gudmundson, “Robust nuclear quadrupole resonance signal detection allowing for amplitude uncertainties”, IEEE Transactions on Signal Processing, vol. 56, no. 3, pp. 887-894, 2008.

[36] S. D. Somasundaram, A. Jakobsson, and N.R.Butt, “Countering Radio frequency interference in single sensor quadrupole resonance”, IEEE Geoscience and Remote Sensing Letters, Vol 6 , no.1, pp 62-66,2009.

[37] S. D. Somasundaram, J. A. S. Smith, K. Althoefer, and L. D. Seneviratne, “Detection of landmines using nuclear quadrupole resonance (NQR): An overview”,2004.

[38] S. L. Tantum, L. M. Collins, L. Carin, I. Gorodnitsky, A. D. Hibbs, D. O. Walsh,G. A. Barrall, D. M. Gregory, R. Matthews, and S. A. Vierk otter, “Signal processing for NQR discrimination of buried landmines," in Proc. SPIE, vol. 3710,pp. 474{482, 1999.

[39] Rabi, I. I.; Zacharias, J. R.; Millman, S.; Kusch, P., “A New Method of Measuring Nuclear Magnetic Moment”, Physical Review, vol. 53, Issue 4, pp. 318-318

[40] S.J. Glaser, “NMR Quantum Computing”, Angew. Chem. Int. Ed. 40, 147-149 (2001); Angew. Chem. 113, 151-153 (2001).

[41] M.D.Rowe and J.A.Smith ,‘ Mine detection by nuclear quadrupole resonance”, Proceedings of UREL International Conference on the detection of abandoned land mines: A Humanitarian imperative seeking a technical solution, pp 62-66,1996

[42] Farrar Thomas, “ Pulse and Fourier Transform NMR”, Academic Press, 1971

[43] E. L. Hahn, “Spin Echoes”, Physical Review, vol. 80, pp. 580-594, 1950

[44] Tinping Niu, Tao Su, Xuehin He, “Weak NQR signal detection based on generalized filter”, Science Direct, 2010 Symposium on Security detection and information processing.

[45] Mark S.Conradi, FET Q switch for pulsed NMR, RSI 48, 359(1977).

[46] V. S. Grechishkin, “NQR device for detecting plastic explosives, mines, and drugs" , Applied Physics A, vol. 55, no. 6, pp. 505-507, 1992.

[47] B. H. Suits, “The noise immunity of gradiometer coils for 14N NQR land mine detection: practical limitations", Applied Magnetic Resonance, vol. 25, no. 3-4, pp. 371-382, 2004.

[48] Gudmundson E, Jakobsson A, and Stoica P, “NQR-Based Explosives Detection—An Overview”, in 9thInternational Symposium on Signals, Circuits and Systems (ISSCS 2009), Iasi, Romania, July 9-10 2009.

[49] Pu Yuan, Yunzhi Mao, Huaming Guo. “Weak signal receiving and processing for nuclear quadrupole resonance detection”, Chinese Journal of Radio Science2006;21(2)

[50] Alan Gregorovic, Tomaz Apih, “TNT detection with ^{14}N NQR: Multipulse sequences and matched filter”, Journal of Magnetic Resonance 2009; 215-221

[51] Sujo C.I, Gopal loshi, “Solid state RF power amplifier at 27 MHz” , Proceedings of international symposium on Antennas and Propogation”, APSYM 2014

[52] Eva Murphy, Colm Slattery, "All about Direct digital synthesis", Analog Dialogue 38-08, August (2004)

[53] Maher Jridi, Ayman Alfalou. "Direct Digital Frequency Synthesizer with CORDIC Algorithm and Taylor Series Approximation for Digital Receivers". European Journal of Scientific Research, EuroJournals, 2009, 30 (4), pp.542-553

[54] João Gonçalves, Jorge R. Fernandes, Manuel M. Silva, "A Reconfigurable quadrature oscillator based on a DDS system", DCIS 2006

[55] C. Ziomek and P. Corredoura, " Digital I/Q Demodulator" Stanford Linear Accelerator Center, Stanford, CA 94309, USA

[56] K. R. Minard, R. A. Wind., 2001, "Solenoidal Micro coil Design-Part1: Optimizing RF Homogeneity and Coil Dimensions". Concepts in Magnetic Resonance 13, p. 128.

[57] I.J.LOWE C.E Tarr, Journal of Physics E1 320(1968).

[58] Fukushima, Roeder, "Experimental Pulse NMR", Nuts and Bolts approach

[59] Xinwang Zhang, Nathan Schemm, Sina Balkır, and Michael W. Hoffman, "A Low-Power Compact NQR Based Explosive Detection System", IEEE sensors journal, vol. 14, no. 2, february 2014.

[60] Jordan Kirsh and Robert Newman, "Digital quadrature detection in nuclear magnetic resonance spectroscopy", Analytical Center, East China Normal University, Shanghai 200062, People's Republic of China

[61] Li Gengyinga and Xie Haibin, "Digital quadrature detection in nuclear magnetic resonance spectroscopy",Analytical Center, East China Normal University, Shanghai 200062, People's Republic of China

[62] Nuclear Magnetism by Abragam, Oxford Publication.

[63] N.J. Stone , "Table of Nuclear Magnetic Dipole and Electric Quadrupole Moments", Oxford Physics

[64] Janez Seliger, Veslko Zagar, "New Methods for detection of ^{14}N NQR frequencies." Applied Magnetic Resonance(2012)

[65] G.Peterson, P.J. Bray ,"^{14}N Nuclear Quadrupole resonance and relaxation measurements of sodium nitrite.", J.Chem.Phys (1976).doi:10.1063/1.432241

[66] Taras N. Rudakov , "Detection of Explosives by NQR method:Main aspects for Export Security", 111-138, series 1874-6500,NATO Science for peace and security, Springer 2009

[67] Ranhong Xie, Youbin Wu, Kang Liu, Mi Liu1 and Lizhi Xiao , "De-noising methods for NMR logging echo signals based on wavelet transform", J. Geophys. Eng. **11** (2014)

[68] Tao Yang, Tao Su, Xuehui He, "NQR Signal Processing Based on Multi-stage Wiener Filter", Symposium on Security Detection and Information , Procedia Engineering 7 (2010) 229–234

[69] Martin Vetterli, "Wavelet and Filter Banks: Theory and Design", IEEE Transactions on Signal Processing, Volume 40, September 1992

[70] G. V. Mozzhukhin, S. V. Molchanov, "Application of the Wavelet Transform for detecting signals of Nuclear Quadrupole Resonance", Russian Physics Journal, Vol. 48, No. 1, 2005.

[71] Nagendra.H, "Application of Wavelet Techniques in ECG Signal Processing", International Journal of Engineering Science and Technology, Volume 3 No.10,October 2011

[72] Yousef M. Hawwar, Ali M. Reza, Robert D. Turney, "Filtering in the Wavelet Transform Domain", University Of Wisconsin-Milwaukee.

[73] David L. Donoho, Iain M. Johnstone, Gerard Kerkyacharianand, Dominique Picard "Density Estimation by Wavelet Thresholding", Technical report no. 162, June 1993

[74] Neema, “Performance analysis of Wavelet Thresholding methods in De-noising Of audio signals of some Indian musical instruments”, International Journal of Engineering Science and Technology, Vol 4 No. 5 May 2012.

[75] Saeed V. Vaseghi, “Advanced Digital signal Processing and Noise reduction.”

[76] R.M.Ramli, “A Review of Adaptive Line Enhancers for Noise Cancellation,” Australian Journal of Basic & Applied Sciences, Jun2012, Vol. 6 Issue 6, p337

[77] B.Widrow, M. E . Hoff ,Wescon Conv. Rec 96-104(1960)

[78] Boroujeny,B.F.(1998). Adaptive Filters: Theory and Applications. Chichester, New York, Weinheim, Brisbane,Singapore, Toronto:JohnWiley & Sons Ltd.

[79] Fenglin, W., & Chris, M. K. (2004),”Frequency Properties of an Adaptive Line Enhancer”, Mechanical Systems and Signal Processing, 797-812.

[80] Alaa Abdulhady Jaber, Robert Bicker,”A Simulation of Non-stationary Signal Analysis Using Wavelet Transform Based onLabVIEW and Matlab**”,** 2014 UKSim-AMSS 8th European Modelling Symposium

[81] J.Zhen, R. Dykstra, C. Eccles, G. Gouws, and S. Obruchkov, “A compact Class D RF power amplifier for mobile nuclear magnetic resonance systems, Review of Scientific Instruments 88, 074704 (2017); doi: 10.1063/1.4994734

[82] Hermann Scharfetter, An electonically tuned wideband probehead for NQR spectroscopy in the VHF range, Journal of Magnetic Resonance 271 (2016) 90-98

[83] Xinwang Zhang, “A Low-Power Compact NQR Based Explosive Detection System”. (2014). Electrical Engineering Theses and Dissertations. Paper 58.